Fundamental Properties and Applications of Physical Gels Composed of Polymer-Grafted Particles and Liquid Crystals

Yuki Kawata

February 2017

Fundamental Properties and Applications of Physical Gels Composed of Polymer-Grafted Particles and Liquid Crystals

Yuki Kawata

Doctoral Program in Nano-Science and Nano-Technology

Submitted to the Graduate School of
Pure and Applied Sciences
in Partial Fulfillment of the Requirements
for the Degree of Doctor of Philosophy in
Science

at the
University of Tsukuba

Contents

Chapter 1

General Introduction

1-1 Soft matter

Soft matter is one of material categories and includes a large variety of materials such as polymers, colloids, liquid crystals, and surfactants (Figure 1-1).[1,2] These components form gels, emulsions, membranes, and rubbers, which play important roles in biological materials, daily necessities, and advanced materials. Now, soft matter is indispensable to our daily life and modern technology. First of all, the individual and common characteristics of several important components of soft matter are briefly described.

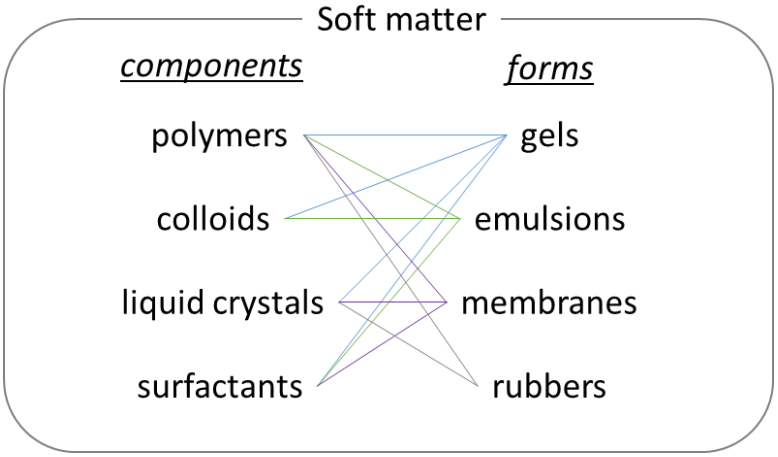

Figure 1-1. Components and forms included in soft matters.

Polymers

Molecules of polymers are long strings-like ones, in which repeating units called monomers are sequentially connected. The number of monomer units in a molecule is typically more than one hundred. Polymers are ubiquitous in our life as plastics, films, rubbers, and fibers. A variety of polymers are produced by using different types of monomers and connecting ways such as linear, branched, and cross-linked. Even if the polymer chains are not chemically cross-linked, long

enough chains behave like cross-linked networks because of entanglement with each other. The entanglement causes unique viscoelastic properties of polymers such as good elasticity in a rubbery state and high viscosity in a molten state.

One of the important characteristics of polymers is the mechanical property, which is a key aspect in the point of view of processing as well as performance of products. The mechanical property is time- and temperature-dependent property and is related to the dynamics inside polymers.[3] Figure 1-2 shows a typical temperature dependence of an elastic modulus of amorphous polymers. In a low enough temperature region (region 1), polymers are hard and show a high elastic modulus over 10^9 Pa. In this state (called a glassy state), the main chains of polymers are frozen and only vibrational motions related to several atoms can be allowed. In a glass transition region (region 2), polymers soften and the modulus drops three orders of magnitude. This region can be interpreted as the onset of the local segmental motions associated with several tens of atoms in a polymer chain. The region 3 is a rubber plateau region in which polymers are rubbery and the modulus exhibit approximately constant value in a certain temperature range. Polymers can be stretched and turned back to their original length. The region appears only if polymers are chemically cross-linked or long enough to form entanglement networks. In the region 4 called a terminal region, polymers begin to flow and the modulus further drops. Polymers in this region behave rubber or fluid for short-time-scale or longer-time-scale experiments, respectively.

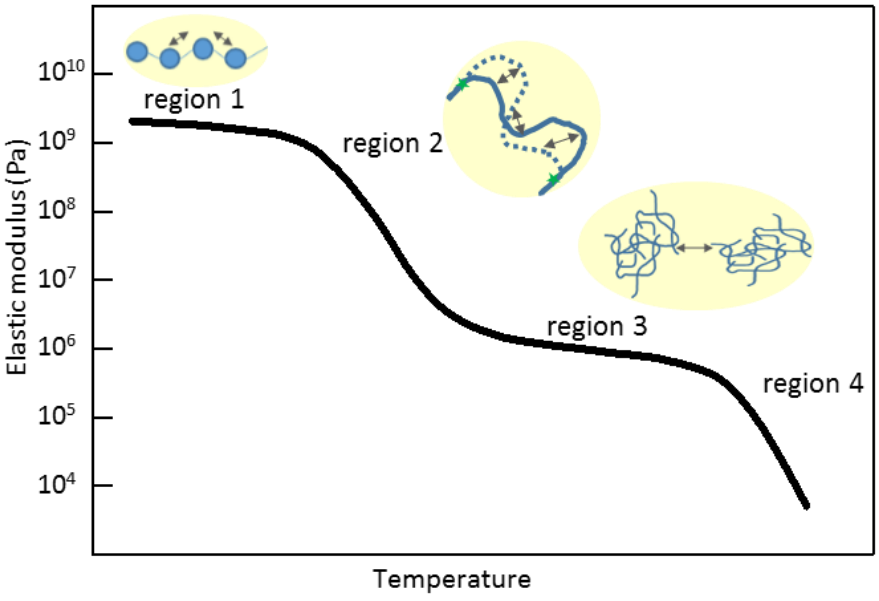

Figure 1-2. Four regions in viscoelastic behavior of a linear amorphous polymer.

Colloids

Colloids are small solid particles or fluid droplets dispersed in other continuous phases. The diameter of the colloids is typically 1 nm – 1 μm. In daily life, colloidal systems can be often seen in foods and cosmetics. Milk is a typical colloidal suspension in which particles made of fats and proteins are homogeneously dispersed in water (Figure 1-3A). On the other hand, tofu is one of colloidal gels in which particles of proteins randomly aggregate and construct network-like structures (Figure 1-3B). In addition, colloids can form regular structures (colloidal crystals) when the particles have a uniform shape and size (Figure 1-3C). The colloidal crystals exhibit strong diffraction of light. Thus, colloids exhibit a variety of states such as fluid and quasi-solid depending on the microstructures.

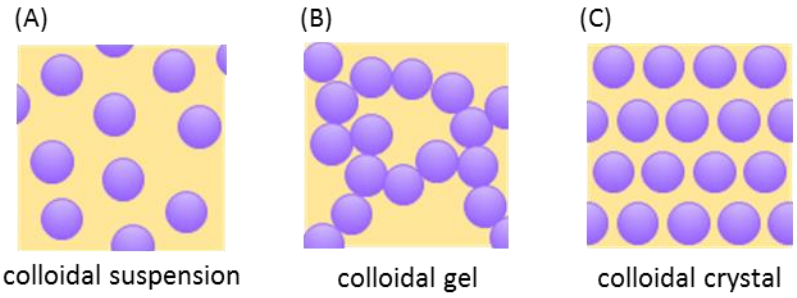

Figure 1-3. A variety of structures formed by colloids: (A) colloidal suspension, (B) colloidal gel, and (C) colloidal crystal.

Liquid crystals

Liquid crystals (LCs) are matter in an intermediate state between liquid and solid and can flow like a liquid and the direction of molecules are (partially) ordered like a crystal.[4] They consist of molecules having strong anisotropy in their shapes: rod, disk, and bend. Nematic (N) LCs which is a typical class of LCs are extensively used in display devices because the optical property can be easily controlled by electric fields. In NLCs, the elongated molecules retain their axes almost parallel each other in a certain direction, while they do not exhibit any positional orders. In the case of thermotropic LCs, N phase turns into an isotropic (I) phase where the long-range orientational order is lost by heating to a temperature above the N–I transition temperature ($T_{N–I}$) (Figure 1-4A). The change in the state of aggregates of LC molecules upon the N–I transition cause the changes in the macroscopic properties of LCs such as the viscosity and transparency. The N–I

transition can be also driven by light in LCs doped with a small amount of azobenzene derivatives.[5] The *trans–cis* photoisomerization of the azo additive in LCs results in lowering of $T_{N–I}$, since the bent-shaped *cis* form suppresses the orientational order of the molecules and cause the LC phase to be unstable. As a result, at an appropriate temperature, the N–I transition can be induced by the irradiation of ultra-violet (UV) light (Figure 1-4B).

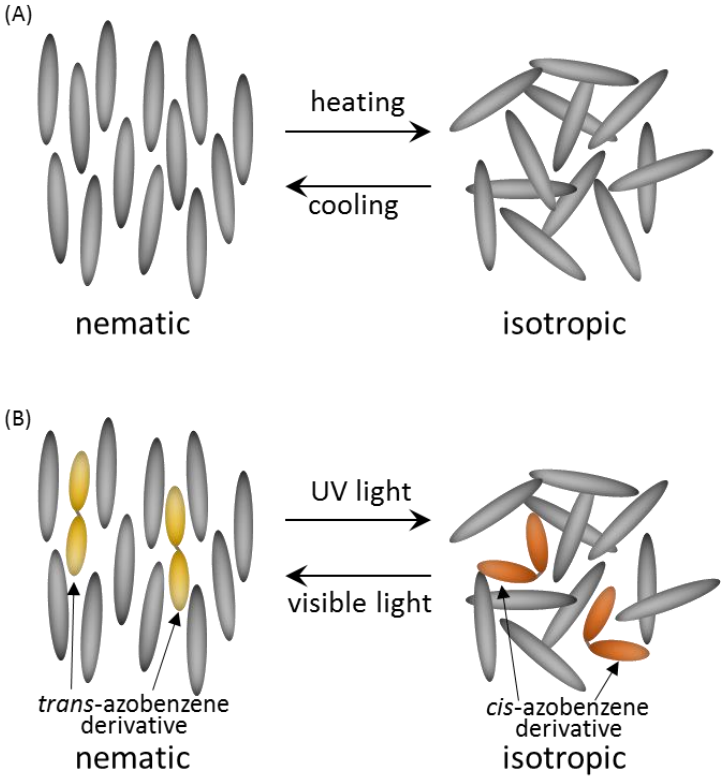

Figure 1-4. Nematic–isotropic transitions driven by (A) heat and (B) light.

Common characteristics

In the above-mentioned materials, their macroscopic physical properties are closely related to mesoscopic aggregates formed by molecules or particles. The structures and stability of the aggregates are significantly affected by small perturbation in the interaction, shape, and dynamics of the components. It is therefore difficult to manipulate the macroscopic properties of the materials and the behaviors of the aggregates. The control of the properties and understanding of the behaviors are significant challenges in academic and industrial researches.

1-2 Development of functional materials using soft matter

Today, a variety of functional materials employing soft matter are under development, for example, self-healing materials and soft actuators using polymer, flexible optical materials using liquid crystals, and cell culture media and artificial cartilage using gels. Self-healing materials have attracted a great deal of attention owing to their potential ability to extend the lifetime of products.[6-8] So far, a great number of materials that can heal cracks and cuts have been proposed on the basis of various approaches (Table 1-1), such as polymerization in cracked areas (Figure 1-5A),[9] and dynamic covalent or non-covalent bonds showing recombination at the contact plane of cutting sections (Figure 1-5B).[6-8, 10-13] In addition, changes in morphology of materials would be potentially applicable to a healing mechanism of surface cracks (Figure 1-6).[14] In liquid-crystalline composites containing microparticles and azo dyes, a reversible gel–sol transition is achieved by the control of the network-like microstructure of the microparticles on the basis of the photochemical phase transition of LC matrices. Utilizing the photoinduced gel–sol transition, the repairing of surface cracks can be realized by the irradiation of UV light. On the other hand, the repairing of surface dents has been achieved in supramolecular materials (Figure 1-5C) and several polyurethanes (Figure 1-5D) by using their elastic property.[13, 15-16] In addition, self-healing of internal delamination damages in fiber-reinforced composites has been recently achieved by the micro-vascular delivery of reactive fluids.[17] An ideal self-healing material should heal various mechanical damages, such as cracks, cuts, dents, and delamination spontaneously or with the aid of external triggers such as light or heat. At present, materials that can heal cuts and dents have been realized with the use of hyperbranched polymers[16] and polyrotaxanes with reversible bonds[13]. However, the development of materials with multiple self-healing abilities is still a significant challenge.

As mentioned above, composite gels consisting of cross-linked polymer particles, LCs, and azobenzene derivatives can photochemically repair surface cracks.[14] The light-assisted mending of surface cracks is successfully achieved by photoindiced gel–sol transition of the composite gels (Figure 1-6). The cracked area of the composite gel is filled up with the composite in a sol state generated by the UV-light irradiation. Then, the fluid area returns to the gel state upon the illumination of visible light, resulting in the recovery of a smooth surface of the composite gels. However, the composites have a low mechanical strength and exhibit a poor elastic behavior. Therefore, unfortunately, surface dents made on the composite gels cannot be repaired. If we

improve the elastic property of such composites significantly in addition to the photoinduced gel–sol transition, the composite gels will be able to possess self-healing abilities of both surface cracks and dents. Thus, the manipulation of the mechanical properties such as fluidity and elasticity will lead to the improvement of functionalities of materials.

Table 1-1. Self-healing materials and their healing mechanisms

damages	healing mechanisms	materials
cracks, cuts	polymerization	materials including encapsulated-polymerizable mobile phases[9] (Fig 1-5A)
	dynamic covalent or noncovalent bond	chemically or physically cross-linked polymer bearing reversible Diels–Alder reaction, π-π stacking interaction, or host–guest molecular recognition units[6-8, 10-13] (Fig 1-5B)
	photoinduced gel–sol transition	particle/azo-doped LC composite gels[14] (Fig 1-6)
delamination	polymerization	fiber-reinforced composites by the micro-vascular delivery of reactive fluids[17]
dents	elastic respond	slide-ring materials[13, 15] (Fig 1-5C)
		polyurethanes (Fig 1-5D)

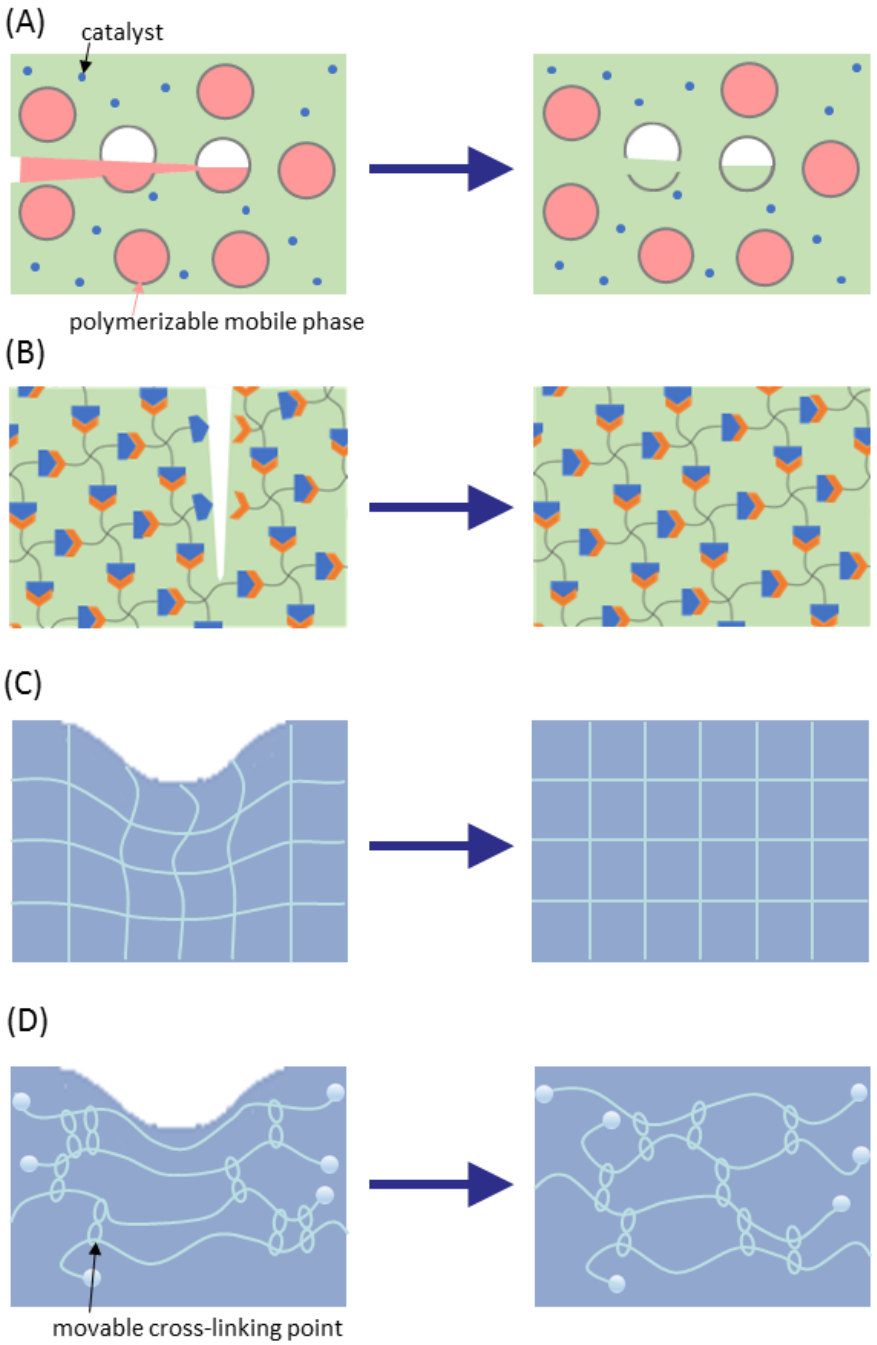

Figure 1-5. Healing mechanisms of self-healing materials which can repair (A and B) cracks and (C and D) dents.

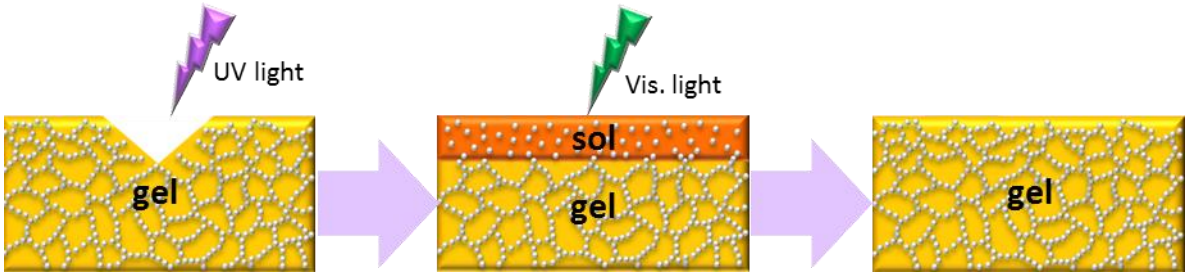

Figure 1-6. Light-mediated repairing of a surface crack in the composite gel of microparticles and LC containing a small amount of an azobenzene derivative.[14]

The manipulation of the mechanical properties can also advance the development of other functional materials such as the cell culture media for tissue engineering and optical materials for flexible devices. One of the technologies in the regenerative medicine is the tissue engineering, where the artificial tissues are constructed from stem cells.[18-19] Recently, Engler et al.[20] reported that the hardness of scaffolds used for the cell culture affects differentiation induction of stem cells, namely, the cells culturing on a harder scaffold differentiate dominantly into a harder tissue. Therefore, the development of scaffolds with tunable hardness will greatly contribute to the progress of the regenerative medicine. On the other hand, in the optical materials, materials applicable to flexible devices are attracting attention.[21] If LCs which are fluid and widely employed as display materials acquire the self-supporting properties, the novel optical materials for flexible devices can be developed. In addition, the fluidity and viscosity are important factors in manufacturing processes. Thus, the control of the mechanical properties such as hardness, elasticity, fluidity, and viscosity is a common subject in the development of functional materials using soft matter.

Focused on the elastic modulus as an index, each functional material requires the manipulation of the elastic modulus in the different ranges. For example, in order to ensure the light-mediated repairing of surface cracks by a photoinduced gel–sol transition, the elastic modulus of the gels should be changed from over 10^3 Pa in a gel state to below 10^2 Pa in a sol state by the photoirradiation. In cell culture media, the control of the elastic modulus in the range of 10^3–10^5 Pa is required for the development of scaffolds with high differentiation induction efficiency of

stem cells. An elastic modulus over 10^4 Pa would be necessary to develop self-supporting optical materials. Therefore, in order to develop these advanced functional materials, the elastic modulus should be manipulated in a wide range from below 10^2 Pa to over 10^5 Pa. At this point, it is noted that the required range of the elastic modulus can be covered with the elastic moduli of gels, which are of a typical form of soft matter. The control using external stimuli is desirable from the stand point of the easy and spatial controls of the elastic modulus.

1-3 Previous studies of the control of the mechanical properties of gels

Gel is a quasi-solid consisting of fluids and infinite three-dimensional networks constructed in the fluids by chemical bonding or physical aggregation of gelators such as polymers, colloids, and hydrogen-bonded molecules. Gels have been used in foods and cosmetics.[22] Since the feeling and texture are important for these products, the mechanical properties of gels have been actively studied. In the previous studies, the mechanical properties of gels has been manipulated by the changes of the structures and stiffness of inner networks, or the viscoelasticity of the fluid.[14, 23-39] The relation between the inner structures and the mechanical properties is one of the subjects gathering the greatest attention.[14, 23-37] For example, in the rubber elasticity theory assuming the homogeneous network consisting of Gaussian chains, the fineness of the network influences the elastic modulus.[40] The shear elastic modulus G is represented as $G = c_p k_B T$, where the c_p is the number density of the chains of which both ends are fixed at respective different cross-linking points, k_B is the Boltzmann constant, and T is the temperature. A higher c_p corresponds to a denser network having more cross-linking points. Moreover, slide-ring gels[35] and double-network gels[36] have been recently reported to exhibit the good elasticity and high mechanical strength by virtue of their unique inner structures. On the other hand, in collagen gels where collagen fibers form the networks, the stiffness of the fibers is also regarded as one of the factors affecting elastic modulus.[34] Furthermore, Bukusoglu et al.[37] reported that the elastic modulus of the composite gels consisting of colloids and nematic LC steeply raised by the increase of the concentration of colloids in the network due to the colloidal glass transition. In the particles/LC composite gels employing an LC matrix showing N and smectic A (SmA) phases, the elastic modulus of the gels notably changed due to the changes in the elasticity of the matrix upon the N–SmA phase transition.[38]

Thermal and photoinduced controls of the mechanical properties of gels have attracted recent attentions due to their potential applications to biomedical devices.[19-20, 24, 28-29, 32] In previously-reported stimuli-responsive gels, their mechanical properties were generally manipulated by means of the stimuli-induced changes of internal structures.[24-33] The control of the elastic modulus has typically been performed in an elastic-modulus range below approximately 10^4 Pa (Figure 1-7). For example, in the hydrogels utilizing temperature-sensitive polymers including poly(*N*-isopropyl acrylamide) or poly(vinyl ether) segments,[24-26] appearance of the hydrophobic parts in polymers by dehydration on heating causes the formation of the network structure by the self-assembly of the polymers.[41] Then, the mechanical properties of the gels changed. The photoinduced changes of the elastic modulus with keeping a gel state have been achieved by the partial decomposition of the inner networks employing photodegradable or photocrosslinkable components.[28-30] On the other hand, only a few papers have reported the temperature-induced changes of the elastic modulus driven by the changes in the stiffness of the network and viscoelasticity of the fluid in particle/LC composite gels.[37-38] In these reports, the change of the elastic modulus is achieved in the relatively higher elastic modulus range of 10^3–10^5 Pa.

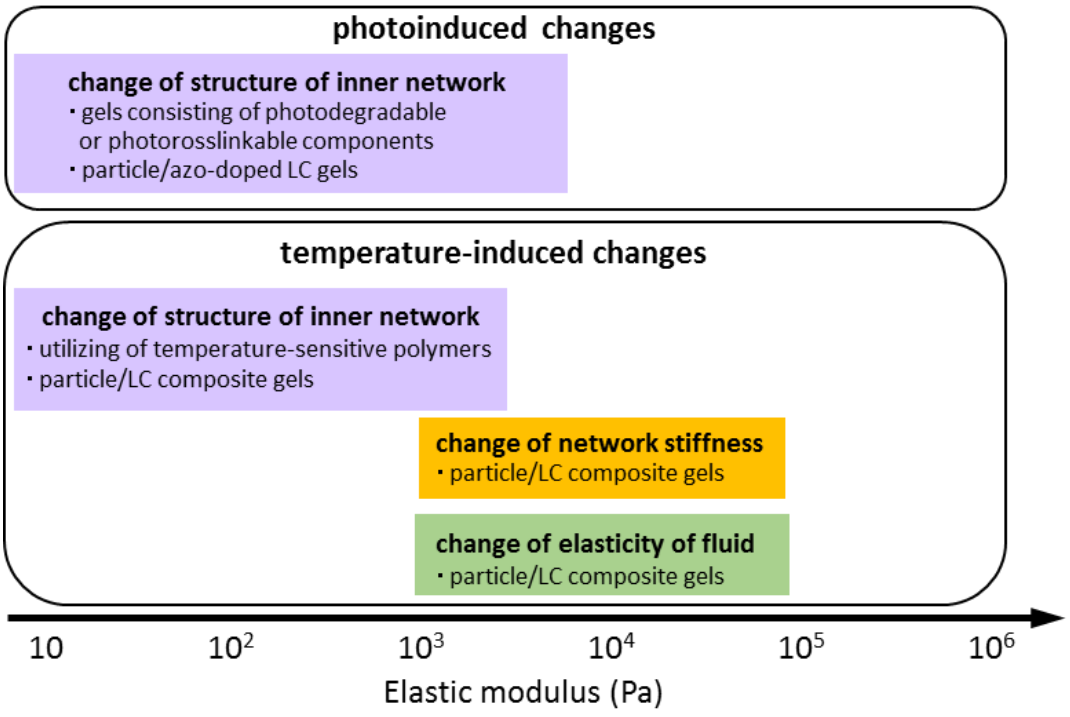

Figure 1-7. Previous studies about the control of the elastic modulus using external stimuli of heat or light.

1-4 Objective of this study

If a mechanism that can easily control the elastic modulus in a wide range from below 10^2 Pa to over 10^5 Pa by the external stimuli is found, the development of the advanced functional materials will rapidly progress. As shown in Figure 1-7, however, the control of the elastic modulus using external stimuli has been achieved only in a narrow range employing a single mechanism. In addition, the photoinduced changes of the elastic modulus have been proposed only below 10^4 Pa employing the structural changes of the inner networks. Putting these in mind, it is considered that the combination of the changes of the structures and stiffness of the inner networks enables the control of the elastic modulus of gels in a wider range. The properties of the networks will be affected by microscopic aspects such as the interaction and dynamics of components. The aim of this thesis is, therefore, to elucidate the role of these microscopic aspects in the mechanism governing the properties of the inner networks and then the mechanical properties of gels. On the basis of the revealed mechanism, the author will attempt the sophisticated tuning of the mechanical properties by the control of the inner networks. Furthermore, the development of improved functional materials is challenged through manipulating the mechanical properties.

In order to investigate the mechanism, the author decided to study the physical gels composed of polymer-brush-afforded silica particles (P-SiPs) and nematic LCs. The P-SiP acting as a gelator is a core-shell particle in which the core is a monodisperse spherical silica particle and the shell consists of poly(methyl methacrylate) (PMMA) chains densely grafted on the core via an atom transfer radical polymerization method. A typical diameter of the P-SiP (the weight-average molecular weight of the grafted PMMA is 248000 g mol^{-1}) is 650 nm in acetone that is a good solvent for PMMA. The P-SiPs are a kind of colloids, which may construct varieties of microstructures as mentioned previously (Figure 1-3). The P-SiP also includes polymer, of which local dynamics would significantly affect the mechanical properties of the polymer materials (Figure 1-2). The properties of P-SiPs as colloids and polymer can be used for control of the structures and stiffness of the inner networks formed by P-SiPs. The LCs showing an N phase at room temperature are employed as a matrix of composites. The LCs are the stimuli-responsive fluids in which the regularity of molecular orientation and their macroscopic properties change upon the thermal N–I phase transition (Figure 1-4A). By the addition of a small amount of an azobenzene derivative to the LCs, the changes of the molecular shape of the azo additive by the photoisomerization could induce the changes of the molecular orientation of LC molecules as if a

little difference in the molecules are amplified to the change in a whole azo-doped LC (Figure 1-4B). The employment of the LCs would efficiently impart the stimuli-responsiveness to the composite.

In chapter 2, the fundamental properties of the P-SiP/LC composites and effects of the microstructures formed with P-SiPs, dynamics of polymer components, and phase structures of liquid crystals on the properties are described. The application of the characteristic mechanical property of the P-SiP/LC composite gels to the self-supporting optical materials is also attempted. In chapter 3, the photoresponsivity of the viscoelasticity of the P-SiP/LC composites containing an azobenzene derivative is examined in detail. The mechanism of the photoresponsivity of the P-SiP/azo-doped LC composites is clarified by analyzing the phase behaviors of PMMA/azo-doped LC blends. The isothermal change of the elastic moduli by UV-light irradiation is performed and the possibility to apply the composite gels to cell culture media for tissue engineering is suggested. In chapter 4, self-healing abilities that are the repairing of surface dents and cracks are investigated on the basis of the precise control of the mechanical properties of P-SiP/azo-doped LC composite gels. In chapter 5, a summary of this study and future perspective are given.

References to chapter 1

(1) Doi, M., *Soft Matter Physics*, First edition. ed; Oxford University Press: Oxford ; New York, 2013.

(2) Gennes, P.-G. d.; Badoz, J., *Fragile Objects : Soft Matter, Hard Science, and the Thrill of Discovery*, Copernicus: New York, 1996.

(3) Sperling, L. H., *Introduction to Physical Polymer Science*, 4th ed; Wiley: Hoboken, N.J., 2006.

(4) de Gennes, P. G.; Prost, J., *The Physics of Liquid Crystals*, 2nd ed; Oxford University Press: Oxford, 1993.

(5) Ikeda, T. Photomodulation of Liquid Crystal Orientations for Photonic Applications. *J. Mater. Chem.* **2003,** *13* (9), 2037-2057.

(6) Murphy, E. B.; Wudl, F. The World of Smart Healable Materials. *Prog. Polym. Sci.* **2010,** *35* (1-2), 223-251.

(7) Hager, M. D.; Greil, P.; Leyens, C.; van der Zwaag, S.; Schubert, U. S. Self-Healing Materials. *Adv. Mater.* **2010,** *22* (47), 5424-5430.

(8) Bergman, S. D.; Wudl, F. Mendable Polymers. *J. Mater. Chem.* **2008,** *18* (1), 41-62.

(9) White, S. R.; Sottos, N. R.; Geubelle, P. H.; Moore, J. S.; Kessler, M. R.; Sriram, S. R.; Brown, E. N.; Viswanathan, S. Autonomic Healing of Polymer Composites. *Nature* **2001,** *409* (6822), 794-797.

(10) Liu, K.; Kang, Y.; Wang, Z.; Zhang, X. 25th Anniversary Article: Reversible and Adaptive Functional Supramolecular Materials: "Noncovalent Interaction" Matters. *Adv. Mater.* **2013,** *25* (39), 5530-5548.

(11) Ying, H.; Zhang, Y.; Cheng, J. Dynamic Urea Bond for the Design of Reversible and Self-Healing Polymers. *Nat. Commun.* **2014,** *5*, 3218.

(12) Yamaguchi, H.; Kobayashi, Y.; Kobayashi, R.; Takashima, Y.; Hashidzume, A.; Harada, A. Photoswitchable Gel Assembly Based on Molecular Recognition. *Nat. Commun.* **2012,** *3*, 603.

(13) Nakahata, M.; Mori, S.; Takashima, Y.; Yamaguchi, H.; Harada, A. Self-Healing Materials Formed by Cross-Linked Polyrotaxanes with Reversible Bonds. *Chem* **2016,** *1*, 766–775.

(14) Yamamoto, T.; Yoshida, M. Viscoelastic and Photoresponsive Properties of Microparticle/Liquid-Crystal Composite Gels: Tunable Mechanical Strength Along with Rapid-Recovery Nature and Photochemical Surface Healing Using an Azobenzene Dopant. *Langmuir* **2012,** *28* (22), 8463-8469.

(15) Noda, Y.; Hayashi, Y.; Ito, K. From Topological Gels to Slide-Ring Materials. *J. Appl. Polym. Sci.* **2014,** *131* (15), 40509.

(16) Wei, Q.; Wang, J.; Shen, X. Y.; Zhang, X. A.; Sun, J. Z.; Qin, A. J.; Tang, B. Z. Self-Healing Hyperbranched Poly(Aroyltriazole)S. *Sci. Rep.* **2013,** *3*, 1093.

(17) Patrick, J. F.; Hart, K. R.; Krull, B. P.; Diesendruck, C. E.; Moore, J. S.; White, S. R.; Sottos, N. R. Continuous Self-Healing Life Cycle in Vascularized Structural Composites. *Adv. Mater.* **2014,** *26* (25), 4302-4308.

(18) Khademhosseini, A.; Langer, R. Microengineered Hydrogels for Tissue Engineering. *Biomaterials* **2007,** *28* (34), 5087-5092.

(19) Lee, K. Y.; Mooney, D. J. Hydrogels for Tissue Engineering. *Chem. Rev. (Washington, DC, U. S.)* **2001,** *101* (7), 1869-1879.

(20) Engler, A. J.; Sen, S.; Sweeney, H. L.; Discher, D. E. Matrix Elasticity Directs Stem Cell Lineage Specification. *Cell* **2006,** *126* (4), 677-689.

(21) Choi, M. C.; Kim, Y.; Ha, C. S. Polymers for Flexible Displays: From Material Selection to Device Applications. *Prog. Polym. Sci.* **2008,** *33* (6), 581-630.
(22) Gallegos, C.; Franco, J. M. Rheology of Food, Cosmetics and Pharmaceuticals. *Curr. Opin. Colloid Interface Sci.* **1999,** *4* (4), 288-293.
(23) Bohidar, H. B.; Dubin, P.; Osada, Y., *Polymer Gels : Fundamentals and Applications*, American Chemical Society Distributed by Oxford University Press: Washington, DC, 2003.
(24) Qiu, Y.; Park, K. Environment-Sensitive Hydrogels for Drug Delivery. *Adv. Drug Delivery Rev.* **2001,** *53* (3), 321-339.
(25) Okabe, S.; Sugihara, S.; Aoshima, S.; Shibayama, M. Heat-Induced Self-Assembling of Thermosensitive Block Copolymer. 1. Small-Angle Neutron Scattering Study. *Macromolecules* **2002,** *35* (21), 8139-8146.
(26) Zhou, X.; Fan, X. S.; He, C. B. Hybrid Starlike Block Copolymer Poss-(Pdmaema-B-Pnipam)(8): Thermal Gelation and Its Blends with Poly(Vinyl Alcohol). *Macromolecules* **2016,** *49* (11), 4236-4244.
(27) Diestra-Cruz, H.; Bukusoglu, E.; Abbott, N. L.; Acevedo, A. Hierarchical Microstructures Formed by Bidisperse Colloidal Suspensions within Colloid-in-Liquid Crystal Gels. *ACS Appl. Mater. Interfaces* **2015,** *7* (13), 7153-7162.
(28) Fairbanks, B. D.; Singh, S. P.; Bowman, C. N.; Anseth, K. S. Photodegradable, Photoadaptable Hydrogels Via Radical-Mediated Disulfide Fragmentation Reaction. *Macromolecules* **2011,** *44* (8), 2444-2450.
(29) Kloxin, A. M.; Kasko, A. M.; Salinas, C. N.; Anseth, K. S. Photodegradable Hydrogels for Dynamic Tuning of Physical and Chemical Properties. *Science* **2009,** *324* (5923), 59-63.
(30) Tibbitt, M. W.; Kloxin, A. M.; Sawicki, L. A.; Anseth, K. S. Mechanical Properties and Degradation of Chain and Step-Polymerized Photodegradable Hydrogels. *Macromolecules* **2013,** *46* (7), 2785-2792.
(31) Vollmer, D.; Hinze, G.; Ullrich, B.; Poon, W. C. K.; Cates, M. E.; Schofield, A. B. Formation of Self-Supporting Reversible Cellular Networks in Suspensions of Colloids and Liquid Crystals. *Langmuir* **2005,** *21* (11), 4921-4930.
(32) Tomatsu, I.; Peng, K.; Kros, A. Photoresponsive Hydrogels for Biomedical Applications. *Adv. Drug Delivery Rev.* **2011,** *63* (14-15), 1257-1266.
(33) Tiefenbacher, K.; Dube, H.; Ajami, D.; Rebek, J. A Transparent Photo-Responsive Organogel Based on a Glycoluril Supergelator. *Chem. Commun. (Cambridge, U. K.)* **2011,** *47* (26), 7341-7343.
(34) Yang, Y. L.; Leone, L. M.; Kaufman, L. J. Elastic Moduli of Collagen Gels Can Be Predicted from Two-Dimensional Confocal Microscopy. *Biophys. J.* **2009,** *97* (7), 2051-2060.
(35) Ito, K. Novel Cross-Linking Concept of Polymer Network: Synthesis, Structure, and Properties of Slide-Ring Gels with Freely Movable Junctions. *Polym J* **2007,** *39* (6), 489-499.
(36) Gong, J. P.; Katsuyama, Y.; Kurokawa, T.; Osada, Y. Double-Network Hydrogels with Extremely High Mechanical Strength. *Adv. Mater. (Weinheim, Ger.)* **2003,** *15* (14), 1155-+.
(37) Bukusoglu, E.; Pal, S. K.; de Pablo, J. J.; Abbott, N. L. Colloid-in-Liquid Crystal Gels Formed Via Spinodal Decomposition. *Soft Matter* **2014,** *10* (10), 1602-1610.

(38) Yamamoto, T.; Kawata, Y.; Yoshida, M. Contrasting Roles of Layered Structures in the Molecular Assembly of Liquid Crystal Matrices on the Viscoelastic Properties of Microparticle/Liquid Crystal Composite Gels Leading to Rigidification and Destabilization. *J. Colloid. Interf. Sci.* **2013,** *397*, 131-136.
(39) Mackintosh, F. C.; Kas, J.; Janmey, P. A. Elasticity of Semiflexible Biopolymer Networks. *Phys. Rev. Lett.* **1995,** *75* (24), 4425-4428.
(40) Strobl, G. R., *The Physics of Polymers : Concepts for Understanding Their Structures and Behavior*, 3rd. rev. and expanded ed; Springer: Berlin ; New York, 2007.
(41) Schild, H. G. Poly (N-Isopropylacrylamide) - Experiment, Theory and Application. *Prog. Polym. Sci.* **1992,** *17* (2), 163-249.

Chapter 2

Thermal Properties of P-SiP/LC Composite Gels

2-1 Introduction

As mentioned in chapter 1 (General Introduction), the micro and mesoscopic aspects would be deeply involved in the macroscopic physical properties of the composites consisting of the P-SiPs and nematic LCs. In this chapter, at first, the fundamental properties, mechanical and optical properties, are examined in the P-SiP/LC composite gels. Then, the effect of the microstructure formed with colloidal particles, dynamics of polymer components, and phase structures of liquid crystals on the properties are investigated using structural and thermal analyses. The structural analyses during the gelation are also performed to clarify the mechanism of gelation in the P-SiP/LC composites.

The P-SiP/LC composite gels are liquid-crystalline physical gels, which would be a possible candidate for novel self-supporting optical materials[1-2] due to the quasi-solid nature of gels and stimuli-responsiveness of LCs. However, in the particle/LC composite gels previously reported[3-6], the photoswitching of optical properties with keeping the quasi-solid nature has not been realized, because the gel state can be observed only in a nematic phase of the LC matrices. In this chapter, using the findings obtained by the above fundamental studies in the P-SiP/LC composite gels, the photochemical switching of the transparency was also attempted while keeping the self-supporting ability.

2-2 Experimental section

2-2-1 Materials

P-SiPs (Figure 2-1A) were kindly supplied by Prof. Kohji Ohno (Kyoto University). The synthesis has been performed by surface-initiated atom transfer radical polymerization (ATRP) of methyl methacrylate on spherical silica cores (diameter = 130 nm).[7-8] In this study, five types of P-SiPs with different weight-averaged molecular weights ($M_{w,graft}$) of the grafted poly(methyl methacrylate) (PMMA) chains were employed: P-SiP (22k), P-SiP (52k), P-SiP (118k), P-SiP

(248k), and P-SiP (600k) with grafted PMMA chains with $M_{w,graft}$ = 22000, 52000, 118000, 248000, and 600000 g mol^{-1}, respectively. The hydrodynamic diameters (D_h) of the P-SiPs were determined based on dynamic light scattering measurements (Zetasizer Nano ZS, Malvern Instruments Ltd., UK) in acetone at 25 °C (Table 2-1). The surface density of grafted PMMA is typically 0.6−0.7 chains/nm^2.[8] The effective graft density σ_{eff} of P-SiP is given by[8]

$$\sigma_{eff} = \sigma_0(D_0/D)^2 \quad (2\text{-}1)$$

where σ_0 is the graft density on the core surface in chains/nm^2, D_0 is the diameter of the core, and D is the distance from the center of the core.

A nematic LC mixture (ZLI-1083) was purchased from Merck and used as supplied. The chemical structures of the components of ZLI-1083 are shown in Figure 2-1B. The nematic–isotropic phase transition temperature ($T_{N–I}$) of ZLI-1083 was determined to be 52.4 °C using polarized optical microscopy. Conventional PMMA for thermal analyses was purchased from Aldrich and purified by reprecipitation (M_w = 102000, M_w/M_n = 2.1). An azobenzene compound BMAB (4-butyl-4'-methoxyazobenzene, Figure 2-1C) was prepared according to a conventional synthetic route[9]

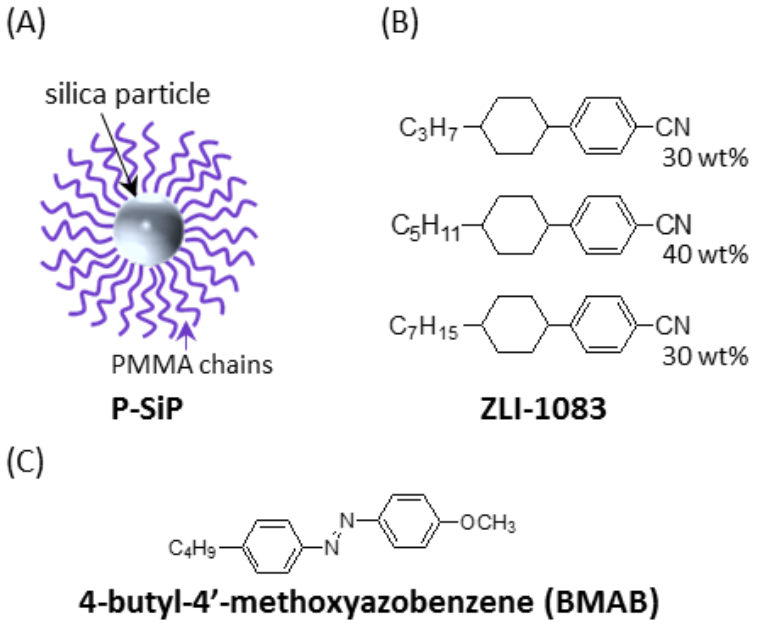

Figure 2-1. (A) Schematic illustration of P-SiP. (B and C) Chemical structures of the components of the nematic LC mixture (B) and an azobenzene compound (C).

Table 2-1. $M_{w,graft}$ of grafted polymer chains and hydrodynamic diameters D_h of P-SiPs.

	P-SiP (22k)	P-SiP (52k)	P-SiP (118k)	P-SiP (248k)	P-SiP (600k)
$M_{w,graft}$/g mol^{-1}	22,000	52,000	118,000	248,000	600,000
D_h/nm	212	360	470	647	863

2-2-2 Methods

Preparation of composite gels

A toluene dispersion of each P-SiP and LCs (ZLI-1083 or azo-doped ZLI-1083 containing 5 mol% of BMAB) was prepared in a glass vial, and toluene was evaporated under reduced pressure at 60–70 °C. The resulting composite was subsequently heated at 120 °C and vigorously mixed, and the composite exhibited a sol state. The composite was then cooled to 25 °C to induce the formation of a gel state. Each composite gel was stored overnight at 25 °C before each experiment was performed.

Scanning electron microscopy

A xerogel was prepared by removing ZLI-1083 from a composite gel consisting of P-SiP (118k). The removal of ZLI-1083 was achieved by soaking the composite gel in hexane and drying repeatedly. The prepared xerogel was cut through and coated with 2-nm-sized Pt–Pd particles. The cutting plane of the xerogel was examined using a scanning electron microscope (SEM, S4300, Hitachi High-Technologies, Tokyo, Japan).

Optical microscopy

The optical textures of the P-SiP (118k)/ZLI-1083 composite gel were examined using an optical microscope (BX51, Olympus, Tokyo, Japan) in cross-polarized and bright-field modes. The cross-polarized mode was employed with a polarizer and an analyzer (the second polarizer)

to examine the textures below $T_{N–I}$. The phase-separation structures above $T_{N–I}$ were examined in the bright-field mode, in which the observation was performed without the analyzer. The composite gels were placed into evaluation cells with a gap thickness of 30 μm and no surface coating. The temperature was controlled using a hot stage (FP80 + FP82, Mettler-Toledo, Tokyo, Japan). To examine the gelation and formation process of the percolation networks in the composite, the optical microscope images were collected in the bright-field mode every 5 s following thermal quench to 107 °C from 114 °C.

A fast Fourier transformation (FFT) was applied to the microscope images using an FFT plug-in with ImageJ (National Institutes of Health, US).[10] To determine the structure factor ($S(q)$), the background FFT image was subtracted from each FFT image of the samples. Then, the obtained images were radially averaged (Figure 2-2). The background image was obtained by observation of a vacant cell. A Gaussian curve or a logarithmic normal distribution curve was fitted to $S(q)$ and the wavenumber q_{max} where the curve reached its maximum was determined.

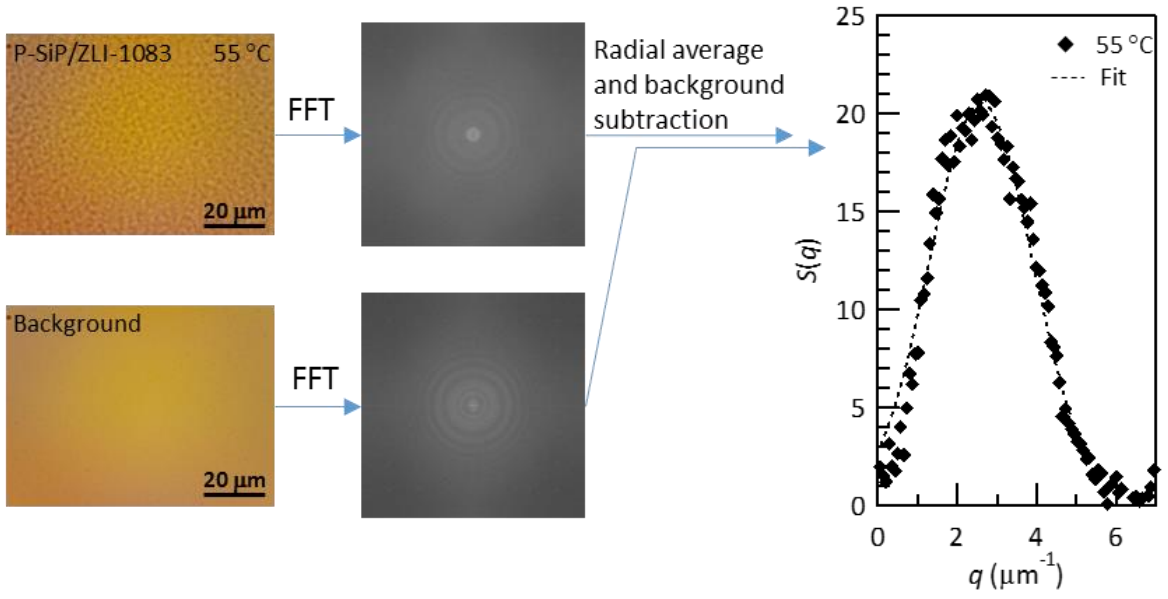

Figure 2-2. FFT analysis method for a micrograph of the P-SiP (118k)/ZLI-1083 composite gel.

Rheology

The fundamental viscoelastic parameters of the composite gels were determined using an advanced rheometric expansion system (ARES-RF, TA Instruments, US) with a parallel-plate type geometry (plate diameter = 25 mm). The measurements were performed with a controlled-strain amplitude. First, a P-SiP/ZLI-1083 composite gel was placed between plates and heated to a sol state. Then, the gap between the plates was adjusted to an appropriate value of 0.5–0.75 mm. After that, the composite gel was cooled to 25 °C. Each sample was maintained for 1.5 h at 25 °C, and the gap was readjusted to an appropriate value. Subsequently, each measurement was performed. The frequency and strain sweep measurements were performed at 25 °C. The temperature dependences of viscoelastic parameters were determined upon heating at a rate of 5 °C/min.

Differential scanning calorimetry

Thermal analyses of the P-SiP (248k)/ZLI-1083 composite gel (particle concentration = 20 wt%) and PMMA/ZLI-1083 blends were conducted using a differential scanning calorimeter (Q200, TA Instruments, USA). The PMMA/ZLI-1083 blends with different ZLI-1083 contents were prepared from an acetone solution of PMMA and ZLI-1083. After evaporation of acetone from the blends under reduced pressure at 60–70 °C, the blends were dried under vacuum at 80 °C for 5 h. The differential scanning calorimetry (DSC) measurements were conducted at scanning rates of +20 and −10 °C/min for the heating and cooling processes, respectively.

Transmittance measurement

The transmittance of the P-SiP (118k)/ZLI-1083 composite gel (particle concentration = 10 wt%) was measured to examine the optical property quantitatively. The composite placed into an evaluation cell (gap = 50 μm) at 120 °C and then cooled to room temperature. The intensity of white light passed through the cell (I) was measured with a photoreceiver (NEWFOCUS Model 2001, NewPort Corporation, US) and a photodetector (Model2000 Multimeter, Keithley Instruments, Inc., US) in the optical microscope with a parallel-polarized mode. The intensity of the light through an absolutely dark field (I_{dark}) was measured in the cross-polarized mode without the sample cell. The intensity of the incident light (I_0) was measured without the sample cell. The transmittance T at each temperature was calculated using the following equation:

$$T = (I - I_{dark})/(I_0 - I_{dark}). \quad (2\text{-}2)$$

Photoresponse of the composite gels

Photoinduced changes of optical properties of the azo-doped composite gel were at first qualitatively evaluated by macroscopic observation of the P-SiP (248k)/azo-doped ZLI-1083 composite (particle concentration = 10 wt%, [BMAB] = 5 mol% for ZLI-1083) film under the irradiation with UV light (wavelength = 365 nm, intensity = 100 mW/cm^2) in an oven (temperature = 45 °C). In order to obtain the films, the composite was heated to a temperature showing a sol state between the glass plates with a gap of 100 μm and cooled to room temperature. Then the glass plates were removed and the obtained gel film was cut into a rectangle (width ≈ 7 mm, length ≈ 5 mm, thickness ≈ 100 μm).

In a quantitative study of the photoinduced changes of the optical properties, the azo-doped composite gel was placed into an evaluation cell (gap = 50 μm) at 120 °C and then cooled to room temperature. The measurements of I, I_{dark}, and I_0 mentioned above were performed in the parallel-polarized mode at 45.0 °C controlled by a hot stage (LK-600PH, LCP94/2, Linkam Scientific, UK) with and without the irradiation of the focused UV light (intensity = 500 mW/cm^2). The transmittance T was calculated using the Equation (2-2).

Photoinduced changes in rheological parameters of azo-doped composite gels were measured using a rheometer (MCR302, Anton-Paar Japan, Tokyo, Japan) with a parallel-plate type geometry (plate diameter = 12 mm) and a transparent quartz stage. An azo-doped composite gel placed between plates was heated to a temperature showing a sol state and the gap between the plates was adjusted to an appropriate value. Next, the composite gel was cooled to room temperature and left for 1.5 h. Subsequently, the composite gel was heated to 48 °C, and the gap was readjusted to 0.2 mm. The measurement was performed at fixed strain = 0.1%, fixed frequency = 1 Hz, and constant temperature = 48 °C with and without irradiation of the UV light (intensity = 150 mW/cm^2).

2-3 Results and discussion

2-3-1 Gel formation in P-SiP/ZLI-1083 composites

The P-SiP (118k)/ZLI-1083 composite (particle concentration = 10 wt%) exhibited a stable gel state and self-supporting ability at room temperature (Figure 2-3A). The ZLI-1083 in the composite gel was confirmed to exhibit a liquid-crystalline nature at 25 °C by observation in the polarized optical microscope (Figure 2-3B). The disturbed optical texture indicates that the surface of P-SiPs affects LC alignment. However, we speculate that the surface of P-SiPs could not induce the specific LC alignment because of the random-coil like conformation of the grafted PMMA chains on the silica core.[8] In the composite gel, ZLI-0183 exhibited $T_{N–I}$ at 52.2 °C, which was almost identical to that of pure ZLI-1083 (52.4 °C). Figure 2-3C presents an SEM image of a xerogel of the composite gel. The P-SiP aggregates form a sponge-like structure that would contribute to the solid-like nature of the P-SiP/ZLI-1083 composites. Interestingly, there was no significant shrinkage of the composite gel even after removing the ZLI-1083. Thus, a xerogel was successfully produced from the composite gel. To the contrary, a xerogel could not be prepared from the particle/LC composite gels in previous reports[6, 11] because of the collapse of particle assemblies caused by the removal of the LC matrices. Therefore, the inner structures of the P-SiP/ZLI-1083 composite gels would be firmly supported by the inter-particle entanglements of the PMMA chains of P-SiPs. The length of the grafted PMMA chains would be long enough to form the entanglements of the polymer chains (molecular weight of grafted PMMA chain was 118,000 g mol^{-1}).

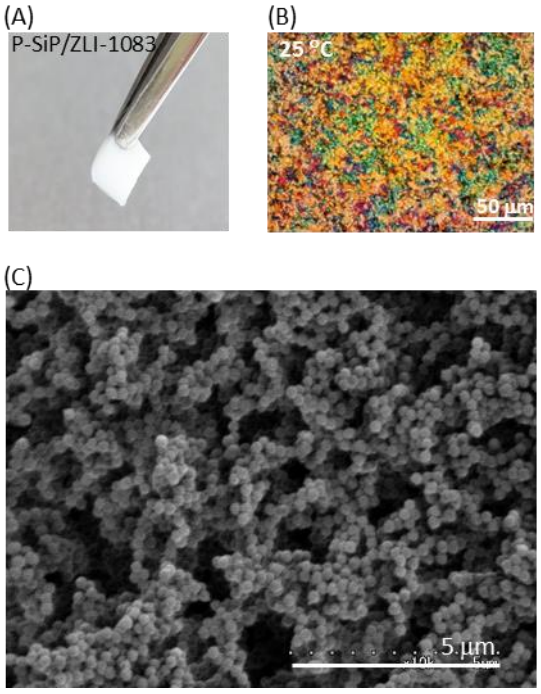

Figure 2-3. (A) Photograph and (B) optical texture of P-SiP (118k)/ZLI-1083 composite gel (particle concentration = 10 wt%) in cross-polarized mode at 25 °C. (C) SEM image of a xerogel prepared from the P-SiP (118k)/ZLI-1083 composite gel.

2-3-2 Viscoelastic properties of P-SiP/ZLI-1083 composites

The dynamic viscoelastic properties of the P-SiP (118k)/ZLI-1083 composite gel (particle concentration = 10 wt%) were examined using the rheometer with a parallel-plate type geometry. Figure 2-4A shows the strain dependence of the storage (G') and loss (G'') moduli of the composite gel (frequency = 1 Hz; temperature = 25 °C). Both moduli had a plateau in the strain region below approximately 1%, indicating that the stress and strain exhibited a linear relation in this region. Frequency and temperature sweep tests were therefore performed at strains below 1%. The frequency sweep test indicated that the P-SiP (118k)/ZLI-1083 composite gel exhibited elastic responses over a broad range of frequency at 25°C, where G' was larger than G'' (Figure 2-4B). As typical values, G' and G'' at the frequency of 1 Hz were 2.8×10^5 and 8.2×10^4 Pa, respectively. G' was ten times higher than the value previously reported for composite gels consisting of polymeric particles without grafted polymers and ZLI-1083.[6] The high moduli of the P-SiP (118k)/ZLI-1083 composite gel resulted from the inner structures reinforced by inter-particle entanglements of the grafted PMMA chains.

The temperature dependences of the viscoelastic parameters were also investigated for the P-SiP (118k)/ZLI-1083 composite. Figure 2-4C presents the G', G'', and loss tangent ($\tan\delta$) values measured as a function of temperature in a heating process at +5 °C/min. Although the majority of previously-reported particle/LC composite gels in which the particles had no grafted polymers exhibited only one gel state,[3-6, 11] the P-SiP (118k)/ZLI-1083 composite exhibited two gel states with distinct elastic moduli. One state is a hard gel state (G_H state) with G' of over 10^4 Pa observed in the temperature region below approximately 65 °C. The other state is a soft gel state (G_S state) with G' of approximately 10^3 Pa observed in the temperature region between 65 and 110 °C. At temperatures above 110 °C, the G_S state transformed into a sol (S) state. We estimate the G_H–G_S and Gs–S transition points ($T_{G_H–G_S}$ and $T_{G_S–S}$) to be 65 and 110 °C, respectively, from the peak of $\tan\delta$ and rapid drop of the moduli. Similar temperature dependences of the viscoelastic parameters were also confirmed in a cooling process (Figure 2-5).

As mentioned above, particle/LC composite gels previously reported usually exhibited only one gel state.[3-6] The gel–sol transition points of the composites were identical to $T_{N–I}$ of their matrices. However, in the present P-SiP (118k)/ZLI-1083 composite, $T_{G_H–G_S}$ (65°C) and $T_{G_S–S}$ (110°C) do not coincide with $T_{N–I}$ (52.2°C) of ZLI-1083. Therefore, the mechanism of gel formation in the P-

SiP/ZLI-1083 composites is different from that of previous composites. In the following sections, we will discuss the G_H–G_S transition, G_S–S transition, and gelation mechanism in detail.

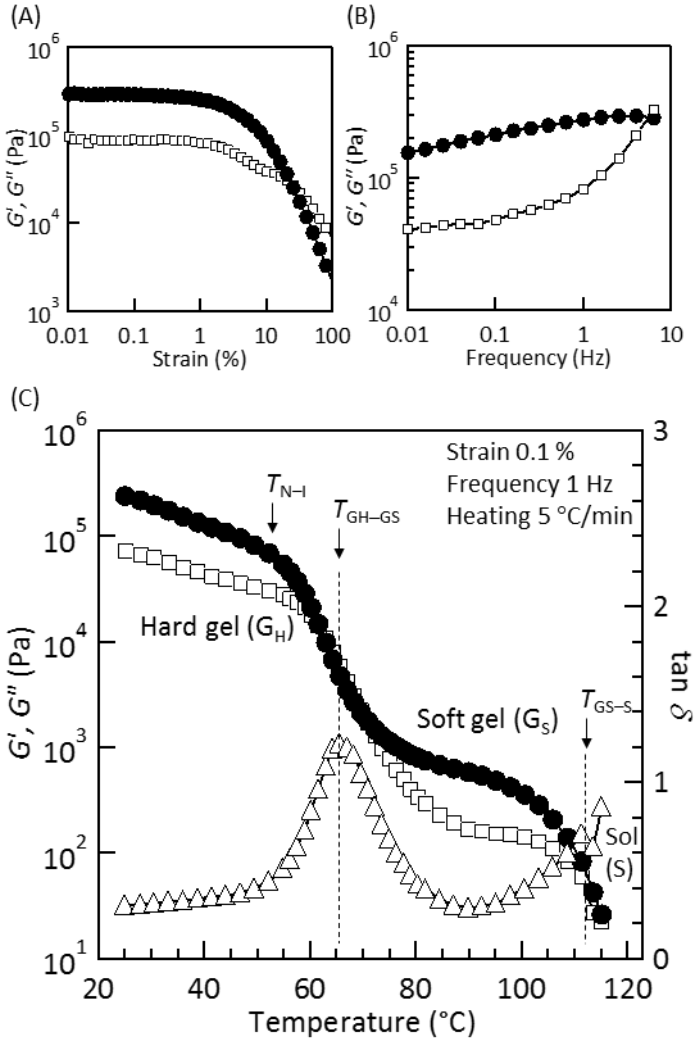

Figure 2-4. (A) G' (circle) and G'' (square) of P-SiP (118k)/ZLI-1083 composite gel (particle concentration = 10 wt%) as a function of the applied strain at a frequency of 1 Hz and 25 °C. (B) G' (circle) and G'' (square) of the composite gel as a function of the frequency at a strain of 0.1 % and 25 °C. (C) Temperature dependence of G' (circle) and G'' (square) and $\tan\delta$ (triangle) of the composite gel with heating at a rate of 5 °C/min.

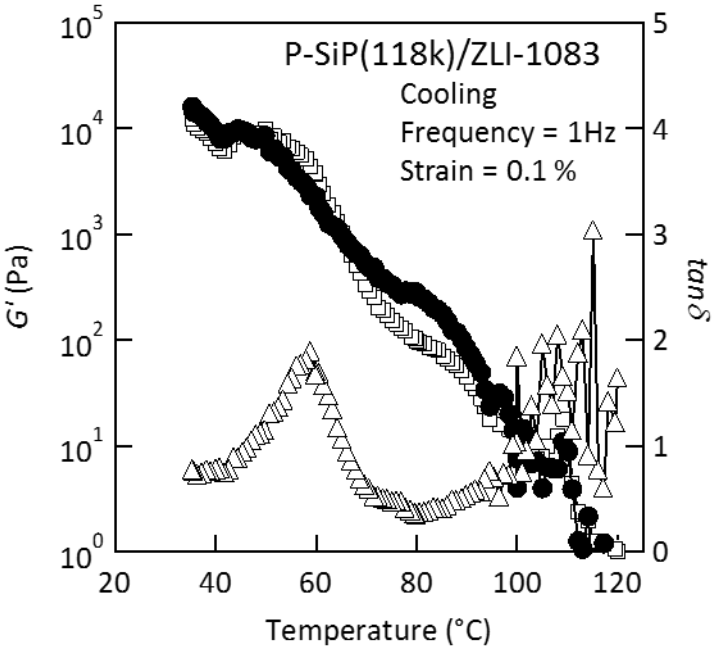

Figure 2-5. Temperature dependence of G' (circles), G'' (squares), and tanδ (triangles) of P-SiP(118k)/ZLI-1083 in a cooling process (−5 °C/min). P-SiP concentration = 10 wt%.

2-3-3 G_S–S transition of the composites: changes of microstructures

The microstructures of the P-SiP (118k)/ZLI-1083 composite gel (particle concentration = 10 wt%) were examined with the bright-field mode in an optical microscope (Figure 2-6). During the heating process, heterogeneous textures were observed until 110 °C (Figure 2-6A–C). These images originate from the percolation network structures formed with P-SiPs. The FFT analysis was conducted on the optical microscope images of the P-SiP (118k)/ZLI-1083 composite gel collected at 55–110 °C. Figure 2-6E plots $S(q)$ as a function of q. The profiles of $S(q)$ obtained at 55–105 °C have a distinct peak at approximately 2.6 μm^{-1}. The peak indicates the existence of periodic microstructures in the micrographs. As observed in Figure 2-6F, the value of q where $S(q)$ reached its maximum (q_{max}) was almost constant, approximately 2.6 μm^{-1}, in the range 55–105 °C, indicating that contours of the microstructures exhibited no significant changes in this temperature region.

The heterogeneous texture slowly disappeared at 110 °C (Figure 2-6D). The change in the optical texture indicates that the percolation network structures of P-SiPs collapsed above 110 °C. This temperature agrees well with the $T_{G_S–S}$ of the P-SiP/ZLI-1083 composite. Here, a solubility test of PMMA in ZLI-1083 was performed to discuss the cause of the collapse of the percolation structures (Figure 2-7). A dilute PMMA/ZLI-1083 blend became a cloudy state and produced precipitations below approximately 110 °C in the cooling process. The cloudy state did not result from the phase transition of ZLI-1083 ($T_{N–I}$ = 52.4 °C) but from the formation of small aggregations of PMMA in the isotropic ZLI-1083. The aggregation can be explained by a phase separation triggered by the thermodynamic instability of polymer/LC systems.[12-14] Consequently, we can conclude that the origins of the G_S–S transition of the P-SiP/ZLI-1083 composites are the collapse of the percolation network structures because of the solubilization of the grafted PMMA of P-SiPs with ZLI-1083 above 110 °C.

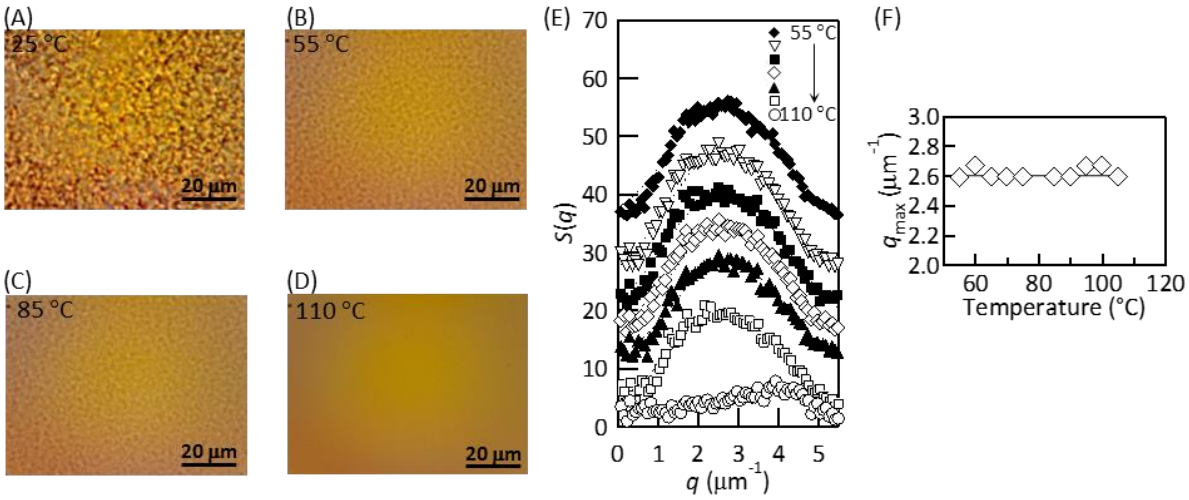

Figure 2-6. (A–D) Optical micrographs of P-SiP (118k)/ZLI-1083 composite gel (particle concentration = 10 wt%) in bright-field mode. (E) $S(q)$ values obtained by FFT analyses of the optical micrographs as a function of wavenumber (q). A certain value was added to the $S(q)$ values to overlay the plots. (F) The wavenumber where $S(q)$ became maximum (q_{max}) in the range 55–105 °C.

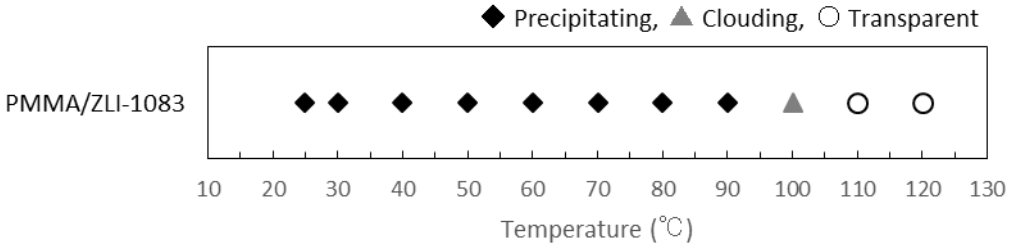

Figure 2-7. Results of visual observations in a dilute PMMA/ZLI-1083 blend upon cooling. M_w of the PMMA was 102000, and the PMMA concentration was 1 wt%.

2-3-4 G_H–G_S transition of the composites: glass–rubber transition of the grafted PMMA

To discuss the G_H–G_S transition of the composites, let us pay attention to the dynamics of the grafted PMMA of P-SiP in the composites. Figure 2-8A shows the result of DSC measurements of PMMA/ZLI-1083 blends with different LC contents as model systems. The conventional PMMA was employed because excessively concentrated P-SiPs easily caused a colloidal crystallization in the composites. In the following paragraphs, the DSC results are described referring to traces in heating runs.

In the blends with LC contents up to 30 wt%, only a step-like shift of the heat flow due to the glass transition (softening to a rubbery state) of PMMA was observed. However, the nematic–isotropic phase transition of ZLI-1083 was not detected. This finding implies that ZLI-1083 was homogeneously mixed with PMMA. Therefore, ZLI-1083 did not exhibit a liquid-crystalline nature macroscopically in these blends. T_g was determined as the center point of the sigmoidal change in the DSC trace. T_g of PMMA in these blends decreased from 103.1 to 59.6 °C as the LC content increased from 0 to 30 wt% (Figure 2-8B). The decrease in T_g clearly indicates that ZLI-1083 acts as a plasticizer for PMMA, similarly to previous reports on several polymer/LC blends.[13-16] However, endothermic peaks due to the nematic–isotropic phase transition of ZLI-1083 appeared at approximately 52 °C in the blends with LC contents of 40 and 50 wt%. These blends consist of PMMA saturated with ZLI-1083 (PMMA phase), and the excess ZLI-1083 separated from the PMMA phase. Although the step-like shifts were not clearly observed due to superposition with the phase transition of ZLI-1083, the gradual decline of the trace from 60 to 80 °C would be assignable to the glass transition of the PMMA saturated with ZLI-1083. Therefore, T_g of PMMA saturated with ZLI-1083 was roughly estimated to be approximately 60 °C.

Figure 2-8C presents DSC traces of the P-SiP (248k)/ZLI-1083 composite gel (particle concentration = 20 wt%) and pure ZLI-1083. The baseline of the DSC trace of the composite gel decreases to some extent above the phase-transition point of ZLI-1083 compared with that of "pure" ZLI-1083. This would imply the occurrence of the glass transition of the grafted PMMA around 60 °C, because the glass transition of grafted PMMA overlaps with the phase transition of ZLI-1083 in the composite. Dang et al. reported T_g values of polystyrene grafted on silica particles (diameter of the core = 120 nm, graft density = 0.5–0.7 nm^{-2}, and degree of polymerization = 130–2000).[17] The T_g values of the grafted polymers with different molecular weights were not

significantly different from that of a linear polymer with high enough degree of polymerization (the differences in T_g are smaller than ±5 °C). Therefore, the grafted PMMA of P-SiP(248k) and P-SiP(118k) (employed for the rheological analyses in Figure 2-4) would have T_g of approximately 60 °C in the composite gels. The glass transition (softening to a rubbery state) of grafted PMMA will cause the softening of the network formed with P-SiPs, resulting in the decrease of the elastic moduli of the P-SiP/ZLI-1083 composites. Consequently, the transition between G_H and G_S states of the P-SiP/ZLI-1083 composite gels ($T_{G_H-G_S}$ = 65 °C) arises from the glass transition of the grafted PMMA of P-SiPs saturated with ZLI-1083.

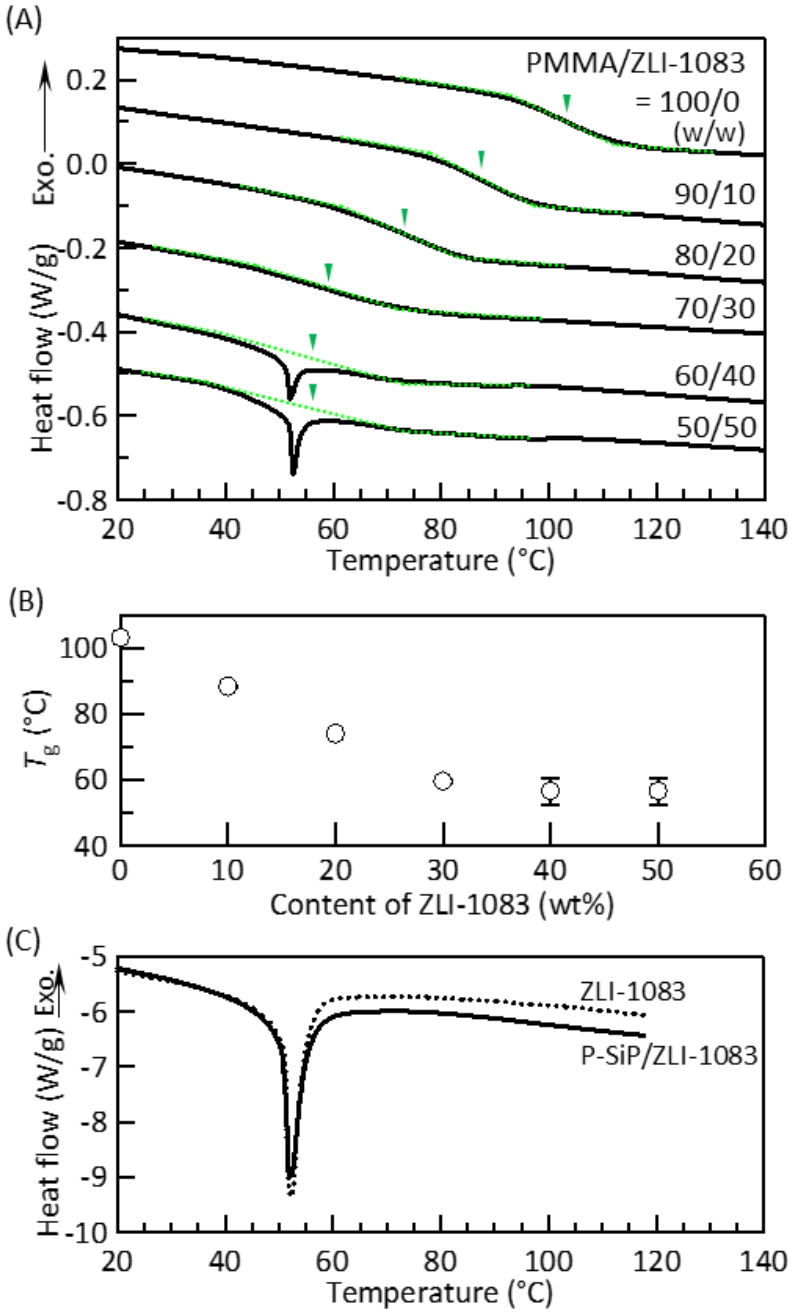

Figure 2-8. (A) DSC traces of PMMA/ZLI-1083 blends with different ZLI-1083 contents in heating runs. The signals were shifted to avoid overlaps. The T_g values are indicated by down-pointing triangles. (B) Dependence of T_g on the ZLI-1083 content in the PMMA/ZLI-1083 blends. (C) DSC traces of P-SiP (248k)/ZLI-1083 composite gel (particle concentration = 20 wt%) (solid line) and ZLI-1083 (dashed line) in heating runs. The traces were shifted to fit each other in the temperature region below the phase transition of ZLI-1083.

2-3-5 Gelation mechanism in P-SiP/ZLI-1083 composites

To discuss the gelation mechanism of P-SiP/ZLI-1083 composites in detail, the rheological and microscopic properties of the P-SiP (118k)/ZLI-1083 composite (particle concentration = 10 wt%) were investigated in a cooling process. Upon cooling, the composites exhibited a rapid increase in G' and turned into the G_S state from the S state around 110 °C (Figure 2-5), at which the heterogeneous microstructures appeared. Hence, the gel state was formed even in the isotropic phase of ZLI-1083 ($T_{N–I}$ = 52.2 °C). As mentioned above, the PMMA/ZLI-1083 blend was in a phase-separated state below 110 °C due to the thermodynamic instability of the homogeneously mixed state. Therefore, the formation of the heterogeneous structures in the composites will be caused by the phase separation of P-SiPs and ZLI-1083.

We infer that the gelation mechanism in P-SiP/ZLI-1083 composites is essentially the same as that reported by Bukusoglu et al.[10] They revealed that the particle networks were formed by the spinodal decomposition of a colloidal dispersion in the isotropic phase of LCs. Following after the previous report, the formation process of the percolation networks was examined in the P-SiP (118k)/ZLI-1083 composite using FFT analyses of bright-field optical microscopy images (Figure 2-9). The images were collected every 5 s after the thermal quench of the composite to 107 °C from 114 °C, and treated by FFT. The heterogeneous microstructures were found to form within 20 s after the thermal quench. These microstructures were bicontinuous structures which would be often developed via spinodal decomposition. Although this growing rate was quite faster than that previously reported (8 min),[10] it was comparable to that of PMMA/LC blends (10 s)[13]. The q_{max}, which corresponds to the inverse of the lateral size of the periodic structures in the images, showed a constant value in the initial stage of the growth of the heterogeneous microstructures. This behavior agrees with the prediction by Cahn-Hilliard theory[18-19] for spinodal decomposition. Thus the P-SiP/ZLI-1083 composites were gelated by the formation of network structures with P-SiPs in the isotropic phase owing to the phase separation based on the spinodal process.

In the colloid/LC gels previously reported,[10] the elastic moduli rapidly increased at $T_{N–I}$ of employed LCs and gradually increased in a nematic phase by cooling. An increase in the concentration of colloids in a colloid-rich continuous phase was responsible for the growth of the mechanical properties. On the other hand, in this study, P-SiP/ZLI-1083 composites exhibited the steep increase in G' between 80 and 55 °C (G_S–G_H transition), though the microstructures hardly changed in this temperature range (Figure 2-10). It is, therefore, difficult to explain the significant

growth in the mechanical properties at the G_S–G_H transition only by the increase in the concentration of P-SiPs in a P-SiP-rich phase. At present, the stiffening of the network structures formed by P-SiPs by the glass transition of the grafted PMMA of P-SiPs is considered to contribute to the significant change in the mechanical properties at G_S–G_H transition.

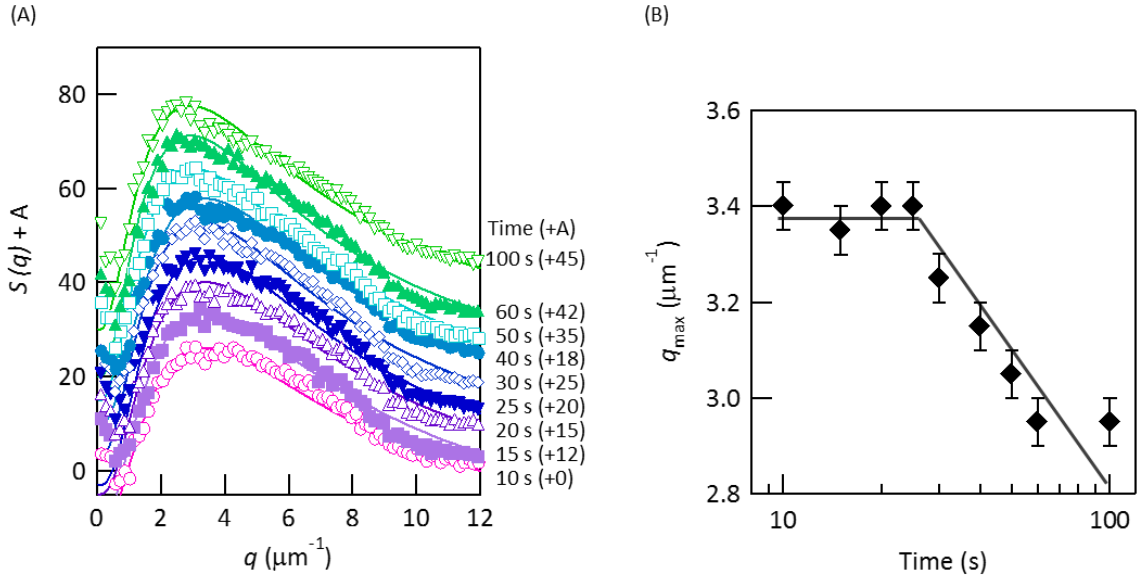

Figure 2-9. (A) Structure factor $S(q)$ with time following the thermal quench from 114 °C to 107 °C as a function of q. (B) Change in the structural peak position q_{max} with the time.

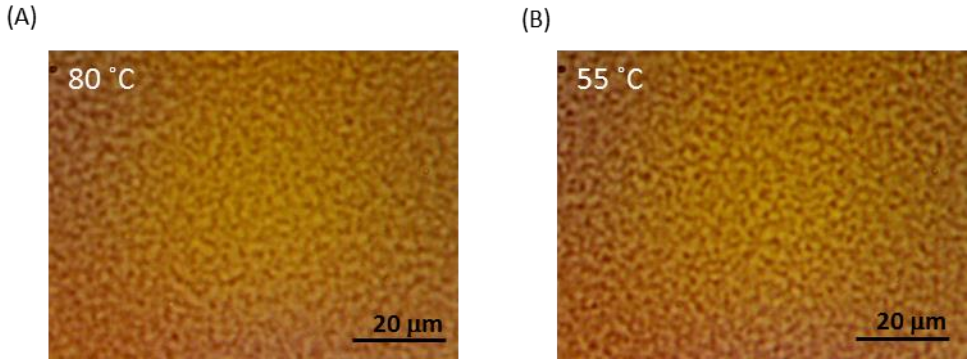

Figure 2-10. (A and B) Optical micrographs of the P-SiP (118k)/ZLI-1083 composite gel (particle concentration = 10 wt%) in a cooling process at 1 °C/min.

2-3-6 Three gel states in P-SiP/LC composites

Figure 2-11 summarizes the viscoelastic and optical properties of the P-SiP/ZLI-1083 composites. The composites exhibited two different optical states (opaque and translucent) in the G_H state depending on the phase structures of the LC matrix. The thermal changes of the transparency were quantitatively examined in the P-SiP (118k)/ZLI-1083 composite film with a thickness of 50 μm (Figure 2-12). Although the transmittance was approximately 0.2 at 25 °C, the value steeply increased at 52 °C, which is $T_{N–I}$ of ZLI-1083, and surpassed 0.95.This change can be simply rationalized in terms of the matching of refractive indices between ZLI-1083 and P-SiPs: the opaque state is due to the mismatching between the P-SiPs ($n_p \approx 1.48$)[7] and ZLI-1083 (n_e = 1.6123, n_o =1.4905) in the nematic phase, whereas the transparent state is due to better matching between the P-SiPs and ZLI-1083 ($n_i \approx 1.5$) in the isotropic phase. Then, the transparent G_S state appeared above the G_H–G_S transition point. Finally, upon the G_S–S transition, the translucent G_S state transforms into the S state. Consequently, the P-SiP/ZLI-1083 composite exhibits three gel states (opaque G_H, transparent G_H, and transparent G_S) depending on temperature. In the composites, although the optical properties of the G_H state were changed by the phase structures of the ZLI-1083 matrices, the mechanical properties were hardly affected because the contribution of the nematic elasticity of the matrices was quite small.[10] Although multiple gel states have been observed in hydrogels using triblock copolymers,[20] the composites studied in this study will be the first example of liquid-crystalline physical gels exhibiting three gel states with distinct viscoelastic and/or optical properties.

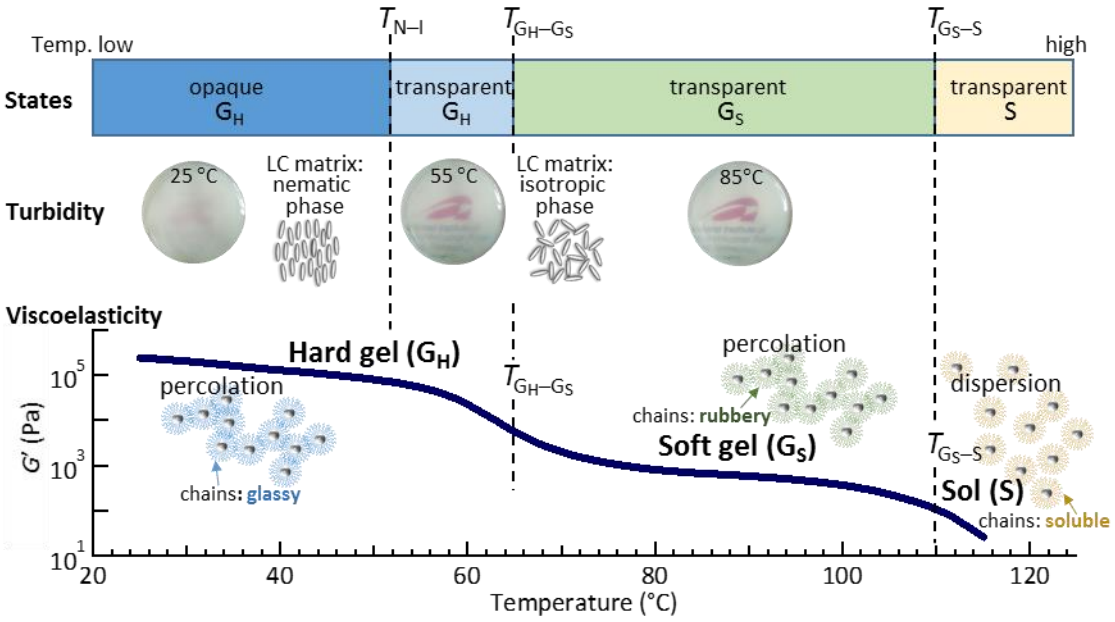

Figure 2-11. Summary of viscoelastic and optical properties of P-SiP/ZLI-1083 composites.

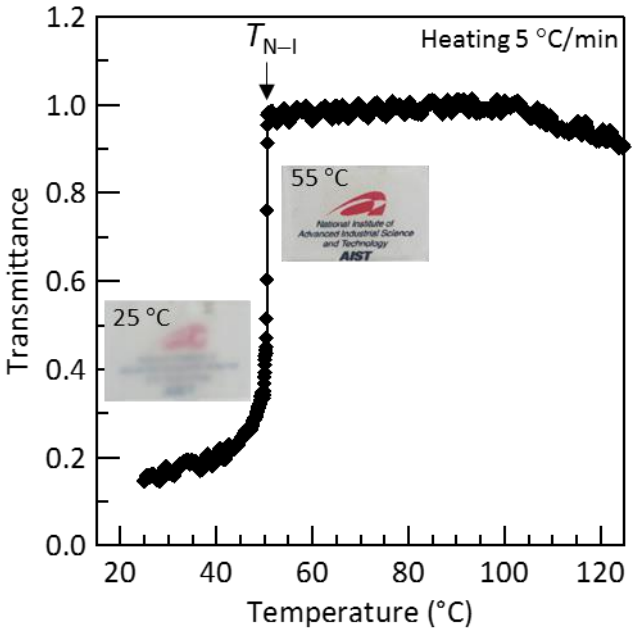

Figure 2-12. Temperature dependence of the transmittance of light through the P-SiP (118k)/ZLI-1083 composite gel with a thickness of 50 μm. The inset photographs of the gel were taken at 25 and 55 °C.

2-3-7 Effects of particle concentration and molecular weight of grafted PMMA chains on the viscoelastic properties

Figure 2-13A shows G' at frequency = 1 Hz of the P-SiP (118k)/ZLI-1083 composite gels as a function of particle concentration at 25 °C. G' monotonically increased with increasing the P-SiP concentration. Notably, the thermal stability of the composite gel was significantly affected by the P-SiP concentration. At 5 wt%, the composite exhibited only one gel state, and the gel state transformed into the sol state above 60 °C (Figure 2-13B). As confirmed by SEM examination (Figure 2-14), the particles formed percolation structures at room temperature even at this concentration. However, the cavity size of the percolation structures of the composite containing 5 wt% P-SiP was larger than that of the composite containing 10 wt% P-SiP. The microstructures with large voids will be easily dismantled when the dynamics of P-SiPs become more active due to the softening of the grafted PMMA above 60 °C.

The molecular weight of the grafted PMMA chains also had significant effects on the viscoelastic properties of the P-SiP/ZLI-1083 composites. In Figure 2-13C, G' of the composites (particle concentration = 10 wt%) at 1 Hz and 25 °C was plotted as a function of the molecular weight of the grafted PMMA of P-SiP. Only the P-SiP (22k)/ZLI-1083 composite exhibited a low G' value of approximately 6×10^3 Pa; in contrast, the other composites exhibited high G' values of the order of 10^5 Pa. Figure 2-15 shows the effective graft density (σ_{eff}) on the outermost surface of the series of P-SiPs. The σ_{eff} were calculated using Equation (2-1) (σ_0 = 0.6 chains/nm^2, D_0 = 130 nm, the D_{h} of the P-SiPs in Table 2-1 were used as D). The σ_{eff} increases with decreasing the molecular weight of the graft PMMA $M_{\text{w,graft}}$. Indeed, σ_{eff} of P-SiP (22k) is more than three times higher than that of the other P-SiPs with longer grafted chains. For P-SiP (22k), the grafted polymers would not deeply interpenetrate each other between the particles, resulting in insufficient inter-particle entanglements. Therefore, the P-SiP (22k)/ZLI-1083 composite exhibited inferior thermal stability as well as lower viscoelastic properties compared with the other composites (Figure 2-13D).

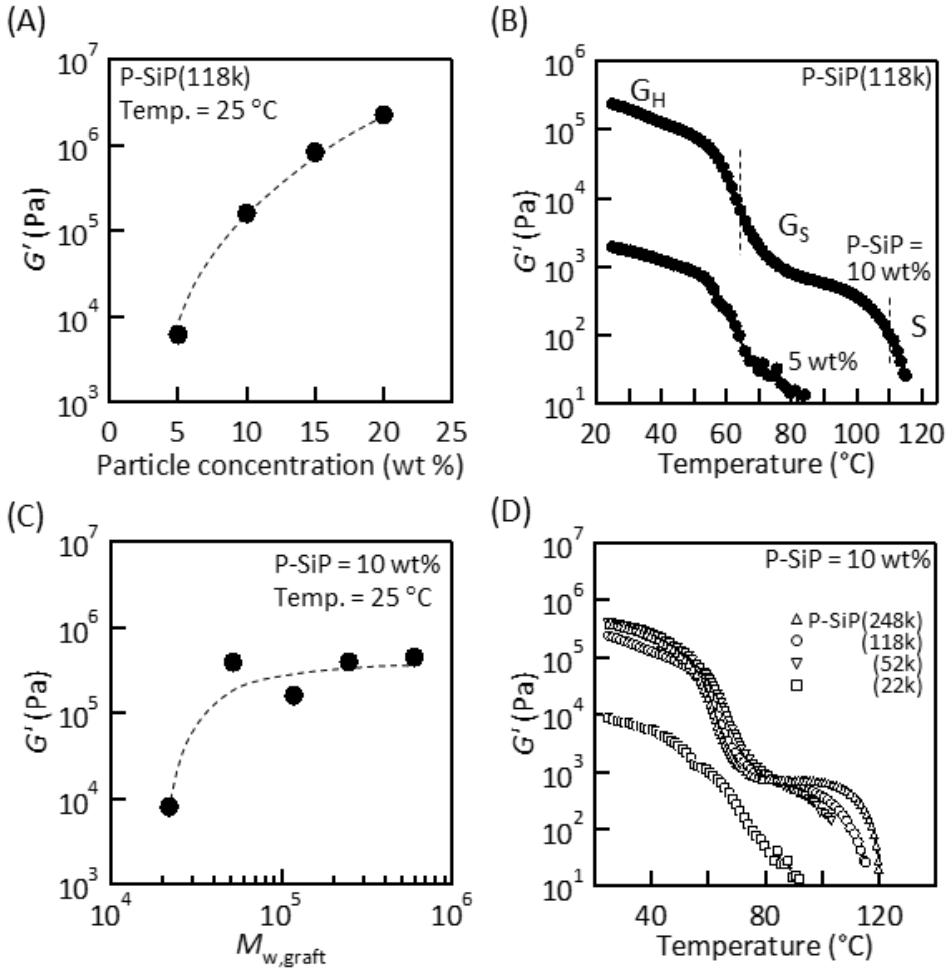

Figure 2-13. Dependence of P-SiP concentration on G' at 25 °C (A) and temperature sweep curves (B) of P-SiP (118k)/ZLI-1083 composite gels at a frequency of 1 Hz and strain in the linear region. Effects of the molecular weight of grafted PMMA ($M_{w,graft}$) on G' at 25 °C (C) and temperature sweep curves (D) of P-SiP/ZLI-1083 composite gels (particle concentration = 10 wt%).

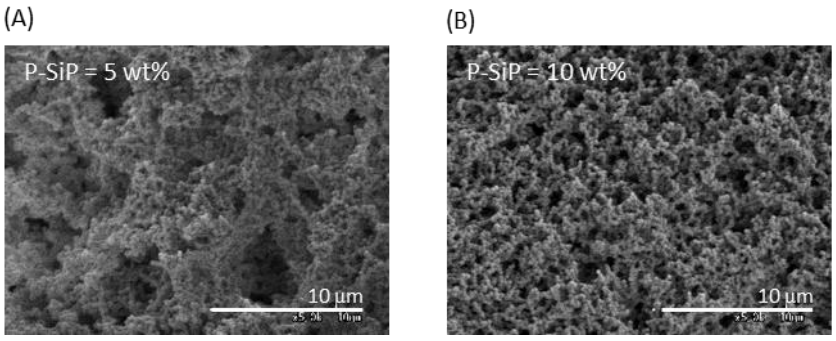

Figure 2-14. SEM images of xerogels prepared from the P-SiP(118k)/ZLI-1083 composite gels with particle concentration of (A) 5 wt% and (B) 10 wt%.

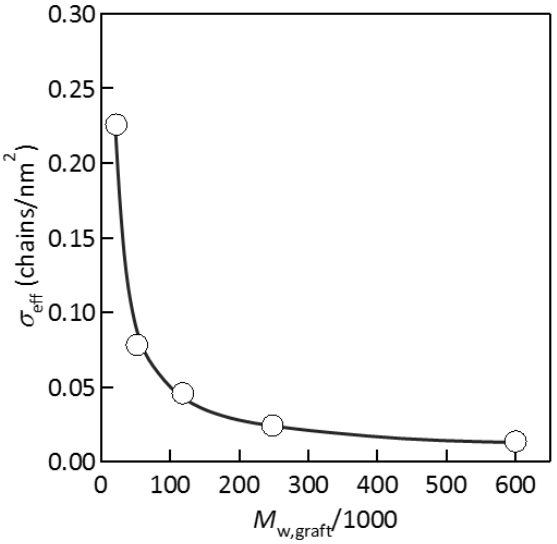

Figure 2-15. σ_{eff} on the outermost surface of P-SiPs with different $M_{w,graft}$ values.

2-3-8 Photochemical switching of the transparency of P-SiP/azo-doped ZLI-1083 composites

Finally, the application of P-SiP/ZLI-1083 composite gels to self-supporting photonic materials was investigated by the addition of the azobenzene compound shown in Figure 2-1(C). As shown in Figure 2-16A, in the initial state, the self-supporting gel film (width ≈ 7 mm, length ≈ 5 mm, thickness ≈ 100 μm) composed of P-SiP (248k) and azo-doped ZLI-1083 was opaque and showed the mechanical strength high enough for picking up with tweezers. Then, upon the irradiation of UV light (wavelength = 365 nm, intensity = 100 mW/cm^2) at 45 °C where the azo-doped ZLI-1083 showed a nematic phase ($T_{N–I}$ = 51.7 °C), the film immediately turned into a transparent state without any changes in the shape of the film (Figure 2-16B). The transmittance of the composite film with a thickness of 50 μm was changed from 0.3 into 0.9 upon the UV-light irradiation at 45°C (Figure 2-16C). The viscoelastic properties of the composite gel were also examined before and after the UV-light irradiation (wavelength = 365 nm, intensity = 150 mW/cm^2) at 48 °C (Figure 2-16D). The G' was 9.8×10^4 Pa and 4.9×10^4 Pa before and after irradiation with the UV light for 15 min, respectively. Although the G' was slightly reduced upon the UV-light irradiation, we confirmed that the P-SiP/azo-doped ZLI-1083 composite gel was still in the G_H state after the UV irradiation. Therefore, the opaque G_H–transparent G_H transition was achieved by not only the thermal manner but also the photochemical one. The photochemical change in the optical property of the composite film is ascribed to the photochemical N–I phase transition of the azo-doped matrix in the same way as shown in the previous study in which the photonic control has been performed in sandwiched cells.[21] It is emphasized here that we fabricated the similar photonic materials based on the self-supporting films.

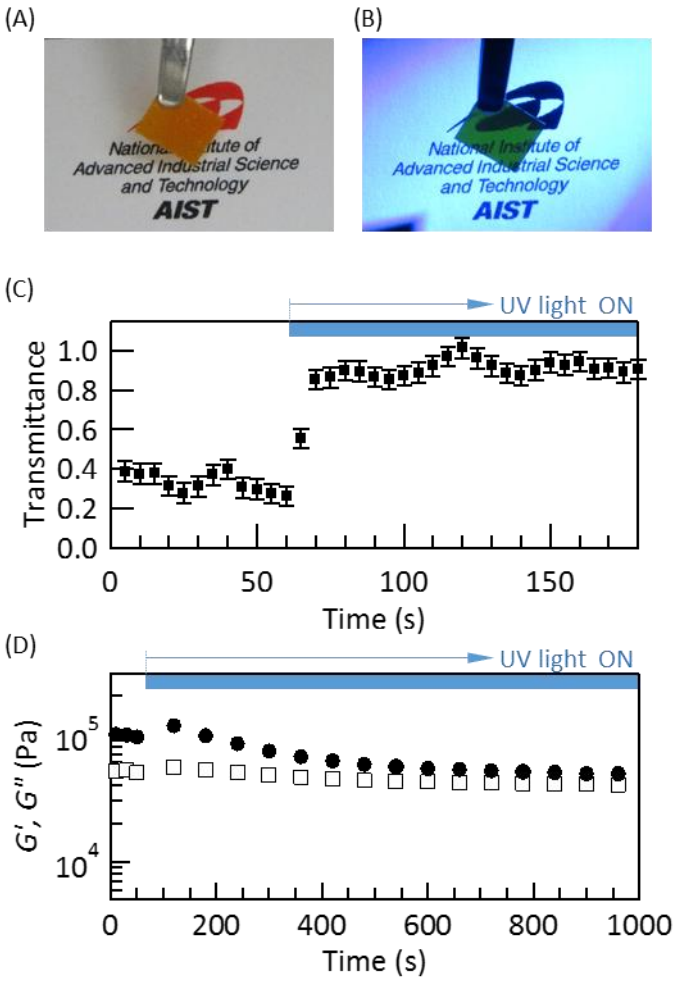

Figure 2-16. (A and B) Photographs of P-SiP (248k)/azo-doped ZLI-1083 composite gel films (particle concentration = 10 wt%, [BMAB] = 5 mol%, width ≈ 7 mm, length ≈ 5 mm, and thickness ≈ 100 μm) picked up with the tweezers at 45 °C without (A) and with (B) UV irradiation for 30s (wavelength = 365 nm, intensity = 100 mW/cm^2). (C) Change in the transmittance of white light passed through the azo-doped composite in a sandwiched cell (cell gap = 50 μm) at 45 °C by irradiating with the UV light (wavelength = 365 nm, intensity = 150 mW/cm^2). (D) Change in rheological parameters of G' (circles) and G'' (squares) of the azo-doped composite (gap = 200 μm, frequency = 1 Hz, strain = 0.1 %, temperature = 48 °C) upon UV irradiation (wavelength = 365 nm, intensity = 150 mW/cm^2).

2-4 Conclusion

In this chapter, the viscoelastic and optical properties of P-SiP/LC composite gels were extensively investigated. The G_H–G_S and G_S–S transitions were confirmed in the viscoelastic measurements of the composite gels. The optical microscope observations suggested that the G_S–S transition was due to the collapse of the percolation network structures of P-SiP in the composite, in which the grafted polymers simultaneously became soluble in the matrices. Thermal analyses clarified that the transition between G_H and G_S was derived from the glass transition of the grafted polymers of P-SiP. Moreover, the transparency of the composites changed with the phase of the LC matrix. Consequently, the composites exhibited three gel states (opaque G_H, transparent G_H, and transparent G_S) with distinct viscoelastic and/or optical properties depending on the liquid crystallinity and polymer dynamics. The viscoelastic properties of the composite gels were tunable in a wide range of *G'* from 10^2 to over 10^6 Pa through controlling the temperature, concentration of P-SiP, and molecular weight of the grafted PMMA. It was revealed that the gelation resulted from the construction of the percolation networks of P-SiPs in the isotropic LC matrix by the phase separation of P-SiPs and the matrix based on the spinodal decomposition. Therefore, the transparent G_H and transparent G_S states were observed in the isotropic phase. Furthermore, we demonstrated the application of the composite gels to self-supporting photonic materials. By the addition of the azobenzene derivative into the LC matrix, the transparency of the composite gel could be controlled by photoinduced opaque G_H–transparent G_H transition based on the photochemical phase transition of the LC matrix. By the combination of properties of gels and LCs, the P-SiP/LC composite gels can be widely applied to not only the self-healing and photonic materials demonstrated in a series of our studies but also vibration-proof and sound-proof insulation materials[22] and cell culture media[23-24].

References to chapter 2

(1) Choi, M. C.; Kim, Y.; Ha, C. S. Polymers for Flexible Displays: From Material Selection to Device Applications. *Prog. Polym. Sci.* **2008,** *33* (6), 581-630.

(2) Baetens, R.; Jelle, B. P.; Gustavsen, A. Properties, Requirements and Possibilities of Smart Windows for Dynamic Daylight and Solar Energy Control in Buildings: A State-of-the-Art Review. *Sol. Energ. Mat. Sol. C.* **2010,** *94* (2), 87-105.

(3) Meeker, S. P.; Poon, W. C. K.; Crain, J.; Terentjev, E. M. Colloid-Liquid-Crystal Composites: An Unusual Soft Solid. *Phys. Rev. E* **2000,** *61* (6), R6083-R6086.

(4) Vollmer, D.; Hinze, G.; Ullrich, B.; Poon, W. C. K.; Cates, M. E.; Schofield, A. B. Formation of Self-Supporting Reversible Cellular Networks in Suspensions of Colloids and Liquid Crystals. *Langmuir* **2005,** *21* (11), 4921-4930.

(5) Wood, T. A.; Lintuvuori, J. S.; Schofield, A. B.; Marenduzzo, D.; Poon, W. C. K. A Self-Quenched Defect Glass in a Colloid-Nematic Liquid Crystal Composite. *Science* **2011,** *334* (6052), 79-83.

(6) Yamamoto, T.; Yoshida, M. Viscoelastic and Photoresponsive Properties of Microparticle/Liquid-Crystal Composite Gels: Tunable Mechanical Strength along with Rapid-Recovery Nature and Photochemical Surface Healing using an Azobenzene Dopant. *Langmuir* **2012,** *28* (22), 8463-8469.

(7) Ohno, K.; Morinaga, T.; Takeno, S.; Tsujii, Y.; Fukuda, T. Suspensions of Silica Particles Grafted with Concentrated Polymer Brush: A New Family of Colloidal Crystals. *Macromolecules* **2006,** *39* (3), 1245-1249.

(8) Ohno, K.; Morinaga, T.; Takeno, S.; Tsujii, Y.; Fukuda, T. Suspensions of Silica Particles Grafted with Concentrated Polymer Brush: Effects of Graft Chain Length on Brush Layer Thickness and Colloidal Crystallization. *Macromolecules* **2007,** *40* (25), 9143-9150.

(9) Tazuke, S.; Kurihara, S.; Ikeda, T. Amplified Image Recording in Liquid-Crystal Media by Means of Photochemically Triggered Phase-Transition. *Chem. Lett.* **1987,** (5), 911-914.

(10) Bukusoglu, E.; Pal, S. K.; de Pablo, J. J.; Abbott, N. L. Colloid-in-Liquid Crystal Gels Formed via Spinodal Decomposition. *Soft Matter* **2014,** *10* (10), 1602-1610.

(11) Yamamoto, T.; Kawata, Y.; Yoshida, M. Contrasting Roles of Layered Structures in the Molecular Assembly of Liquid Crystal Matrices on the Viscoelastic Properties of Microparticle/Liquid Crystal Composite Gels Leading to Rigidification and Destabilization. *J. Colloid. Interf. Sci.* **2013,** *397*, 131-136.

(12) Mucha, M. Polymer as an Important Component of Blends and Composites with Liquid Crystals. *Prog. Polym. Sci.* **2003,** *28* (5), 837-873.

(13) Ahn, W.; Kim, C. Y.; Kim, H.; Kim, S. C. Phase-Behavior of Polymer Liquid-Crystal Blends. *Macromolecules* **1992,** *25* (19), 5002-5007.

(14) Benmouna, F.; Daoudi, A.; Roussel, F.; Leclercq, L.; Buisine, J. M.; Coqueret, X.; Benmouna, M.; Ewen, B.; Maschke, U. Effect of Molecular Weight on the Phase Diagram and Thermal Properties of Poly(styrene)/8CB Mixtures. *Macromolecules* **2000,** *33* (3), 960-967.

(15) Huh, W. S.; Weiss, R. A.; Nicolais, L. Thermal and Rheological Properties of Blends of Polystyrene and Thermotropic Liquid-Crystals. *Polym. Eng. Sci.* **1983,** *23* (14), 779-783.

(16) Patwardhan, A. A.; Belfiore, L. A. Thermodynamic Miscibility of Polymer-Liquid Crystal Blends. *Polym. Eng. Sci.* **1988,** *28* (14), 916-925.

(17) Dang, A.; Hui, C. M.; Ferebee, R.; Kubiak, J.; Li, T. H.; Matyjaszewski, K.; Bockstaller, M. R. Thermal Properties of Particle Brush Materials: Effect of Polymer Graft Architecture

on the Glass Transition Temperature in Polymer-Grafted Colloidal Systems. *Macromol. Symp.* **2013,** *331* (1), 9-16.
(18) Cahn, J. W.; Hilliard, J. E. Free Energy of a Nonuniform System .1. Interfacial Free Energy. *J. Chem. Phys.* **1958,** *28* (2), 258-267.
(19) Cahn, J. W. Phase Separation by Spinodal Decomposition in Isotropic Systems. *J . Chem. Phys.* **1965,** *42* (1), 93-99.
(20) Park, M. J.; Char, K. Two Gel States of a PEO-PPO-PEO Triblock Copolymer Formed by Different Mechanisms. *Macromol. Rapid Commun.* **2002,** *23* (12), 688-692.
(21) Lee, H. K.; Kanazawa, A.; Shiono, T.; Ikeda, T.; Fujisawa, T.; Aizawa, M.; Lee, B. All-Optically Controllable Polymer Liquid Crystal Composite Films Containing the Azobenzene Liquid Crystal. *Chem. Mater.* **1998,** *10* (5), 1402-1407.
(22) Noda, Y.; Hayashi, Y.; Ito, K. From Topological Gels to Slide-Ring Materials. *J. Appl. Polym. Sci.* **2014,** *131* (15), 40509.
(23) Agarwal, A.; Huang, E.; Palecek, S.; Abbott, N. L. Optically Responsive and Mechanically Tunable Colloid-In-Liquid Crystal Gels that Support Growth of Fibroblasts. *Adv. Mater. (Weinheim, Ger.)* **2008,** *20* (24), 4804-4809.
(24) Lee, K. Y.; Mooney, D. J. Hydrogels for Tissue Engineering. *Chem. Rev. (Washington, DC, U. S.)* **2001,** *101* (7), 1869-1879.

Chapter 3

Photochemical Control of Elastic Modulus by Changing Network Stiffness

3-1 Introduction

Recently, gel materials of which mechanical properties can be controlled by the photoirradiation attract a great deal of attention owing to their potential for application to biomedical devices.[1-6] The photoinduced changes of the elastic modulus were previously reported through the structural changes of the inner networks formed with photodegradable[2-4] or photocrosslinkable[5-6] components. In these photoresponsive gels, the control of the elastic modulus has been performed only in an elastic-modulus range below approximately 10^4 Pa. On the other hand, as described in chapter 2, P-SiP/LC composites exhibited drastic changes of the elastic moduli by the temperature dependence of their network stiffness without the significant changes of their network structure.

The aim of this chapter is the photocontrol of the mechanical property on the basis of the photoinduced change in the stiffness of the inner networks. For this purpose, the photoresponsivity of the P-SiP/LC composites containing an azobenzene derivative is examined in detail. The photocontrol of the elastic modulus with the change of the network stiffness is carried out. To clarify the mechanism of the photoresponsivity of the P-SiP/azo-doped LC composites, the phase behavior of PMMA/azo-doped LC blends is investigated using the Flory-Huggins theory. In addition, the viscoelastic properties of the composites using the different host nematic LCs are studied in order to realize a sophisticated tuning of the physical properties.

3-2 Experimental Section

3-2-1 Materials

P-SiP(248k) is employed as particle components in this chapter. Details of the particles were described in chapter 2. Nematic LCs (7CB, 5CB, and ZLI-1083) shown in Figure 3-1A were purchased from Merck and used as supplied. BMAB (Figure 3-1B) and conventional PMMA (M_w = 102000, M_w/M_n = 2.1) were prepared as described in chapter 2. $T_{N–I}$ of 7CB, 5CB, ZLI-1083, and BMAB were determined to be 41.9, 35.5, 52.4, and 48.5 °C, respectively, by polarized optical microscopy.

3-2-2 Methods

Preparation of P-SiP/azo-doped LC composite gels

Azo-doped LCs were prepared by the addition of BMAB to each LC ([BMAB] = 5 or 10 mol%). Then, azo-doped LCs were heated at 60 °C to ensure homogeneous mixtures. A toluene dispersion of P-SiPs and the azo-doped LCs was weighed and mixed in a glass vial. The homogeneous dispersion was heated under reduced pressure at 60–70 °C to evaporate toluene. The resultant samples were vigorously mixed at 120 °C where the samples were in a sol state. Then, the samples were cooled to room temperature to form a gel state. All of gel samples used in this chapter were prepared at the P-SiP concentration of 10 wt%.

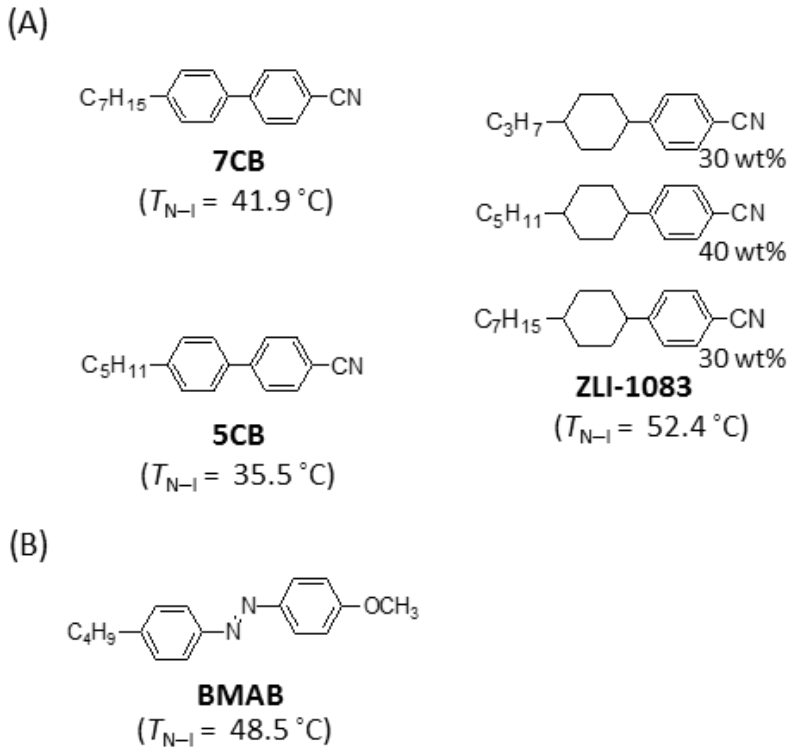

Figure 3-1. Chemical structures of LCs (A) and an azobenzene compound (B).

Rheology

Rheological parameters of the P-SiP/azo-doped LC gels were measured using the rheometer (MCR302, Anton-Paar Japan, Tokyo, Japan) with a parallel-plate type geometry (plate diameter = 12 mm) and a transparent quartz stage. The measurements were performed with a controlled-strain amplitude. The composite gel placed between plates was heated to sol state and the gap between the plates was adjusted to 0.23–0.25 mm. Then, the composite gel was cooled to room temperature and left for 1 h. The gap was readjusted to approximately 0.2 mm. The frequency and strain dependences of the rheological parameters were measured at 25 °C. The temperature sweep tests were performed in a heating process at 1 °C/min at fixed frequency = 1 Hz and fixed strain = 0.1%, where the stress and strain exhibit a linear relation. The temperature sweep tests were also carried out under irradiation of the UV light (wavelength = 365 nm, intensity = 150 mW/cm^2) after preliminary UV-light irradiation for 10 min at 25 °C. It was confirmed that there was a slight deviation between the actual temperatures of the sample and the temperatures indicated by the rheometer during temperature sweep tests at 1 °C/min, because the temperature control unit and

sensor are set on the outside of the fused quartz stage owing to ensure the transparency. Although the $T_{N–I}$ of azo-doped 7CB ([BMAB] = 5 mol%) was determined to be 46.6 °C by the measurement of the shear viscosity using the rheometer (Figure 3-2), this temperature was approximately +3 °C higher than that determined by polarized optical microscopy. Isothermal changes of the rheological parameters induced by the UV irradiation were measured at fixed strain = 0.1%, fixed frequency = 1 Hz, and fixed temperature = 42 °C.

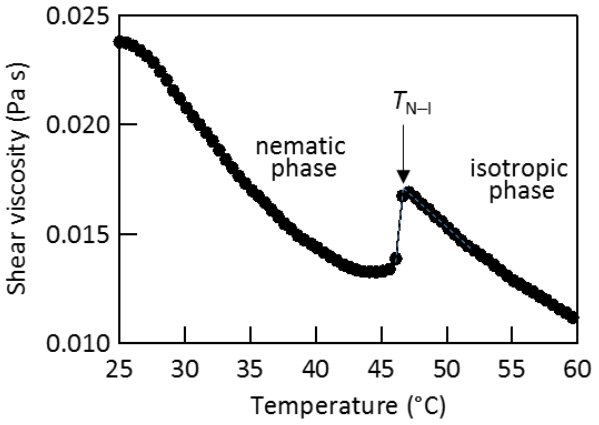

Figure 3-2. Temperature dependence of shear viscosity of azo-doped 7CB ([BMAB] = 5 mol% for 7CB).

Transmittance measurements

The clouding points and $T_{N–I}$ were determined from the transmittance of PMMA/azo-doped 7CB blends to construct the phase diagrams of the blends. PMMA/azo-doped 7CB blends were prepared by dissolving PMMA and azo-doped 7CB in acetone at various concentrations of azo-doped 7CB. Then acetone was evaporated under reduced pressure at 60 °C. The PMMA/azo-doped LC blends were heated to 120 °C between the glass plates with a gap of 200 μm and cooled to room temperature. The intensity of red light (wavelength > 600 nm) passed through the sample (I) was measured in a cooling process at −1 °C/min without and with the irradiation of a focused UV beam (wavelength = 365 nm, intensity = 150 mW/cm^2), using the optical microscope in the bright-field mode as mentioned in chapter 2. The temperature was controlled using a hot stage (FP80 + FP82, Mettler-Toledo, Tokyo, Japan). The measurements under the UV-light irradiation were performed after preliminary irradiation of UV light for 10 min. The intensity in a dark field (I_{dark}) was

measured without the incident light. The intensity of the incident light (I_0) was measured without the sample cell. The transmittance T at each temperature was calculated using the Equation (2-2).

Optical Microscopy

The optical textures of the P-SiP/azo-doped LC composites and PMMA/azo-doped LC blends were observed using the optical microscope in the cross-polarized and bright-field modes. The $T_{N–I}$ of the composites were determined with and without irradiation of the UV light (wavelength = 365 nm, intensity = 150 mW/cm^2) by observation in the cross-polarized mode. The images above $T_{N–I}$ were collected in the bright-field modes. The samples were interposed between two glass slides with the gap of approximately 30 μm.

X-ray diffraction

X-ray diffraction experiments on azo-doped 7CB ([BMAB] = 5 mol% for 7CB) were performed using R-AXIS diffractometer (Rigaku, Japan) with Cu Kα radiation (λ = 1.542 Å, half width = 0.005 Å, beam size = 0.5 mm φ, and (intensity of Cu Kβ)/(intensity of Cu Kα) < 0.1 %). The X-ray generator was operated at 40 kV and 30 mA. The azo-doped 7CB was inserted into a quartz glass tube (outside diameter = 1.5 mm, wall thickness = 0.01 mm). The temperature of the sample tube was controlled using a hot stage (FP82HT, Mettler-Toledo, Tokyo, Japan). The exposure time of the X-ray for the collection of the diffraction images was 60 s. The camera length was 100.0 mm. A series of the diffraction images of the initial azo-doped 7CB were collected at every 5 °C in the temperature range from 25 °C to 55 °C. Then, the diffraction images were collected at each temperature after the irradiation of the UV-light (λ = 365 nm, intensity = 150 mW/cm^2) for 5 min with keeping the temperature. The intensity of the diffracted X-ray was circularly averaged to get results.

3-3 Results

3-3-1 Characteristic viscoelasticity of P-SiP/azo-doped LC composite gels.

Figure 3-3A and B shows the frequency and strain dependences of the G', G'', and tanδ of the P-SiP (248k)/azo-doped 7CB composite gel ([BMAB] = 5 mol% for 7CB) at 25 °C. The G' is larger than G'' over a broad range of frequency, indicating that the azo-doped composite exhibits a stable gel state at room temperature similarly to an azo-undoped composite investigated in chapter 2. Figure 3-3C shows the temperature dependences of the rheological parameters of the composite in a heating process at +1 °C/min. The composite exhibits two gel states with distinct elastic moduli: a hard gel (G_H) state and a soft gel (G_S) state. The G_H–G_S transition temperature ($T_{G_H–G_S}$) was determined by the temperature where the tanδ shows the maximum. The G_S–sol (S) transition temperature ($T_{G_S–S}$) was estimated as the temperature where the tanδ become 1, i.e., where G' and G'' crosses each other as shown in Figure 3-3C. The $T_{G_H–G_S}$ and $T_{G_S–S}$ are 51 °C and 87 °C, respectively. These viscoelastic transition temperatures do not agree with $T_{N–I}$ (46.6 °C) of the azo-doped 7CB matrix, similarly to the case mentioned in chapter 2.

Two gel states were also observed in the other P-SiP/azo-doped LC composite gels in which 5CB or ZLI-1083 were employed as the host LC (Table 3-1). This unique rheological property is a characteristic of P-SiP/LC composite gels. The origin of the viscoelastic transitions in P-SiP/LC composite gels have already been revealed in chapter 2.

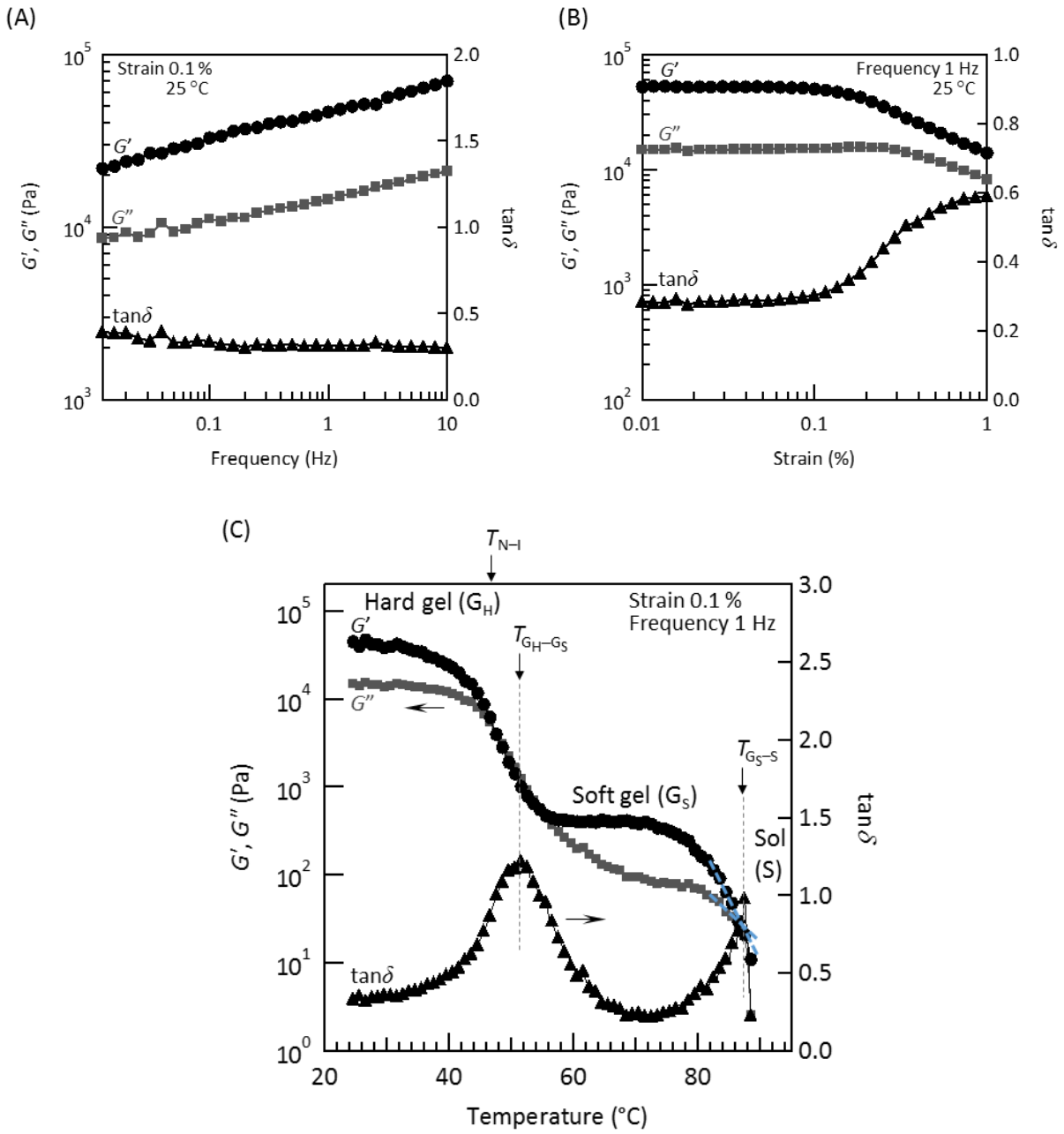

Figure 3-3. (A) Frequency, (B) strain, and (C) temperature dependences of the storage (G', circles) and loss (G'', squares) elastic moduli and loss tangent (tanδ, triangles) in the P-SiP/azo-doped 7CB composite gel ([BMAB] = 5 mol% for 7CB). The measurements were performed at 25 °C (A and B) and with heating at 1 °C/min (C). The $T_{N–I}$ is determined from measurement of the shear viscosity of azo-doped 7CB.

Table 3-1. Transition temperatures of P-SiP/azo-doped LC composite gels without and with the UV-light irradiation.

Host LCs	BMAB	initial			with UV irradiation		
		$T_{N–I}$ [a, b]	$T_{G_H–G_S}$	$T_{G_S–S}$	$T_{N–I}$ [a, c] ($\Delta T_{N–I}$) [c]	$T_{G_H–G_S}$ ($\Delta T_{G_H–G_S}$) [c]	$T_{G_S–S}$ ($\Delta T_{G_S–S}$) [c]
7CB	5 mol%	43.8 °C [a] 46.6 °C [b]	51 °C	87 °C	32.2 °C (−11.6 °C)	40 °C (−11 °C)	71 °C (−16 °C)
	10 mol%	44.9 °C [a]	53 °C	91 °C	20.1 °C (−24.8 °C)	36 °C (−17 °C)	62 °C (−29 °C)
5CB	5 mol%	36.2 °C [a]	29 °C	52 °C	23.2 °C (−13.0 °C)	15 °C (−14 °C)	35 °C (−17°C)
ZLI-1083	5 mol%	49.6 °C [a]	82 °C	117 °C	38.8 °C (−10.8 °C)	73 °C (−9 °C)	110 °C (−7 °C)

[a] determined by polarized optical microscopy observation. [b] determined from the temperature dependence of the shear viscosity. [c] ΔT = (*transition temperature in initial state*) – (*transition temperature with UV irradiation*)

3-3-2 Photoinduced changes in the rheological properties of P-SiP/azo-doped LC composite gels

Figure 3-4 shows the temperature dependence of the rheological parameters of P-SiP/azo-doped 7CB composite gels in the initial state (without irradiation) and with the irradiation of UV light (wavelength = 365 nm, intensity = 150 mW/cm^2). Interestingly, the viscoelastic curves are sifted toward a lower temperature region with the UV-light irradiation. $T_{G_H–G_S}$ and $T_{G_S–S}$ were clearly decreased by the *trans–cis* photoisomerization of BMAB in the composites, while the $T_{N–I}$ also decreased upon the photoirradiation. Moreover, the degree of reduction of the transition temperatures upon the photoirradiation ($\Delta T_{G_H–G_S}$, $\Delta T_{G_S–S}$, and $\Delta T_{N–I}$) becomes large with increasing the concentration of BMAB in the composite gel.

In Figure 3-4B, it is expected that the UV-light irradiation at 42 °C will cause a G_H–G_S transition of the P-SiP/azo-doped 7CB composites ([BMAB] = 10 mol%). Figure 3-5A shows the isothermal change in the elastic moduli by the UV-light irradiation at the above-mentioned condition. The G' is over 10^4 Pa in the initial state. Upon the photoirradiation, G' gradually decreases to

approximately 10^3 Pa after the irradiation for 10 min. The G'' is lower than G' before and after the sufficient irradiation. This indicates that the composite keeps stable quasi-solid states, even though the elastic moduli notably decrease by the photoirradiation. The drastic change in the elastic modulus is successfully induced by the irradiation of UV light with keeping the gel state. Upon the G_H–G_S transition, the PMMA grafted on P-SiP changes into the rubbery state from glassy one. Therefore, the softening of the inner network by the glass transition (the rubber softening) of grafted polymers would account for the decrease in the elastic moduli of the composite gels with the UV-light irradiation (Figure 3-5B). Consequently, the hardness of the gel could be successfully controlled by the photoinduced change of the stiffness of the inner network. On the other hand, in previous studies,[3-4] the photoinduced changes of the elastic modulus have been achieved by the structural change of the inner network employing photodegradable components. The present result is therefore the first example that the rheological properties of the gel is controlled by the photoinduced change of stiffness of the inner network.

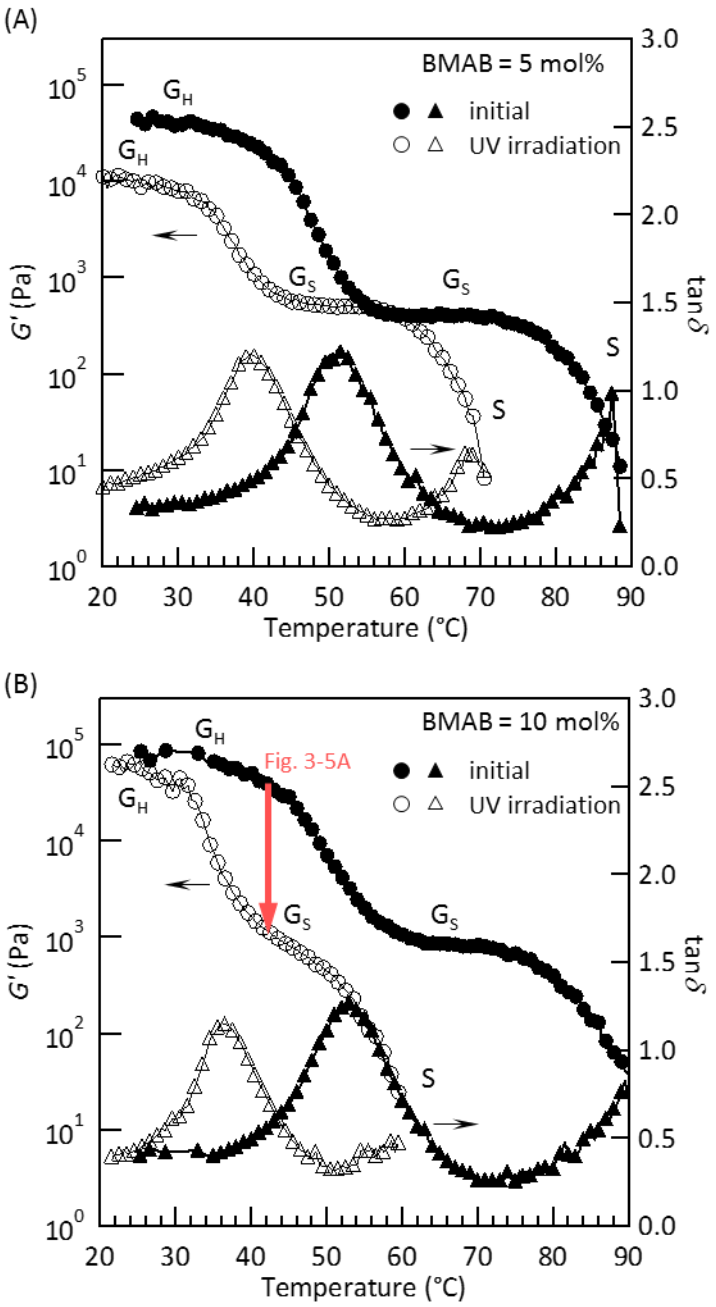

Figure 3-4. Temperature dependences of G' (circle) and tanδ (triangle) of the P-SiP/azo-doped 7CB composite gels (BMAB = 5 mol% for 7CB) in initial state (closed symbols) and with UV-light irradiation (open symbols) (wavelength = 365 nm, intensity = 150 mW/cm^2). Both measurements were performed in the heating process at 1 °C/min.

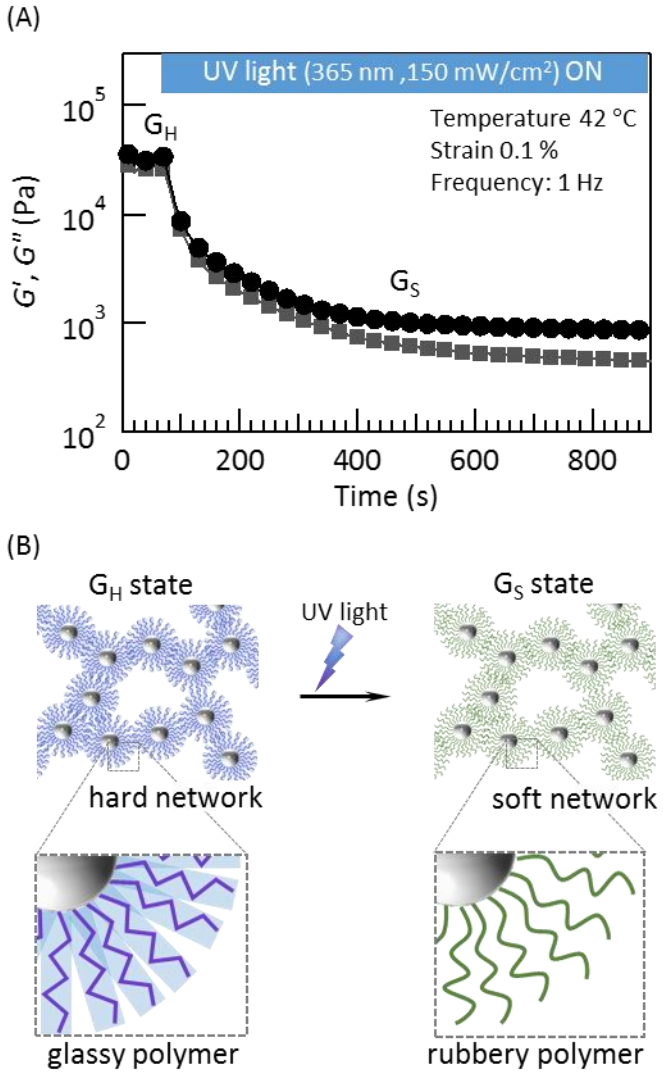

Figure 3-5. (A) Isothermal change in the G' (circles) and G'' (squares) of the P-SiP/azo-doped 7CB composite gel (BMAB = 10 mol%) by the UV-light irradiation (wavelength = 365 nm, intensity = 150 mW/cm^2) at 42 °C. (B) Schematic illustrations of the photoinduced G_H-G_S transition.

3-4 Discussion

3-4-1 Effects of UV-light irradiation on the phase behavior of PMMA/azo-doped 7CB composites

To discuss the change in the viscoelastic transition temperatures upon the UV-light irradiation, the phase behavior of PMMA/azo-doped 7CB blends was investigated without and with the UV-light irradiation. Figure 3-6A shows the temperature dependence of the transmittance of the PMMA/azo-doped 7CB blend (azo-doped 7CB concentration = 60 wt%, in which [BMAB] = 5 mol% for 7CB, and sample thickness = 200 μm) without the photoirradiation in the cooling process at −1 °C/min. The transmittance of the composites is approximately 90 % at 80 °C, where the optical microscope image is homogeneous (Figure 3-6B). The transmittance begins to decrease around 70 °C upon cooling and at the same time the phase separation structure appears in optical microscope images (Figure 3-6C). Thus the decrease of the transmittance originates from the UCST-type phase separation in the PMMA/azo-doped 7CB blend. The difference in the refractive indices between PMMA-rich and azo-doped LC-rich phases would cause the light scattering and the decrease of the transmittance.[7] Here, the clouding point is determined to be 66.7 °C as shown in Figure 3-6A. In addition, the abrupt drop of the transmittance at 43.4 °C is due to the N–I phase transition of the LC-rich phase. The clouding points and $T_{N–I}$ of PMMA/azo-doped 7CB blends are plotted against the weight fraction of azo-doped 7CB in Figure 3-6D. The clouding points (circles) reflect a phase boundary between single-phase state and two-phases state of PMMA-rich and isotropic LC-rich phases. A coexistence curve shows the maximum at approximately 87 °C, that is UCST of PMMA in azo-doped 7CB. This temperature well agreed with the $T_{G_S–S}$ of the P-SiP/azo-doped 7CB as expected from the mechanism of the G_S–S transition mentioned in chapter 2. The $T_{N–I}$ (triangles) displays the phase boundary between two-phases states (PMMA-rich–isotropic LC-rich phases state and PMMA-rich–nematic LC-rich phases state). The $T_{N–I}$ of the blends are roughly constant independent of the concentration and almost identical to that of the azo-doped 7CB alone. This indicates that a small amount of PMMA included in the LC-rich phase does not affect the thermal stability of the nematic phase.

The clouding points under the UV-light irradiation were also examined. Figure 3-6E shows the coexistence curves of the blends before and under the photoirradiation. The coexistence curve is shifted toward a lower temperature upon the UV-light irradiation, indicating the reduction of the UCST of PMMA in azo-doped 7CB. The reduction of UCST would account for the reduction of

$T_{G_S–S}$ of the P-SiP/azo-doped 7CB composite with the photoirradiation. Moreover, Fig. 3-6E also indicates that the concentration of azo-doped 7CB in the PMMA-rich phase is increased by the UV-light irradiation. For example, the concentrations of the azo-doped 7CB in PMMA-rich phase at 60 °C were 52 wt% (point A) and 71 wt% (point B) before and under the photoirradiation, respectively. It is known that the molecularly homogeneous PMMA blends containing the higher concentration of LCs exhibit the lower T_g because LCs act as plasticizers.[7] Therefore, T_g of PMMA in the blends would decrease by the increase of the concentration of a plasticizer in the PMMA-rich phase upon the UV-light irradiation. The reduction of $T_{G_H–G_S}$ of the P-SiP/azo-doped 7CB composite gel by the UV-light irradiation was derived from the photoinduced reduction of T_g of the grafted PMMA shell. Consequently, the decrease of the viscoelastic transition temperatures of the P-SiP/azo-doped 7CB composites would be attributable to the changes in the phase behavior of the grafted PMMA/the isotropic LC system by the UV-light irradiation.

Several literatures reported the photoinduced changes of UCST and LCST (lower critical solution temperature) of solutions of photoresponsive polymers containing azobenzene parts in their main chains, side chains, or terminal groups.[8-12] They suggested that an increase of polarity of polymers by the generation of *cis* azobenzene parts whose dipole moment was generally higher than a *trans* form would lead to the changes in the critical solution temperatures. The dipole moment of BMAB used in this study would be also increased by its *trans*–*cis* photoisomerization. Indeed, the dipole moments were calculated as 1.48 and 4.55 D for *trans* and *cis* forms of BMAB, respectively, using MOPAC AM1. Here, we will consider the effect of the increase of the polarity of the azo-doped 7CB matrix by the increase of the dipole moment of BMAB. The dielectric constant is an index of the polarity and contains the contribution of the orientation polarization associated with the permanent dipoles of molecules.[13] 7CB and BMAB are polar molecules which possess permanent dipoles. Ignoring the interaction between dipoles, the dielectric constant is proportional to $\Sigma_i \Sigma_j x_i x_j \mu_i \mu_j$, where x_i is the mole fraction and μ_i is the dipole moment of each components. The ratio of the above equation between before and after photoirradiation is calculated as 1.08 using the mole fractions and dipole moments estimated with MOPAC AM1 (1.48, 4.55, and 4.14 D for *trans*-BMAB, *cis*-BMAB, and 7CB). The ratio indicates that the increase of the dipole moment of BMAB by its isomerization would not induce the significant change in the polarity of the azo-doped solvent. The large dipole moment of the host LC and the low concentration of the azo additive are responsible for the small change of the polarity. Zhang

et al.[9] reported the reduction of approximately 3 °C in the UCST upon the UV-light irradiation in the aqueous ethanol solution of a methacrylate copolymer with the side chains bearing azobenzene parts (the content of the azobenzene comonomer was 6 mol%), where the polarity of the copolymer is expected to increase slightly upon the photoisomerization of the azobenzene parts similarly to the case of the azo-doped 7CB studied in this thesis. On the other hand, in contrast to the expectation of a small change of the UCST from the slight increment of the polarity, the UCST of the PMMA/azo-doped 7CB blend was decreased by nearly 20 °C upon the UV-light irradiation. Thus, in this study, it is difficult to explain the photoinduced changes of the phase behavior only by the increment of polarity of the azo-doped solvent.

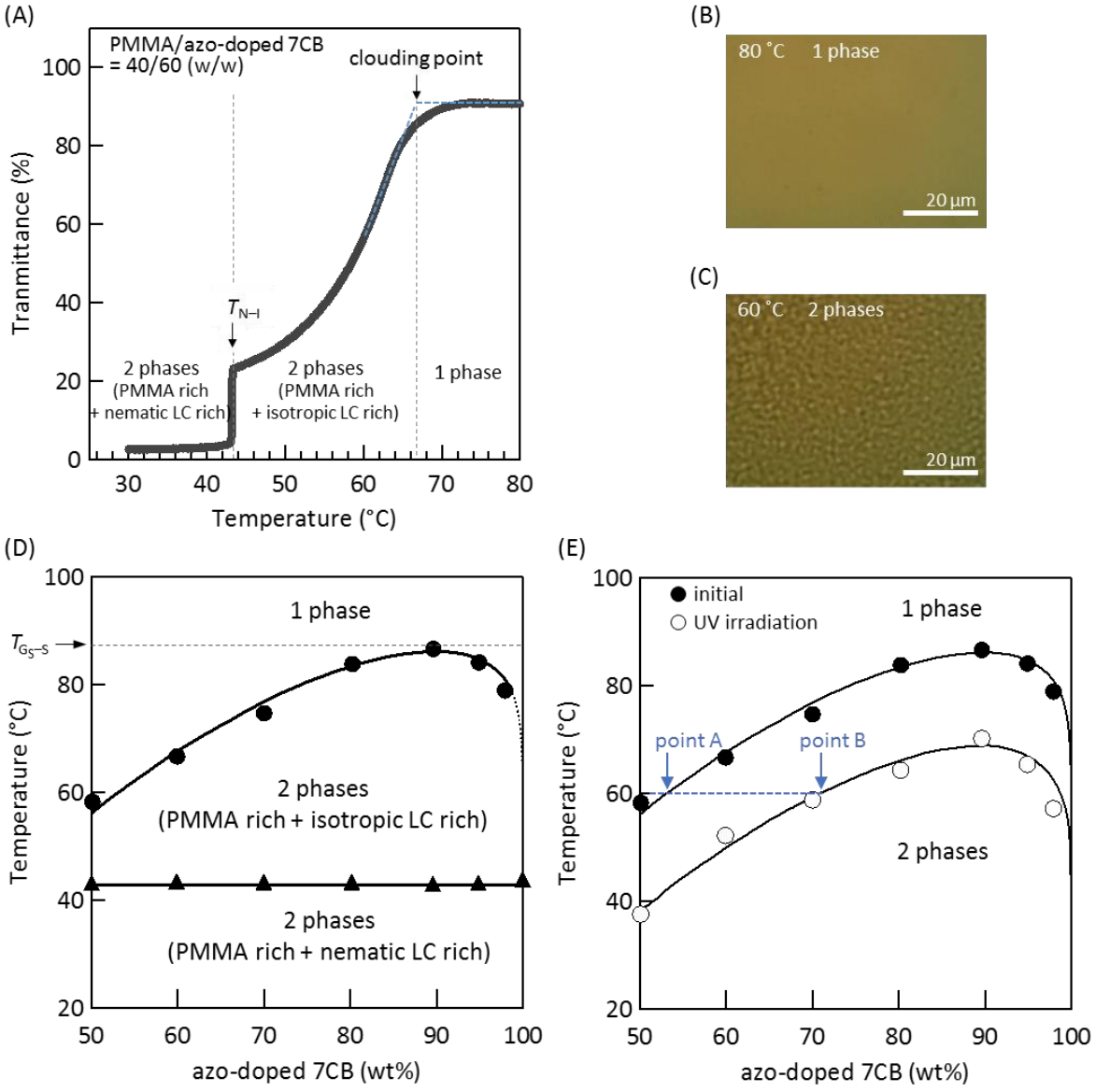

Figure 3-6. (A) Temperature dependence of the transmittance of the PMMA/azo-doped 7CB blends (azo-doped 7CB = 60 wt%, BMAB = 5 mol% for 7CB) without irradiation in a cooling process at −1 °C/min. (B and C) Optical micrographs of the blends at 80 (B) and 60 °C (C). (D) Phase diagram of the PMMA/azo-doped 7CB blends in initial state. The clouding points (circles) and T_{N-I} (triangles) are plotted as a function of weight fraction of azo-doped 7CB. (E) Coexistence curves of the PMMA/azo-doped 7CB blend in initial state (closed circles) and under irradiation of the UV light (wavelength = 365 nm, intensity = 150 mW/cm^2) (open circles). The continuous lines were calculated assuming the following parameters: $\chi = -0.28 + (154.1\ \mathrm{K})/T$, $N_1 = 4$, and $N_2 = 485$ in initial state; $\chi = -0.25 + (136.4\ \mathrm{K})/T$, $N_1 = 4$, and $N_2 = 485$ with UV irradiation.

3-4-2 Flory-Huggins theory

Phase behaviors of blends of polymers and nematic LCs are generally treated using combination of Flory-Huggins theory[14-16] for the mixtures of polymers and solvents and Maier-Saupe theory[17] with consideration of anisotropic contribution for nematic ordering of the LC matrices.[18-21] However, the photoinduced changes observed in the PMMA/azo-doped 7CB blend occurs in the temperature range where azo-doped 7CB is in the isotropic phase. Therefore, the changes in the phase behavior of the blends upon the UV-light irradiation can be simply discussed by considering the Flory-Huggins theory alone.

In the Flory-Huggins theory, the thermodynamics of binary mixture including polymer is considered using a lattice model (Figure 3-7). The lattice is occupied by solvent and chain molecules which consist of repeating units. The repeating units are represented by spheres, radii of which are assumed the same in polymer and the solvent. The chemical species of molecules (solvent or polymer solute) are discriminated by the number of spheres. Since the two bonded spheres must occupy the neighboring sites, the number of possible arrangements of the bonded spheres in the lattice is much less than that in a lattice for a mixture of non-bonded spheres. With consideration of the restriction of the arrangement, the entropy of mixing of the polymer and solvent ($\Delta_{\mathrm{mix}}S$) is

$$\begin{aligned}\Delta_{\mathrm{mix}}S &= -k_{\mathrm{B}}\left[n_1 ln\left(\frac{n_1N_1}{n_1N_1+n_2N_2}\right)+n_2 ln\left(\frac{n_2N_2}{n_1N_1+n_2N_2}\right)\right]\\ &= -k_{\mathrm{B}}(n_1 lnx_1+n_2 lnx_2)\end{aligned} \tag{3-1}$$

where n_1 and n_2 are the numbers of solvent and polymer molecules, N_1 and N_2 are the numbers of repeating units in a respective molecule, and x_1 and x_2 are the mole fractions of repeating units of solvent and polymer on the basis of the numbers of spheres.

There are three types of the first neighbor contacts, namely, pairs between solvent units ([1,1]), solvent and polymer units ([1,2]), and polymer units ([2,2]). The mixing of polymer and solvent cause the change of the first neighbor site as follows; (1/2)[1,1] + (1/2)[2,2] →[1,2]. Using the interaction between these respective pairs (ε_{11}, ε_{12}, and ε_{22}), the change in energy with taking turn in the arrangement ($\Delta\varepsilon$) is

$$\Delta\varepsilon = \varepsilon_{12} - (\varepsilon_{11} + \varepsilon_{22})/2 \tag{3-2}$$

The $\Delta\varepsilon$ is an index of the miscibility between polymer and solvent. The enthalpy of mixing ($\Delta_{mix}H$) is given by

$$\Delta_{\mathrm{mix}}H = z\Delta\varepsilon n_1 N_1 x_2 = k_B T\chi n_1 N_1 x_2 \tag{3-3}$$

$$\chi = \frac{z\Delta\varepsilon}{k_B T} \tag{3-4}$$

The χ in eq. (3-4) is called the Flory-Huggins interaction parameter and z is the number of the nearest neighbor sites. The mole fractions can be replaced to the volume fractions in the lattice model and then the free energy of mixing of polymer and solvent in a unit cell ($\Delta_{mix}g$) is expressed as[14-16]

$$\frac{\Delta_{\mathrm{mix}}g}{k_B T} = \frac{\varphi_1}{N_1}\ln\varphi_1 + \frac{\varphi_2}{N_2}\ln\varphi_2 + \chi\varphi_1\varphi_2 \tag{3-5}$$

where φ_1 and φ_2 are the volume fractions of the solvent and polymer.

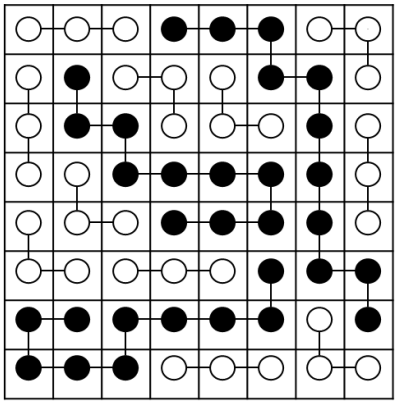

Figure 3-7. Lattice model for a binary mixture consisting of chain molecules.

Equation (3-5) successfully accounts for the phase separation driven by the thermodynamic instability in polymer solutions. In the case of UCST-type phase separation, the coexistence curve that is the phase boundary associated with the phase separation is convex upward. At the critical point where the curve shows a maximum, $(d^2\Delta_{mix}g/d\varphi_2^2) = 0$ and $(d^3\Delta_{mix}g/d\varphi_2^3) = 0$. Thus the volume fraction of polymer (φ_{2c}) and χ parameter at the critical point (χ_c) are expressed as follows.

$$\varphi_{2c} = \frac{\sqrt{N_1}}{\sqrt{N_1} + \sqrt{N_2}} \tag{3-6}$$

$$\chi_c = \frac{\left(\sqrt{N_1} + \sqrt{N_2}\right)^2}{2N_1N_2} \tag{3-7}$$

3-4-3 Origin of photoinduced change in phase behavior of PMMA/azo-doped 7CB blend

The parameter χ is determined by fitting of the experimental data with Equation (3-5) and often assumed to be the function of the temperature: $\chi = A + B/T$, where A and B are constants.[15, 18-21] A term independent of the temperature in the equation is added in order to improve the agreement with experimental data. The weight fractions of the experimental data are converted to the volume fractions to conduct the fitting, assuming that the partial molar volumes in the blends are identical to the molar volumes of the polymer and solvent alone. The N_2 is set to 485 on the basis of the number-averaged degree of polymerization of PMMA, and N_1 are then determined as 4 according to Equation (3-6). The clouding points in Figure 3-6E were fitted using Equation (3-5) while referring to Equation (3-7), yielding $\chi = -0.28 + (154.1\ \mathrm{K})/T$ in the initial state and $\chi = -0.25 + (136.4\ \mathrm{K})/T$ under the UV-light irradiation. The curves in Figure 3-6D and 3-6E were calculated with the obtained χ parameters. The fitted results indicate that the χ under the UV-light irradiation is smaller in magnitude than that in the initial state at a constant temperature. Thus, it was revealed that the χ parameter decreases by the *trans*−*cis* photoisomerization of BMAB in the PMMA/azo-doped 7CB blends. Although the χ is related to the $\Delta\varepsilon$ and z as indicated by Equation (3-4), the UV-light irradiation would not notably affect z. Consequently, the photoisomerization of BMAB in the blends would result in the decrease of $\Delta\varepsilon$, that is, the change in the interactions in the blends

The main interaction between the polar molecules is the dipole-dipole interaction, which is directly related to the magnitude of the dipole moments. In the blends of azo-doped 7CB (solvent) and PMMA (polymer), the energies for the dipole-dipole interactions[22] between molecular pairs of the solvent-polymer (u_{12}) and solvent-solvent (u_{11}) are expressed as

$$u_{12} = -2x_{1a}x_2\frac{\mu_{1a}\mu_2 f}{4\pi\varepsilon_0 r^3} - 2x_{1b}x_2\frac{\mu_{1b}\mu_2 f}{4\pi\varepsilon_0 r^3} = -\frac{C_{12}f}{r^3} \tag{3-8}$$

$$C_{12} = \frac{2x_2\mu_2[x_{1a}\mu_{1a} + x_{1b}\mu_{1b}]}{4\pi\varepsilon_0} \tag{3-9}$$

and

$$u_{11} = -x_{azo}\frac{\mu_{1a}^2 f}{4\pi\varepsilon_0 r^3} - 2x_{azo}(1-x_{azo})\frac{\mu_{1a}\mu_{1b} f}{4\pi\varepsilon_0 r^3} - (1-x_{azo})^2\frac{\mu_{1b}^2 f}{4\pi\varepsilon_0 r^3} = -\frac{C_{11}f}{r^3} \tag{3-10}$$

$$C_{11} = \frac{x_{azo}^2\mu_{1a}^2 + 2x_{azo}(1-x_{azo})\mu_{1a}\mu_{1b} + (1-x_{azo})^2\mu_{1b}^2}{4\pi\varepsilon_0} \tag{3-11}$$

where x_{1a}, x_{1b}, and x_2 are the mole fractions of monomer units of BMAB, 7CB, and PMMA in the blend and x_{azo} is the mole fraction of BMAB in the azo-doped 7CB. Thus x_{1a} and x_{1b} are written as $x_{azo}(1-x_2)$ and $(1-x_{azo})(1-x_2)$, respectively. The μ_{1a}, μ_{1b}, and μ_2 are the dipole moments of BMAB, 7CB, and a monomer unit of PMMA, respectively. ε_0 is the permittivity of vacuum and r is the intermolecular distance. The f is a factor representing the orientation between dipoles, for example, $f = 1$ for two dipoles aligned parallel. The C_{12} and C_{11} are constants indicating the strength of the dipole-dipole interactions. The changes in the constants by the *trans–cis* transition of BMAB (ΔC_{12} and ΔC_{11}) are described by

$$\Delta C_{12} = C_{12,cis} - C_{12,trans} = \frac{x_2 x_{1a}\mu_2\left(\mu_{1a,cis} - \mu_{1a,trans}\right)}{4\pi\varepsilon_0} \tag{3-12}$$

$$\Delta C_{11} = C_{11,cis} - C_{11,trans} = \frac{x_{azo}^2\left(\mu_{1a,cis}^2 - \mu_{1a,trans}^2\right) + 2x_{azo}(1-x_{azo})\mu_{1b}\left(\mu_{1a,cis} - \mu_{1a,trans}\right)}{4\pi\varepsilon_0} \tag{3-13}$$

The $\mu_{1a,trans}$ and $\mu_{1a,cis}$ are the dipole moments of *trans* and *cis* forms of BMAB. The constants in the PMMA/azo-doped 7CB blends where BMAB is *trans* form ($C_{12,trans}$ and $C_{11,trans}$), ΔC_{12}, and ΔC_{11} were calculated (Table 3-2) using the dipole moments estimated with MOPAC AM1. The dipole moment of methyl 2-methyl propionate (1.82 D, MOPAC AM1), which is a model compound of the monomer unit of PMMA, was used as μ_2. Both the ΔC_{12} and ΔC_{11} show positive values, which indicate that the intermolecular interactions become stronger by the *trans–cis* isomerization of BMAB in the blend. Since the ΔC_{11} exhibits comparatively high value, the slight change in the strength of the interaction between solvents may possibly cause the change of the phase behavior. Then the strengthening of the intermolecular attraction between solvents (leading to the decrease of ε_{11}) would cause the worse miscibility between the polymer and solvent (increase of $\Delta\varepsilon$) and rising of the clouding points of the blend (increase of χ). However, as shown in Figure 3-6E, the clouding points of the blends are reduced by the UV-light irradiation. Besides, the ΔC_{12} and ΔC_{11} are much smaller than C_{12} and ΔC_{11}. We can thus infer that the intermolecular interactions would not be notably influenced by the increase of the dipole moment of BMAB with its isomerization if the aggregation state remains the same.

Table 3-2. The constants for dipole-dipole interactions and the difference upon the *trans–cis* isomerization of BMAB in PMMA/azo-doped 7CB blends.

$C_{12,trans}$ /10^{-49} J m^3	ΔC_{12} /10^{-49} J m^3	$C_{11,trans}$ /10^{-49} J m^3	ΔC_{11} /10^{-49} J m^3
3.65	0.140	16.0	1.25

calculated using $\mu_{1a,trans}$ = 1.48 D, $\mu_{1a,cis}$ = 4.55 D, μ_{1b} = 4.14 D, μ_2 = 1.82 D, and x_2 = 0.5, and x_{azo} = 0.05.

In the *trans–cis* isomerization of azobenzene derivatives, we can observe the changes in not only the dipole moment of a BMAB molecule but also the geometry of the molecules. The changes in the geometry of the azobenzene derivatives could affect ε_{11} through the effect on the local structure in molecular level. Although ε_{11} of the PMMA/azo-doped 7CB blends can be regarded as the mean interaction energy between solvent pairs of 7CB-7CB, 7CB-BMAB, and BMAB-BMAB, here we will focus on the interaction between 7CB and BMAB to discuss the photoinduced changes. In the nematic phase with long-range orientational order, the molecules align roughly

parallel their long axis. Although the long-range order disappears upon the N–I phase transition, it is known that the short-range order between LC molecules remains even in an isotropic phase.[23-25] Therefore, it is considered that the most probable intermolecular interactions between 7CB and BMAB are anisotropic interactions including a dipole-dipole interaction between the molecules arranged their dipole moments in an antiparallel way (Figure 3-8) even in the isotropic phase of the azo-doped 7CB. Here, the intermolecular distance (r) between 7CB and *cis*-BMAB would be longer than that between 7CB and *trans*-BMAB due to the steric hindrance of the bent-shaped *cis*-BMAB. Thus the interaction would become weaker (ε_{11} would become higher) by the *trans–cis* photoisomerization of BMAB. According to Equations (3-2) and (3-4), $\Delta\varepsilon$ and χ become lower because of the higher ε_{11}. Therefore, the photoinduced shift of the coexistence curve to the lower temperature side in the PMMA/azo-doped 7CB blends (decrease of χ) will be attributable to the decrease in $\Delta\varepsilon$ due to the weakening of the intermolecular force of azo-doped 7CB (increase of ε_{11}) by the *trans-cis* photoisomerization of BMAB. Although the larger steric hindrance of *cis*-BMAB is possible to bring about the higher ε_{12}, the ε_{12} would not efficiently affect the phase behavior due to few opportunities of formation of interaction pairs of polymer-azo additive.

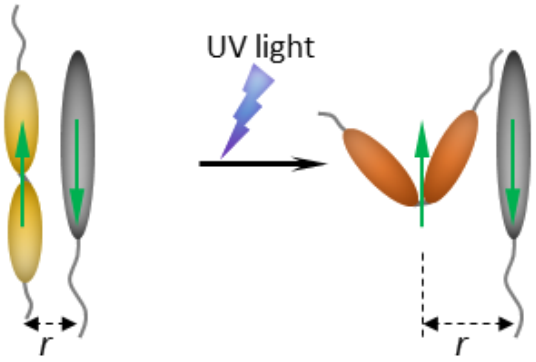

Figure 3-8. Schematic illustration of the photoinduced change of the intermolecular interaction in azo-doped 7CB.

In order to verify the hypothesis that the intermolecular interaction (ε_{11}) of azo-doped 7CB would be weakened through the change in the intermolecular distance upon the photoisomerization

of BMAB, the X-ray diffraction measurements of the azo-doped 7CB ([BMAB] = 5 mol%) were performed before and after the UV-light irradiation. Figure 3-9A and B show the X-ray diffraction patterns of the azo-doped 7CB before and after the irradiation. The single diffraction halo based on the distance between molecules of which positions are randomly arranged is observed at a wide-angle (approximately 14 nm^{-1}). The peak positions of the halo (q_{max}) were determined from Gaussian curves fitted to the diffraction patterns. As shown in Figure 3-9C, the q_{max} after the UV-light irradiation are smaller than those before the irradiation independent of the phase structure of the azo-doped 7CB. The decrease of q_{max} by the UV-light irradiation indicates the increase of the intermolecular distance of the azo-doped 7CB by the *trans–cis* photoisomerization of the azo dopant. It was thus revealed that the change of molecular geometry of a small amount of the azo dopant by its photoisomerization resulted in the change of the intermolecular distance of the whole azo-doped 7CB.

The energy for the interaction between dipoles aligned antiparallel is expressed as $-\mu^2/4\pi\varepsilon_0\varepsilon_r r^3$ using the dipole moment μ, relative permittivity ε_r, and distance between the dipoles r.[22] For example, at 45 °C where the azo-doped 7CB exhibits an isotropic phase both before and after the irradiation, it was calculated from the q_{max} that r was 0.454 and 0.457 nm before and after the irradiation, respectively. The attractive interaction energy between the dipoles of μ = 4.14 D, which is the same as the dipole moment of the 7CB molecules in the system, could be roughly estimated as -19.3×10^{-22} and -18.9×10^{-22} J before and after the irradiation, respectively, using the ε_r of 7CB at 45 °C (ε_r = 9.5).[26] Thus, the difference in the intermolecular interaction energy of the azo-doped 7CB before and after the UV-light irradiation was approximately 0.4×10^{-22} J. This indicates that the UV-light irradiation could change the ε_{11} higher and $\Delta\varepsilon$ lower in the order of 10^{-23} J in PMMA/azo-doped 7CB blends. Moreover, the expected decrease of the $\Delta\varepsilon$ by the irradiation roughly agreed with the decrease estimated from the photoinduced change in the phase diagrams of the blends shown in Figure 3-6E. It was calculated from the χ parameters that the decrease of the $\Delta\varepsilon$ was 0.1×10^{-22} J at 45 °C ($\Delta\varepsilon$ calculated from Equation (3-4) and χ were 1.1×10^{-22} and 0.98×10^{-22} J before and after the irradiation, respectively). Therefore, the observed change of the intermolecular distance of the solvent by the UV-light irradiation would be large enough to induce the improvement of miscibility between the polymer and solvent and the significant change of the phase behavior of the PMMA/azo-doped 7CB blends.

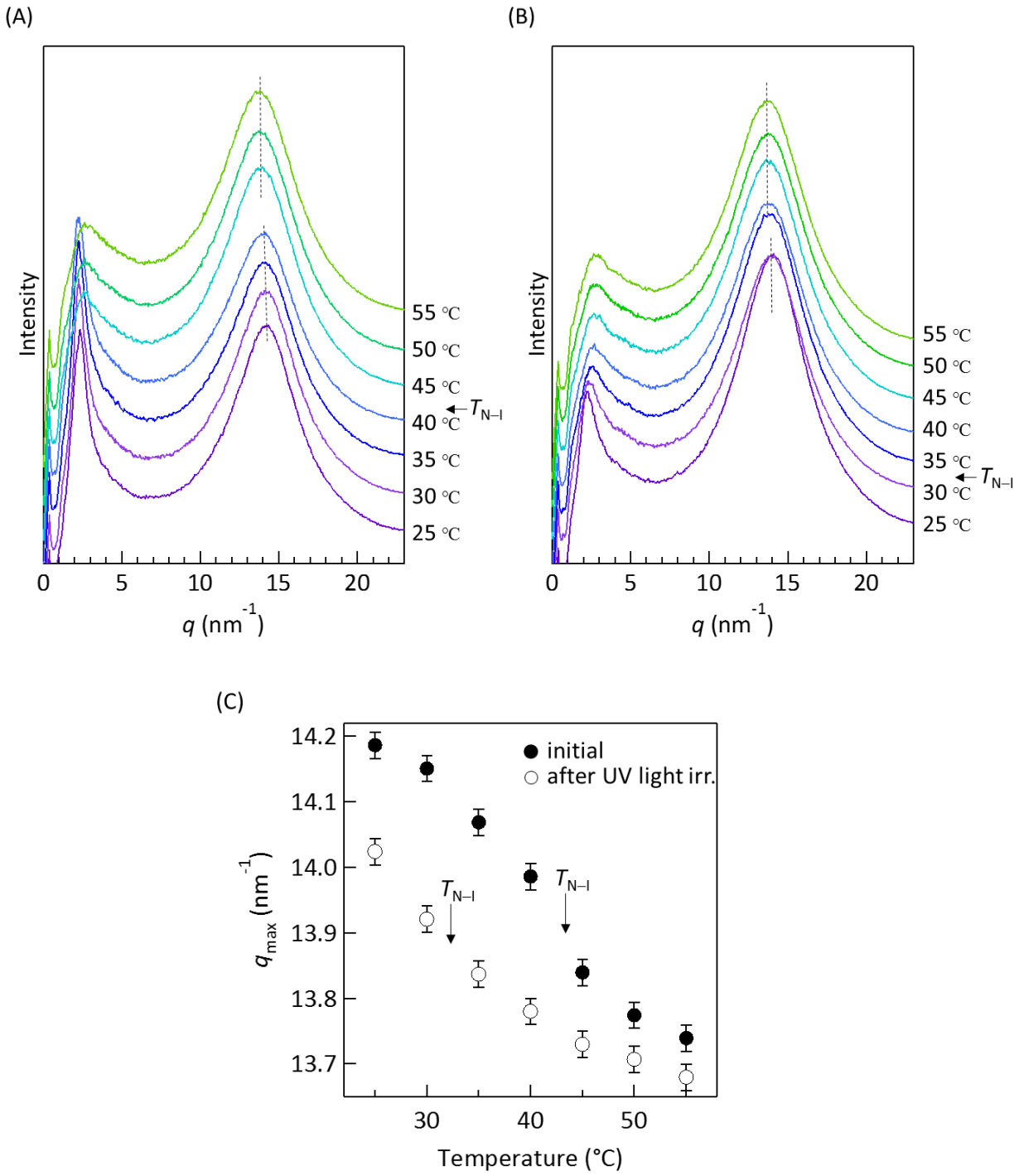

Figure 3-9. (A and B) X-ray diffraction patterns of the azo-doped 7CB ([BMAB] = 5 mol%) (A) before and (B) after the irradiation of the UV-light (λ = 365 nm, intensity = 150 mW/cm^2) for 5 min. (C) Temperature dependences of the q_{max} determined from the diffraction patterns before and after the irradiation.

3-4-4 Mechanism of the photoinduced change in rheological property of P-SiP/azo-doped LC composite gels

From the above discussions, the mechanism of the photoinduced G_H–G_S transition of P-SiP/azo-doped LC composite gels (presented in Figure 3-5) can be summarized as follows and Figure 3-10:

Step 1: The photoisomerization of the azo-dye in the composite weakens the intermolecular interaction of azo-doped LC.

Step 2: The reduction of intermolecular force of the azo-doped LC matrix results in the improvement of the miscibility between grafted PMMA and the matrix

Step 3: The improvement of miscibility causes the more azo-doped LC molecules to dissolve into the grafted PMMA shell of P-SiP.

Step 4: The increase of the concentration of azo-doped LC molecules acting as plasticizers in the shell induces the reduction of the T_g of the grafted PMMA in the composite, namely, the reduction of the $T_{G_H–G_S}$ of the P-SiP/azo-doped LC composite gels.

Step 5: Consequently, at an appropriate temperature, the P-SiP/azo-doped LC composite exhibits the transition from G_H state where the grafted PMMA are glassy into the G_S state where they are rubbery due to the lowering of $T_{G_H–G_S}$with the UV-light irradiation.

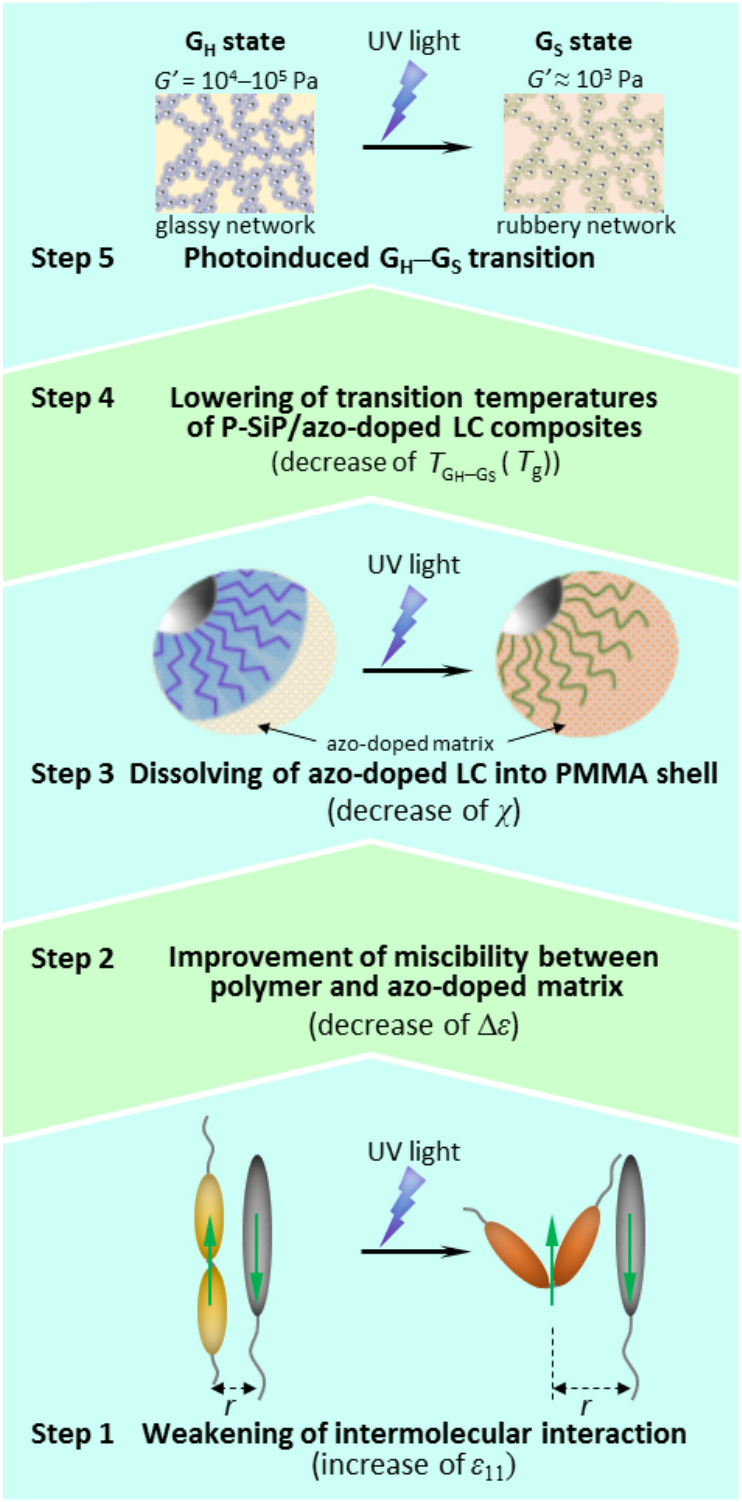

Figure 3-10. A possible mechanism of the change in rheological properties by the UV-light irradiation in P-SiP/azo-doped LC composite gels.

3-4-5 Effect of $T_{N–I}$ of the matrix on the viscoelastic transition temperatures

Figure 3-11 shows $T_{G_H–G_S}$ and $T_{G_S–S}$ of the P-SiP/azo-doped LC composite gels plotted as a function of $T_{N–I}$ (determined by polarized optical microscopy) of the LC matrices. Interestingly, these viscoelastic transition temperatures linearly increases with increasing the $T_{N–I}$ of the LC matrices, although the N–I transition does not directly contribute to the elastic moduli of the composites as mentioned in chapter 2. It is known that $T_{N–I}$ of LCs is directly related to the magnitude of angle-dependent interactions between LC molecules.[17, 23-24, 27]. In other words, LC with the higher $T_{N–I}$ would exhibit the stronger interaction between LC molecules, which leads to the lower ε_{11} in Equation (3-2). Thus, the higher $T_{N–I}$ is expected to bring about lower miscibility between grafted PMMA and azo-doped LC matrix (the higher $\Delta\varepsilon$). Indeed, the blends with the higher $T_{N–I}$ exhibited the higher clouding points (suggesting the higher $\Delta\varepsilon$): The clouding points were 44, 84, and 112 °C for the PMMA/azo-doped LC blends (PMMA = 20 wt%) employing 5CB, 7CB, and ZLI-1083 as host LC, respectively (Figure 3-6D and Figure 3-12). The lower miscibility between the grafted PMMA and the LC with the higher $T_{N–I}$ would result in the higher viscoelastic transition temperatures of the P-SiP/azo-doped LC composites. Furthermore, the reduction of the transition temperatures upon the UV-light irradiation were also confirmed in the other azo-doped composite gels as shown in Table 3-1 and Figure 3-13. The combination of the photocontrol and $T_{N–I}$ dependence of the transition temperatures would enable the advanced control of the mechanical properties of the composite gels.

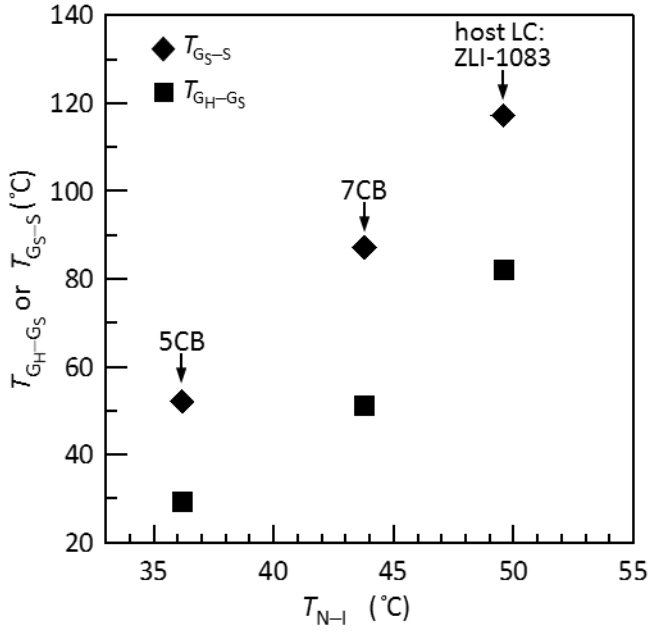

Figure 3-11. Correlation between transition temperatures of $T_{G_H-G_S}$ (squares), T_{G_S-S} (rhombuses) and T_{N-I} in P-SiP/azo-doped LC composite gels

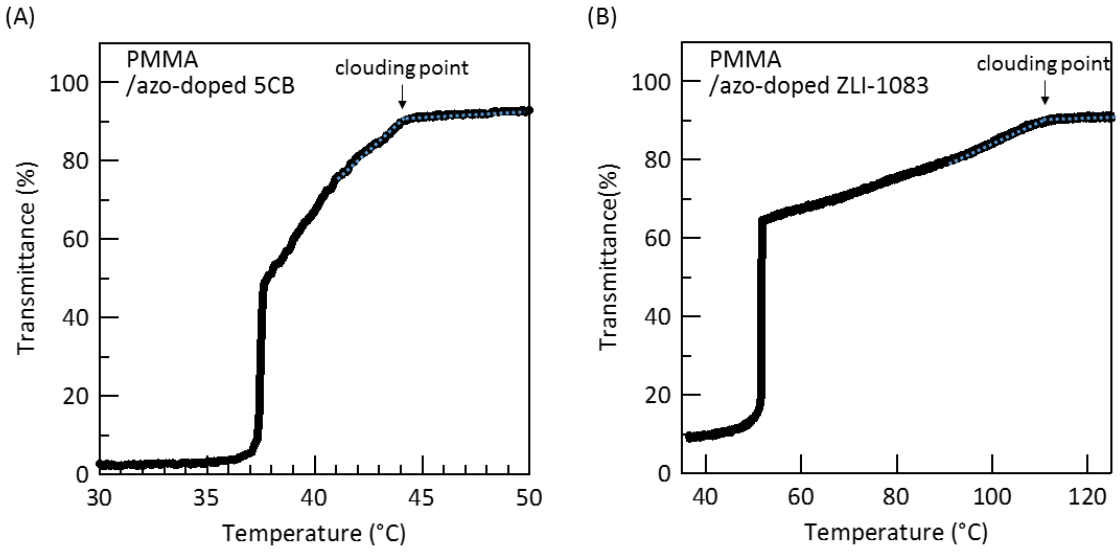

Figure 3-12. Temperature dependence of the transmittance of (A) the PMMA/azo-doped 5CB and PMMA/azo-doped ZLI-1083 blends (PMMA = 20 wt%, BMAB = 5 mol%) in a cooling process at 1 °C/min.

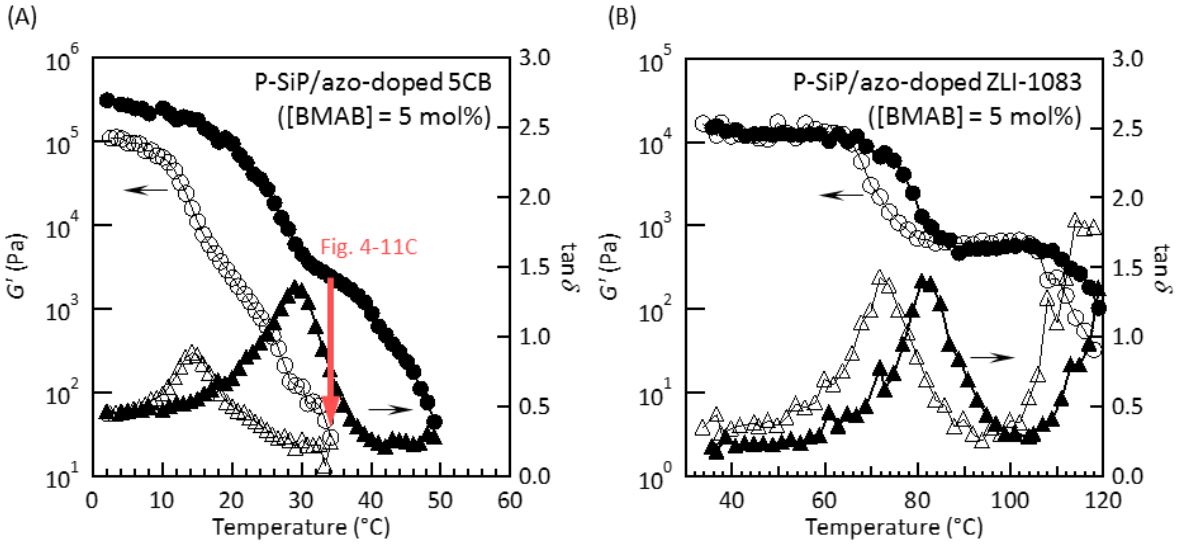

Figure 3-13. Temperature dependences of G' (circle) and $\tan\delta$ (triangle) of (A) the P-SiP/azo-doped 5CB and (B) P-SiP/azo-doped ZLI-1083 composite gels (BMAB = 5 mol% for LC) in the initial state (closed symbols) and with UV-light irradiation (open symbols) (wavelength = 365 nm, intensity = 150 mW/cm^2) in the heating process at 1 °C/min.

3-5 Conclusion

In this chapter, the photochemical changes of the viscoelasticity of P-SiP/azo-doped LC composites were investigated. The P-SiP/azo-doped LC composite gels possess two gel states (G_H and G_S states) with distinct viscoelastic properties similarly to the composite gel described in chapter 2. The G_H–G_S and G_S–S transition temperatures are reduced by the irradiation of UV light. Using the photoinduced reduction of the viscoelastic transition temperatures, the isothermal G_H–G_S transition and the decrease of the elastic moduli were successfully achieved. The photoinduced change of viscoelasticity would result from the softening of the inner network by the glass transition (rubber softening) of the grafted PMMA of P-SiPs. The hardness of the composite gels could be tuned by the photochemical control of stiffness of inner networks formed with P-SiPs in the composite gel.

In addition, the phase behavior of PMMA/azo-doped LC blends was investigated to clarify the mechanism of the photoresponsivity of P-SiP/azo-doped LC composites. The coexistence curve indicative of UCST-type phase separation in the blends is shifted toward the lower temperature region upon the UV-light irradiation. Within the framework of the Flory-Huggins theory, it was suggested that the photoinduced shift of the coexistence curve originated from the improvement of the miscibility between PMMA and the azo-doped LC upon the photoisomerization of the azo additive. We infer that the better miscibility under the photoirradiation originates from the weaker intermolecular interaction between azo-doped LC molecules owing to the larger steric hindrance of *cis* form of azo additives. The improvement of miscibility between polymer components and the azo-doped matrix by the UV-light irradiation successfully accounts for the photoinduced change in the viscoelasticity of P-SiP/azo-doped LC composite gels.

The viscoelastic transition temperatures of P-SiP/azo-doped LC exhibit the tendency to increase with the increase of $T_{N–I}$ of the employed LC. Consequently, the viscoelasticity of the P-SiP/azo-doped LC composite gels can be controlled in a wide range of elastic moduli (10^3–10^5 Pa) by the optimization of the experimental conditions such as light irradiation, temperature, and host LCs. Such good controllability of viscoelastic properties will make possible to develop composite gels applicable to cell culture media for tissue engineering,[3, 28] in which the sophisticated control of gel properties is required.

References to chapter 3

(1) Engler, A. J.; Sen, S.; Sweeney, H. L.; Discher, D. E. Matrix Elasticity Directs Stem Cell Lineage Specification. *Cell* **2006,** *126* (4), 677-689.

(2) Tomatsu, I.; Peng, K.; Kros, A. Photoresponsive Hydrogels for Biomedical Applications. *Adv. Drug Delivery Rev.* **2011,** *63* (14-15), 1257-1266.

(3) Kloxin, A. M.; Kasko, A. M.; Salinas, C. N.; Anseth, K. S. Photodegradable Hydrogels for Dynamic Tuning of Physical and Chemical Properties. *Science* **2009,** *324* (5923), 59-63.

(4) Fairbanks, B. D.; Singh, S. P.; Bowman, C. N.; Anseth, K. S. Photodegradable, Photoadaptable Hydrogels Via Radical-Mediated Disulfide Fragmentation Reaction. *Macromolecules* **2011,** *44* (8), 2444-2450.

(5) Hahn, M. S.; Miller, J. S.; West, J. L. Three-Dimensional Biochemical and Biomechanical Patterning of Hydrogels for Guiding Cell Behavior. *Adv. Mater. (Weinheim, Ger.)* **2006,** *18* (20), 2679-2684.

(6) Khademhosseini, A.; Langer, R. Microengineered Hydrogels for Tissue Engineering. *Biomaterials* **2007,** *28* (34), 5087-5092.

(7) Ahn, W.; Kim, C. Y.; Kim, H.; Kim, S. C. Phase-Behavior of Polymer Liquid-Crystal Blends. *Macromolecules* **1992,** *25* (19), 5002-5007.

(8) Niskanen, J.; Tenhu, H. How to Manipulate the Upper Critical Solution Temperature (UCST)? *Polym. Chem.* **2017,** *8*, 220-232.

(9) Zhang, Q. L.; Schattling, P.; Theato, P.; Hoogenboom, R. Uv-Tunable Upper Critical Solution Temperature Behavior of Azobenzene Containing Poly(Methyl Methacrylate) in Aqueous Ethanol. *Eur. Polym. J.* **2015,** *62*, 435-441.

(10) Irie, M.; Tanaka, H. Photoresponsive Polymers .5. Reversible Solubility Change of Polystyrene Having Azobenzene Pendant Groups. *Macromolecules* **1983,** *16* (2), 210-214.

(11) Ueki, T.; Nakamura, Y.; Yamaguchi, A.; Niitsuma, K.; Lodge, T. P.; Watanabe, M. UCST Phase Transition of Azobenzene-Containing Random Copolymer in an Ionic Liquid. *Macromolecules* **2011,** *44* (17), 6908-6914.

(12) Akiyama, H.; Tamaoki, N. Synthesis and Photoinduced Phase Transitions of Poly(N-Isopropylacrylamide) Derivative Functionalized with Terminal Azobenzene Units. *Macromolecules* **2007,** *40* (14), 5129-5132.

(13) Gaiduk, V. I., *Dielectric Relaxation and Dynamics of Polar Molecules*, World Scientific: Singapore ; River Edge, N.J., 1999.

(14) Flory, P. I. Thermodynamics of High Polymer Solutions. *J. Chem. Phys.* **1942,** *10* (1), 51-61.

(15) Huggins, M. L. Theory of Solutions of High Polymers. *J. Am. Chem. Soc.* **1942,** *64*, 1712-1719.

(16) Flory, P. J., *Principles of Polymer Chemistry*, Cornell University Press: Ithaca,, 1953.

(17) Maier, W.; Saupe, A. Eine Einfache Molekular-Statistische Theorie Der Nematischen Kristallinflussigen Phase .1. *Z. Naturforsch. Pt. A* **1959,** *14* (10), 882-889.

(18) Benmouna, F.; Bedjaoui, L.; Maschke, U.; Coqueret, X.; Benmouna, M. On the Phase Behavior of Blends of Polymers and Nematic Liquid Crystals. *Macromol. Theory Simul.* **1998,** *7* (6), 599-611.

(19) Mucha, M. Polymer as an Important Component of Blends and Composites with Liquid Crystals. *Prog. Polym. Sci.* **2003,** *28* (5), 837-873.

(20) Soule, E. R.; Rey, A. D. Modelling Complex Liquid Crystal Mixtures: From Polymer Dispersed Mesophase to Nematic Nanocolloids. *Mol. Simul.* **2012,** *38* (8-9), 735-750.

(21) Srivastava, J. K.; Singh, R. K.; Dhar, R.; Singh, S. Phase Diagrams and Morphology of Polymer-Dispersed Liquid Crystals: An Analysis. *Liq. Cryst.* **2012,** *39* (11), 1402-1413.
(22) Israelachvili, J. N., *Intermolecular and Surface Forces*, 3rd ed; Academic Press: Burlington, MA, 2011.
(23) Chandrasekhar, S., *Liquid Crystals*, second edition ed; Cambridge University Press: 1992.
(24) de Gennes, P. G.; Prost, J., *The Physics of Liquid Crystals*, 2nd ed; Oxford University Press: Oxford, 1993.
(25) Sasaki, T.; Goto, M.; Ishikawa, Y.; Yoshimi, T. Enhancement of Photorefractivity in the Isotropic Phase of Polymer Liquid Crystals. *J. Phys. Chem. B* **1999,** *103* (11), 1925-1929.
(26) Ratna, B. R.; Shashidhar, R. Dielectric Properties of 4'-*n*-alkyl-4-cyanobiphenyls in Their Nematic Phases. *Pramana* **1976**, *6*(5), 278-283.
(27) Stephen, M. J.; Straley, J. P. Physics of Liquid-Crystals. *Rev. Mod. Phys.* **1974,** *46* (4), 617-704.
(28) Agarwal, A.; Huang, E.; Palecek, S.; Abbott, N. L. Optically Responsive and Mechanically Tunable Colloid-in-Liquid Crystal Gels That Support Growth of Fibroblasts. *Adv. Mater. (Weinheim, Ger.)* **2008,** *20* (24), 4804-4809.

Chapter 4

Dual Self-Healing Abilities Based on Precise Control of Mechanical Properties

4-1. Introduction

Self-healing materials have been in the spotlight over the past two decades owing to their potential ability to extend the lifetime of products.[1-11] So far, a great number of materials that can heal damages such as cracks, cuts, delamination, and dents have been proposed on the basis of various approaches. An ideal self-healing material can heal various mechanical damages made on/in a material spontaneously or with the aid of external triggers such as light or heat. However, the development of materials with multiple self-healing abilities is still a significant challenge.

In the previous chapters, the thermal behavior and photoinduced change of the viscoelastic property of the series of P-SiP/LC composite gels were investigated in detail and the control of the viscoelastic properties was enabled by the optimization of the experimental conditions such as light irradiation, temperature, and kinds of host LCs. Utilizing the control of the property, the repairing of surface cracks due to the photoinduced gel–sol transition as well as the repairing of surface dents owing to the elasticity derived from polymer components would be realized in the composites Thus, in this chapter, the self-healing abilities of the P-SiP/LC and P-SiP/azo-doped LC composites will be investigated.

4-2 Experimental Section

4-2-1 Materials

P-SiP (248k) or P-SiP (600k) as particles, 5CB as a host nematic LC, and BMAB as a photoresponsive additive were employed in this chapter. The details of the materials have been already described in chapters 2 and 3. Conventional PMMA (M_w = 102000 and M_w/M_n = 2.1) and particles without grafted polymer (Micropearl, ϕ = 3.6 μm, Sekisui Chemical, Japan) were used for comparison with P-SiPs.

4-2-2 Methods

Preparation of composite gels

P-SiP/5CB and P-SiP/azo-doped 5CB composite gels (particle concentrations = 10 wt%) were prepared by the same manner described in previous chapters. The composite gel using Micropearl was prepared by vigorously mixing the suspension of the particles and LC at 80 °C and then cooling.

Scanning electron microscopy

The cutting plane of xerogel prepared from the P-SiP (248k)/5CB composite gel was observed on the SEM in the same way described in chapter 2.

Optical microscopy

The optical textures of the composite gels in the evaluation cells with a gap thickness of 30 μm were observed with and without the irradiation of a focused UV light (wavelength = 365 nm, intensity = 1.6 mW/cm^2) as mentioned in chapters 2 and 3.

Rheology

The fundamental rheological analyses without the UV-light irradiation were performed using ARES-RF. The isothermal measurement at 34 °C with the UV-light irradiation (wavelength = 365 nm, intensity = 180 mW/cm^2) was carried out with MCR302, after the composite gel was left at room temperature for 1.5 h. The details of the measurements are described in previous chapters.

Spontaneous repairing of surface dents

A tool in slotted screwdriver form (the contact surface was 0.3 mm × 10 mm) attached on a digital force gauge (FGP-50, Nidec-shimpo, Kyoto, Japan) was pressed onto the molded P-SiP (248k)/5CB composite gels at 25 °C. After removing the mechanical stress, the repairing process of the resulted surface dent was monitored at 25 °C.

To evaluate the restoration of the mechanical property, the normal force which acts parallel to the direction of the indentation was measured using MCR302 with a tool in slotted screwdriver form (the contact surface was 1.0 mm × 5.5 mm). A disk-shaped sample with the thickness (d_0) of 1.6 mm was prepared with the P-SiP(600k)/5CB composite gel on the stage of MCR302. The measurements of normal force were performed twice with changing the distance between the tool and stage (d) at a rate of 0.01 mm/s. An interval between runs was 10 min. The compressive stress and strain were calculated from the equations; *stress* = (*normal force*)/(*contact area*) and *strain* = (d_0-d)/d_0, respectively.

Photoinduced repairing of surface cracks

The cracked area made on the P-SiP (248k)/azo-doped 5CB composite gel was irradiated with a focused UV light (wavelength = 365 nm, intensity = 8.5 mW/cm^2) at 30 °C. Then, the UV-irradiated gel was illuminated with visible light (wavelength = 450 nm, intensity = 40 mW/cm^2) at room temperature. The photochemical repairing behavior was evaluated by visual observation.

4-3 Results and discussion

4-3-1 Spontaneous repairing of a surface dent

The P-SiP (248k)/5CB composite formed a stable gel, of which G' and G'' moduli were 4.6×10^4 and 5.2×10^4 Pa at 25 °C, respectively (Figure 4-1A). As similar to the P-SiP/ZLI-1083 composite gel mentioned in chapter 2, the formation of the inner percolation network structure was confirmed through the SEM observation of the xerogel prepared from the P-SiP(248k)/5CB composite gel (Figure 4-1B). To examine the spontaneous repairing of a surface dent that is one of self-healing abilities, mechanical stress tests were performed with a tool in slotted screwdriver form (the contact area was 0.3 mm × 10 mm) at a given stress on the P-SiP (248k)/5CB composite gel at 25 °C. The composite gel was locally deformed by the indentation at a pressure of 3 MPa with the tool, at which the gel was not broken (Figure 4-2A). Subsequently, after leaving the dented P-SiP/5CB composite gel for 10 min, the dent completely disappeared, indicating that the surface dent was repaired spontaneously (Figure 4-2B). Although there are variations in the breaking strength of the P-SiP/5CB composite gels depending on experimental conditions such as room temperature, none of the composite gels was broken by the indentation at pressures below 1.5 MPa, and several composite gels showed the high breaking strength of approximately 10 MPa (Figure 4-3). If the composite gel was not broken by the indentation, every dent made on the gel disappeared spontaneously within several tens of minutes at 25 °C after removing the mechanical stress. On the other hand, a previously reported particle/LC composite gel[10] was easily broken by the indentation at a pressure below 1 MPa (Figure 4-4). The inferior mechanical properties of the previous composite gels were attributed to the brittle networks formed by weak physical interactions between particles that had no grafted polymer chains on their surface. Thus, the composite gel could not deform without the collapse of the networks. Such phenomenon has often been observed in physical gels. In contrast, as mentioned above, the P-SiP/5CB composite gels showed an elastic nature despite being a physical gel, which suggests that the network in the composite gel could be elastically deformed with mechanical stress and return to an original state after removing the stress.

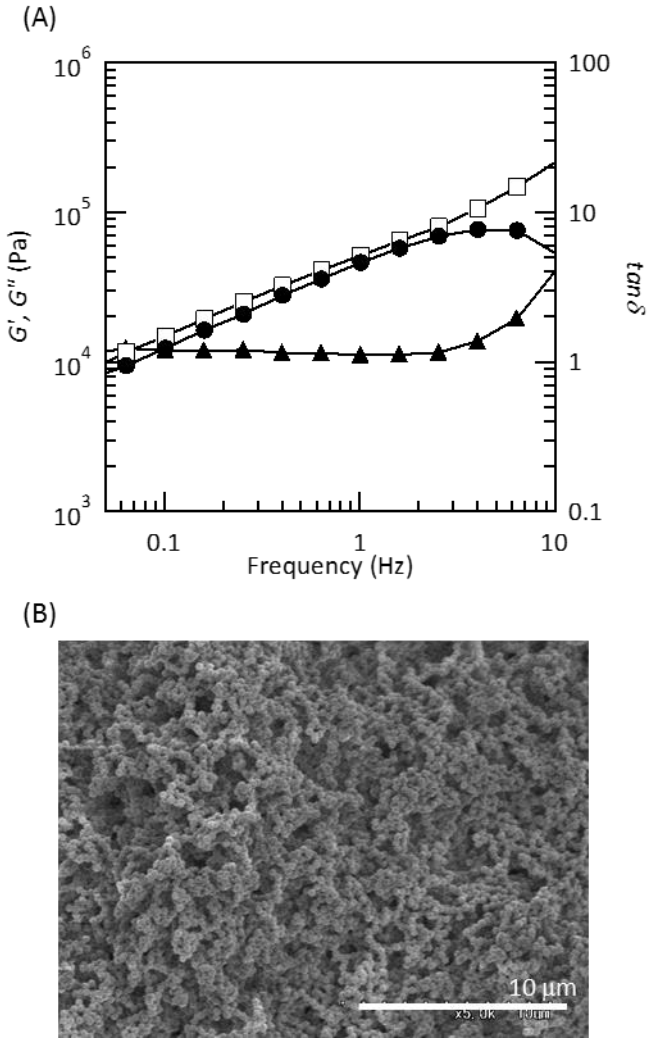

Figure 4-1. (A) Frequency dependences of the G' (circles), G'' (squares), and tanδ (triangles) of the P-SiP (248k)/5CB composite gel (particle concentration = 10 wt%). (B) SEM image of a xerogel prepared from the P-SiP (248k)/5CB composite gel.

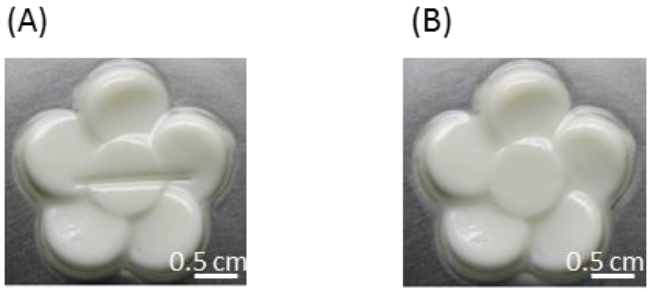

Figure 4-2. Photographs of P-SiP (248k)/5CB composite gel (particle concentration = 10 wt%) at 25 °C taken (A) immediately after being pressed with a tool in slotted screwdriver form at 3 MPa and (B) 10 min after the press.

Figure 4-3. A mechanical stress test of the P-SiP (248k)/5CB composite gel at 25 °C: **(**A) initial state; (B) immediately after being pressed with a digital force gauge with a tool in slotted screwdriver form (the contact surface was 0.3 mm × 10 mm) at 10 MPa (in circle); (C) after leaving the composite gel for 1 hour. The concentration of P-SiP was adjusted to 10wt%.

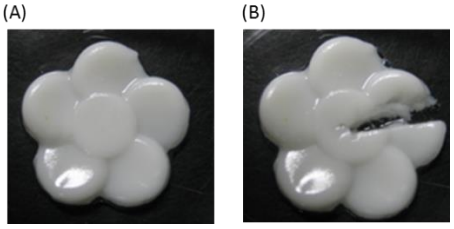

Figure 4-4. A mechanical stress test of the previously reported particle/LC composite gel[10] at 25 °C (A) before and (B) after indentation at 1 MPa. In this composite gel, LC was a mixture showing a nematic phase (ZLI-1083) purchased from Merck. The concentration of the particle was adjusted to 20 wt%.

Figure 4-5 shows a temperature dependence of the rheological parameters of the P-SiP (248k)/5CB composite gel. The G_H–G_S transition can be observed around room temperature. Thus the grafted PMMA would be in the glass transition region at room temperature, in which the local segmental motion of polymer is permitted and the conformation of PMMA can change due to the rotation around the backbone.[12] The PMMA chains in the P-SiP/5CB composite gel would respond to mechanical stress by their conformational change and entropically return to a stable conformation after removing the stress. Furthermore, in the sponge-like structure formed with P-SiPs, PMMA chains would be cross-linked not only physically but also chemically (Figure 4-6). The physical cross-linking points consist of inter-particle entanglement of PMMA chains. The chemical points are chemical bonds between the silica cores of P-SiPs and PMMA chains. The chemical cross-linking points would regulate the spatial positions of the PMMA chains even if the physical cross-linking points slide by the application of the mechanical stress. Consequently, although the P-SiP/5CB composite gel was classified into a physical gel, the sponge-like structures consisting of P-SiPs also behaved like a chemically cross-linked rubber network. Thus, compared with the previous composite gels,[10] the P-SiP/5CB composite gel showed high mechanical strength and efficient repairing of surface dents. On the other hand, in the case of free PMMA/5CB blends, while they had high storage modulus similar to that of the P-SiP/5CB composite gel (Figure 4-7A), a surface dent made on the PMMA/5CB blend was not completely repaired within several tens of minutes (Figure 4-7B and C). The inner structure of the PMMA/5CB blend had only physical cross-links consisting of the entanglement of PMMA chains. The mechanical indentation could cause positional changes of the PMMA chains as well as the slide of the entanglement points. Therefore, the shape recovery of the PMMA/5CB blend did not occur efficiently.

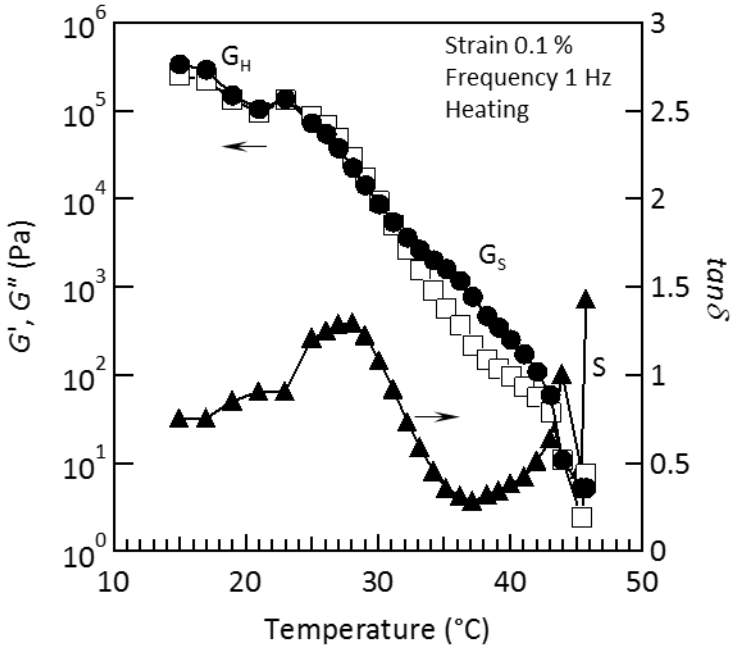

Figure 4-5. Temperature dependence of the G' (circles), G'' (squares), and tanδ (triangles) in the P-SiP (248k)/5CB composite gel (particle concentration = 10 wt%).

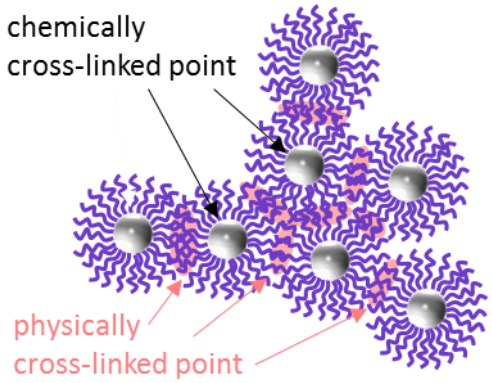

Figure 4-6. Schematic illustration of a sponge-like structure formed in P-SiP/5CB composite gels.

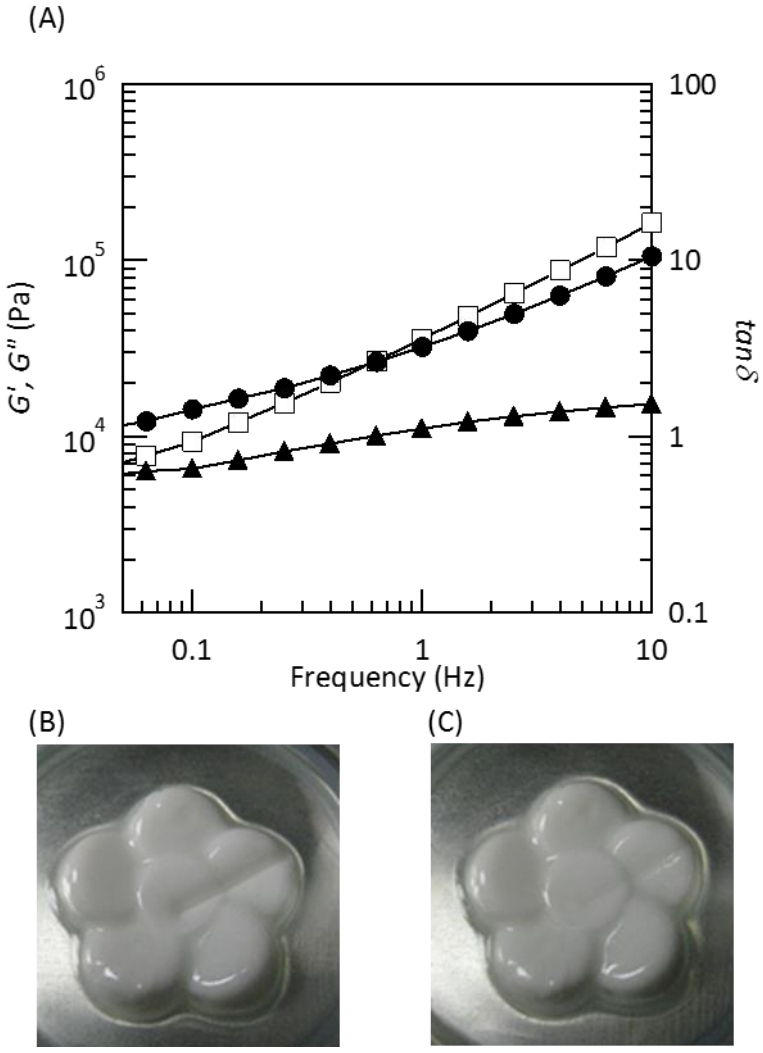

Figure 4-7. (A) Frequency dependences of the G' (circles), G'' (squares), and tanδ (triangles) in the PMMA/5CB blend (PMMA concentration = 10 wt%). (B and C) Photographs of the blend at 25 °C taken (A) immediately after being pressed with a tool in slotted screwdriver form at 3 MPa and (B) 45 min after the press.

In addition, the repeated compression tests were performed in the P-SiP (600k)/5CB composite gel (particle concentration = 10 wt%) using the tool in slotted screw driver form (the contact surface was 1.0 mm × 5.5 mm) in the rheometer. The normal force that acts parallel to the direction of the compression was measured with changing the distance between the tool and stage (*d*) at the rate of 0.01 mm/s (Figure 4-8A). The loading/unloading tests were performed twice and the composite gel was left with removing the stress for 10 min between the first and second runs. Figure 4-8B shows the stress-strain curves calculated from the data of Figure 4-8A. The unloading curve did not agree with a loading curve. This disagreement means that the composite gel was damaged by the compression and a surface dent was produced. Nevertheless, after repairing for 10 min, the surface dent was not visually observed and the strain-stress curve of the second run exactly coincided with that of the first run. Thus, it was obvious that not only the shape but also the mechanical property were fully recovered spontaneously.

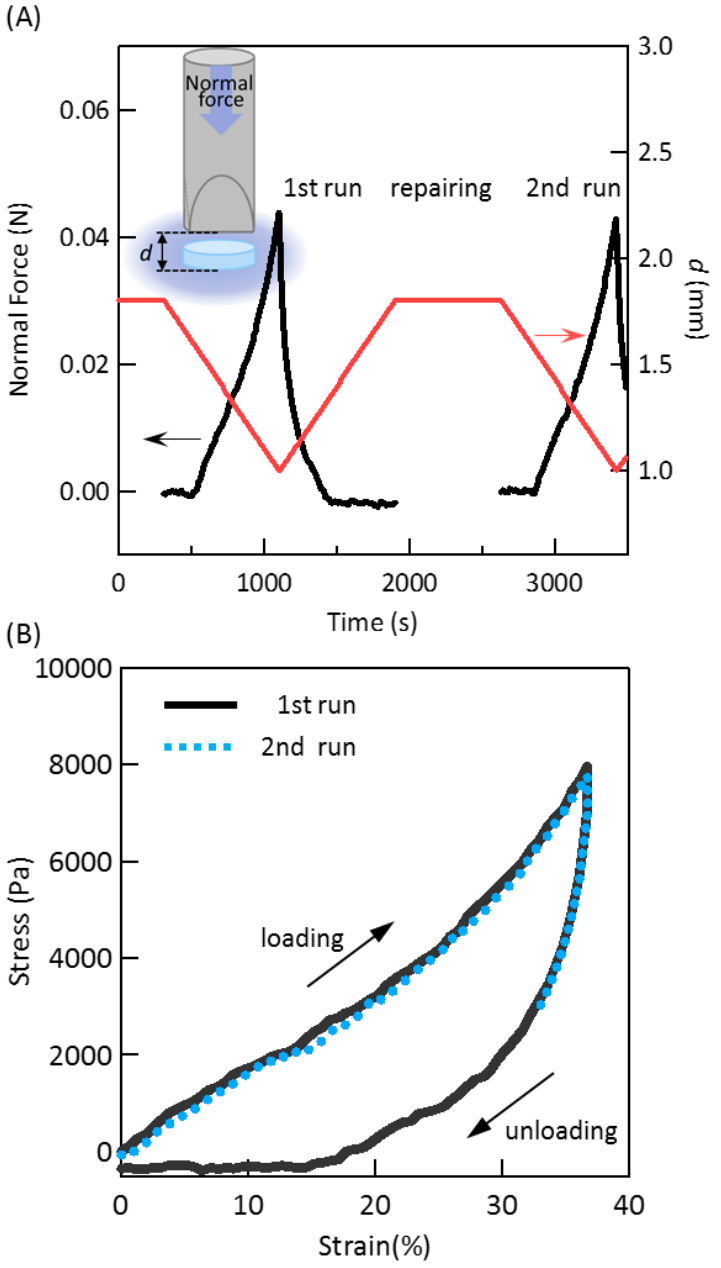

Figure 4-8. (A) Repeating tests of loading/unloading the mechanical stress with the tool in slotted screw driver form (the contact surface was 1.0 mm × 5.5 mm) to the P-SiP (600k)/5CB composite gel. The chainging rate of *d* is 0.01 mm/s. The interval time between 1st and 2nd cycles was approximately 10 min. (B) Compressive strress-strain curves of the composite gel calculated from Figure 4-8A.

4-3-2 Thermal properties of the composite gels

The thermal properties of the P-SiP (248k)/5CB composite gel were examined in optical microscopy (Figure 4-9). The matrix of the composite gel exhibited a nematic phase at room temperature (Figure 4-9A). Although the LC matrix changed into an isotropic phase at 36 °C, a heterogeneous microstructure (Figure 4-9B), which would originate from a phase separation between P-SiP-rich and 5CB-rich phases, was observed until 45 °C. The heterogeneous structure disappeared at 45 °C (Figure 4-9C), where the composite macroscopically changed into a sol (S) state. Of course, the thermal gel–sol transition and the transformation between heterogeneous and homogeneous structures were reversible. In a cooling process, the sol-gel transition and appearance of heterogeneous microstructures were observed at almost the same temperature as the heating process.

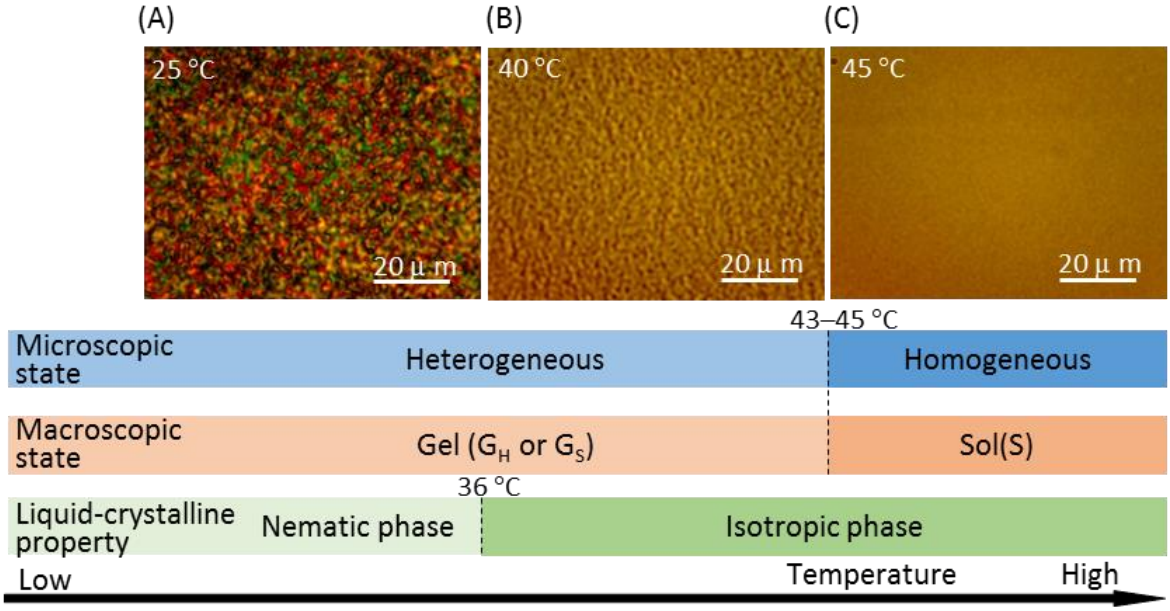

Figure 4-9. Thermal changes of microscopic and macroscopic states, and LC phases of P-SiP/5CB composite gels: (A–C) Optical micrographs of P-SiP (248k)/5CB composite gel (P-SiP = 10 wt%) at each temperature (upper part); (A) in the cross-polarized mode; (B and C) in the bright-field mode.

4-3-3 Photoresponsive properties of azo-doped composite gels

Figure 4-10 shows the $T_{N–I}$ and the disappearance temperatures of heterogeneous structures corresponding to $T_{G_S–S}$ of P-SiP (248k)/azo-doped 5CB composite gels ([BMAB] = 0–10 mol% for 5CB) with and without the irradiation of UV light (wavelength = 365 nm, intensity = 1.6 mW/cm^2). The transition temperatures were determined by microscope observation. Both temperatures of the azo-doped composite gels were significantly reduced by the photoirradiation. Here, we can expect that the photoirradiation at point A induces a transition from the heterogeneous (gel) state to a homogeneous (sol) one of the P-SiP/azo-doped 5CB composite. Figure 4-11 shows the changes in the optical textures and the viscoelastic property of the P-SiP/azo-doped 5CB composite gel ([BMAB] = 5 mol% for 5CB) with irradiation of the focused UV light (intensity = 0.05 mW) at 34 °C (point A in Figure 4-10). In the cross-polarized mode (Figure 4-10A), an optical texture in and around the irradiated area changed into the dark state by the generation and diffusion of the *cis* form of BMAB. This indicates that *trans–cis* photoisomerization of BMAB caused the isothermal nematic–isotropic phase transition of the LC matrix[13]. Upon the photoirradiation, the heterogeneous microstructure in the irradiated area was found to slowly disappear for several minutes in the bright-field mode (Figure 4-11B). Thus, the *trans–cis* photoisomerization triggered changes not only in the phase structures of the LC matrix, but also in the microscopic morphologies of the composite gel. Figure 4-11C shows the rheology of the P-SiP/azo-doped 5CB composite gel under irradiation of UV light. The initial G' of the composite gel was over 10^3 Pa at 34 °C. With the irradiation of the UV light (intensity = 180 mW/cm^2), G' slowly decreased and became below10 Pa after 300 s. The elastic moduli agreed with the values expected from Figure 3-11A. From macroscopic observations (inset of Figure 4-11C), the composite was confirmed to show a liquid-like nature after the photoirradiation. As we expected in Figure 4-10, the gel–sol transition of a P-SiP/5CB composite gel was successfully induced by means of the *trans–cis* photoisomerization. The liquid-like P-SiP/azo-doped 5CB composite induced by UV light irradiation reverted back to the solid-like composite after irradiation of visible light (wavelength = 450 nm, intensity = 40 mW/cm^2) and then leaving it at room temperature in dark for 1 h (Table 4-1). The G' of the composite gel before the UV-light irradiation and after visible-light irradiation were 3.1×10^4 and 2.0×10^4 Pa, respectively (strain = 0.1%; frequency = 1 Hz; temperature = 20 °C).

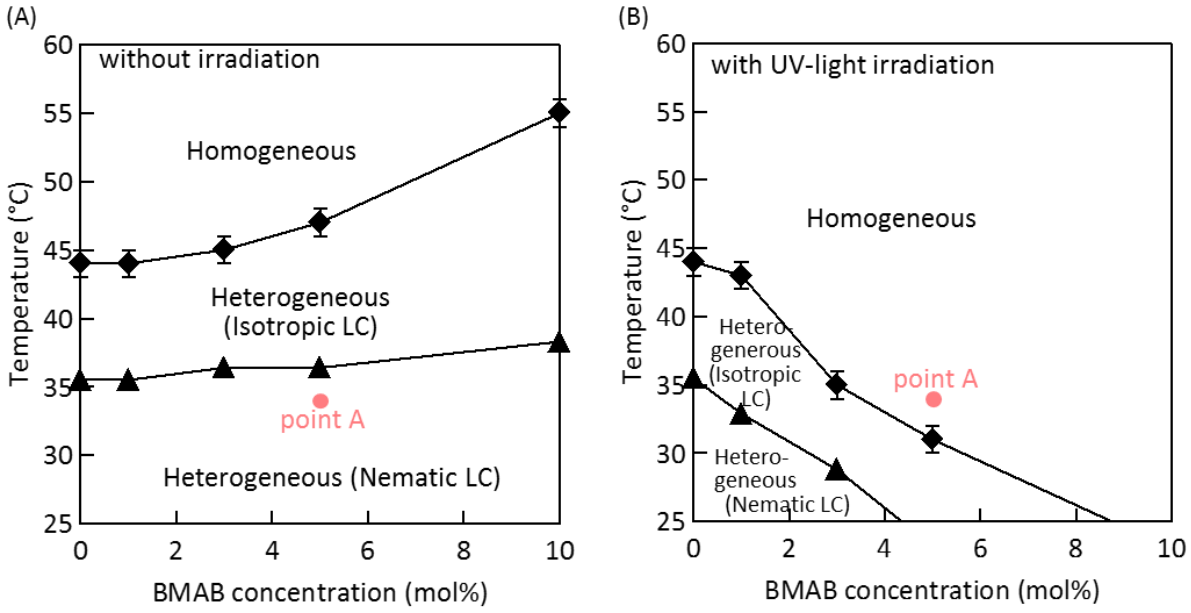

Figure 4-10. Phase diagrams of P-SiP (248k)/azo-doped 5CB composite gel (particle concentration = 10 wt%) as a function of the concentration of BMAB (A) without and (B) with irradiation of UV light (wavelength = 365 nm, intensity = 1.6 mW/cm^2). The heterogeneous–homogeneous transition temperature (rhombuses) and $T_{N–I}$ (triangles) were determined by optical microscopic observations of the composite gels in a heating process at 1 °C/min. At point A, gel–sol transition can be induced by irradiation of UV light.

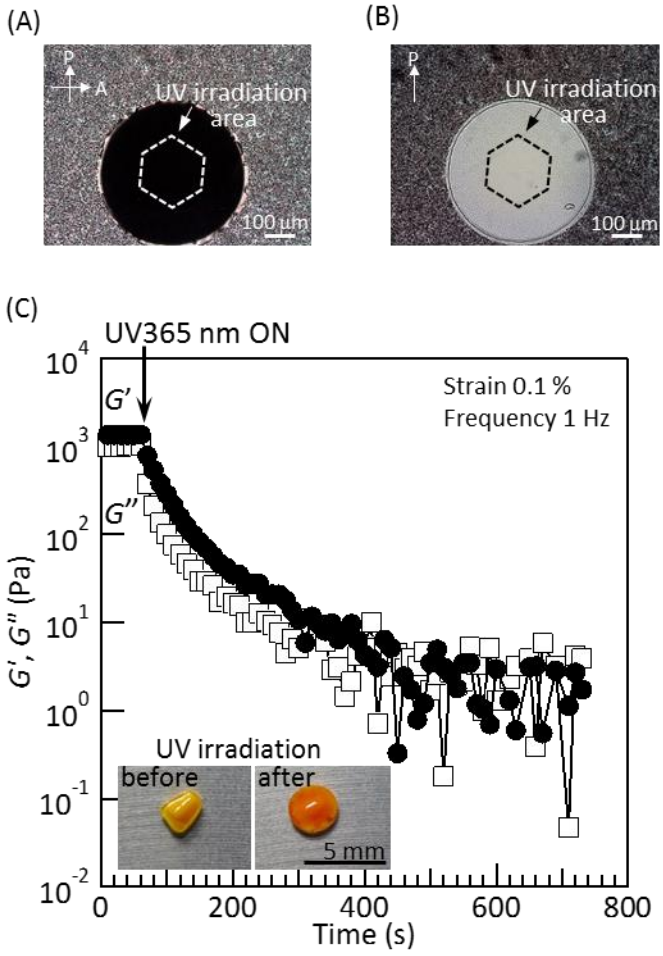

Figure 4-11. Photoinduced change in the microscopic structure and viscoelastic property of the P-SiP (248k)/azo-doped 5CB composite gel (particle concentration = 10 wt%, [BMAB] = 5 mol% for 5CB). Optical textures of the composite gel at 34 °C during irradiation of focused UV light (wavelength = 365 nm, intensity = 0.05 mW) were obtained in (A) cross-polarized and (B) bright-field modes. (C) Dynamic storage (G′, circles) loss moduli (G″, squares) at a strain of 0.1%, frequency of 1 Hz, and temperature of 34 °C were measured with irradiation of UV light (wavelength = 365 nm, intensity = 180 mW/cm2). Inset photographs in C) are the composite gel before and after irradiation with the UV light.

Table 4-1. Viscoelastic parameters of the P-SiP (248k)/azo-doped 5CB composite gel in the light-assisted mending process. The concentration of particles and BMAB were adjusted to 10 wt% for the gel and 5 mol% for 5CB, respectively. UV light (wavelength = 365 nm, intensity = 180 mW/cm^2) and visible light (wavelength = 450 nm, intensity = 10 mW/cm^2) were used.

Step	Condition	Temperature [°C]	G'[a)] [kPa]	G''[a)] [kPa]
1	initial state	20	31	29
2		34	1.9	1.1
3	during irradiation of UV light	34	0.018	0.002
4	during irradiation of visible light	34	0.17	0.045
5	1 h after irradiation	20	20	17
6	1 day after irradiation	20	85	45

a) Storage (G') and loss (G'') moduli at strain = 0.1% and frequency = 1 Hz.

4-3-4 Dual self-healing abilities of the azo-doped composite gel

Finally, using the improved elastic properties and the photoinduced gel–sol transition mentioned above, the dual self-healing abilities of P-SiP/azo-doped 5CB composite gels were investigated (Figure 4-12). Mechanical stress (pressure = 3 MPa) was applied on the surface of the P-SiP (248k)/azo-doped 5CB composite gel ([BMAB] = 10 mol% for 5CB) with the tool mentioned earlier. With this external stress, a crack and a dent were produced at the central part and the left edge of the surface of the composite gel, respectively (Figure 4-12A). The surface dent spontaneously disappeared when the composite gel was left for 10 min at 25 °C, while the cracked area did not show any healing events (Figure 4-12B). Subsequently, we irradiated the cracked area with a focused UV light (intensity = 8.5 mW/cm^2) at 30 °C. The composite gel was transformed into the sol state in the irradiated area and the surface crack was filled up with the composite sol (Figure 4-12C). Subsequently, the UV light-induced sol area was illuminated with visible light (intensity = 40 mW/cm^2) to induce sol–gel transition, resulting in the recovery of a smooth surface of the composite gel (Figure 4-12D).

The self-healing characteristics discussed in this study will be strongly dependent on various factors. For example, in the case of the spontaneous repairing of surface dents, T_g of the grafted polymer will affect the efficiency of the self-healing because the polymer chains need to act like rubbery chains. Then, it is preferred that T_g of the grafted polymer is around room temperature. Actually, in this chapter, the P-SiP/5CB composite gel successfully exhibits efficient repairing of surface dents around room temperature, because the grafted PMMA chains show a rubbery nature even at room temperature by 5CB as plasticizer. In the case of the photochemical mending of surface cracks, gel–sol transition triggered by *trans–cis* photoisomerization of the doped azobenzene compound is required. The operating temperature range of the photochemical mending can be tuned by the concentration of the doped azobenzene compound as shown in Figure 4-10. With increasing the concentration of the azo-dopant, the photochemical mending can be achieved at a lower temperature.

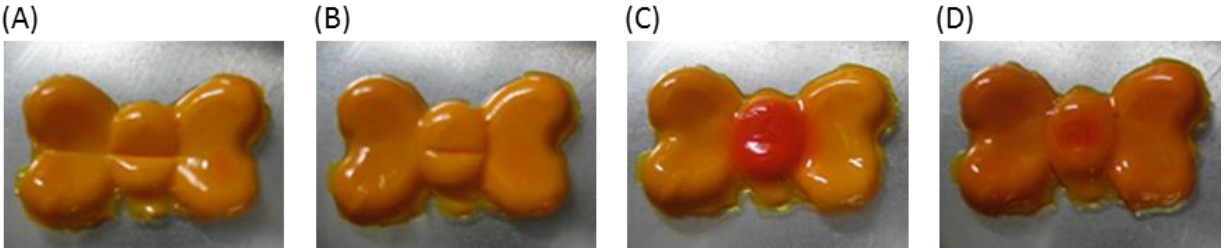

Figure 4-12. Photographs of a P-SiP (248k)/azo-doped 5CB composite gel (particle concentration = 10 wt%, [BMAB] = 10 mol% for 5CB): (A) immediately after being pressed with a tool in slotted screwdriver form at 3 MPa and 30 °C; (B) 10 min after the press; (C) after irradiation of a cracked area with focused UV light (wavelength = 365 nm, intensity = 8.5 mW/cm^2) for 20 min at 30 °C; (D) after illumination of the UV-irradiated area with visible light (wavelength = 450 nm, intensity = 40 mW/cm^2) for 20 min at 25 °C.

4-4 Conclusion

In this chapter, the P-SiP/5CB composite gel was found to show high strength against mechanical stress and good shape recoverability. These mechanical properties of the composite gels was attributed to a combination of the rubbery nature of PMMA chains plasticized with 5CB in the shells of P-SiP and the regulatory effect of the silica core on the spatial positions of the chemically-grafted PMMA chains. In addition, the composite gels doped with an azobenzene compound exhibited gel–sol transition by the *trans–cis* photoisomerization of the azo dopant. The P-SiP/azo-doped 5CB composite gel exhibited dual self-healing abilities comprising of the spontaneous repairing of a surface dent and the light-assisted mending of a surface crack in a material.

References to chapter 4

(1) Murphy, E. B.; Wudl, F. The World of Smart Healable Materials. *Prog. Polym. Sci.* **2010,** *35* (1-2), 223-251.

(2) Hager, M. D.; Greil, P.; Leyens, C.; van der Zwaag, S.; Schubert, U. S. Self-Healing Materials. *Adv. Mater.* **2010,** *22* (47), 5424-5430.

(3) White, S. R.; Sottos, N. R.; Geubelle, P. H.; Moore, J. S.; Kessler, M. R.; Sriram, S. R.; Brown, E. N.; Viswanathan, S. Autonomic Healing of Polymer Composites. *Nature* **2001,** *409* (6822), 794-797.

(4) Bergman, S. D.; Wudl, F. Mendable Polymers. *J. Mater. Chem.* **2008,** *18* (1), 41-62.

(5) Zhang, H. J.; Xia, H. S.; Zhao, Y. Poly(Vinyl Alcohol) Hydrogel Can Autonomously Self-Heal. *Acs Macro Lett.* **2012,** *1* (11), 1233-1236.

(6) Liu, K.; Kang, Y.; Wang, Z.; Zhang, X. 25th Anniversary Article: Reversible and Adaptive Functional Supramolecular Materials: "Noncovalent Interaction" Matters. *Adv. Mater.* **2013,** *25* (39), 5530-5548.

(7) Ying, H.; Zhang, Y.; Cheng, J. Dynamic Urea Bond for the Design of Reversible and Self-Healing Polymers. *Nat. Commun.* **2014,** *5*, 3218.

(8) Cordier, P.; Tournilhac, F.; Soulie-Ziakovic, C.; Leibler, L. Self-Healing and Thermoreversible Rubber from Supramolecular Assembly. *Nature* **2008,** *451* (7181), 977-980.

(9) Yamaguchi, H.; Kobayashi, Y.; Kobayashi, R.; Takashima, Y.; Hashidzume, A.; Harada, A. Photoswitchable Gel Assembly Based on Molecular Recognition. *Nat. Commun.* **2012,** *3*, 603.

(10) Yamamoto, T.; Yoshida, M. Viscoelastic and Photoresponsive Properties of Microparticle/Liquid-Crystal Composite Gels: Tunable Mechanical Strength Along with Rapid-Recovery Nature and Photochemical Surface Healing Using an Azobenzene Dopant. *Langmuir* **2012,** *28* (22), 8463-8469.

(11) Nakahata, M.; Mori, S.; Takashima, Y.; Yamaguchi, H.; Harada, A. Self-Healing Materials Formed by Cross-Linked Polyrotaxanes with Reversible Bonds. *Chem* **2016,** *1*, 766–775.

(12) Ferry, J. D., *Viscoelastic Properties of Polymers*, 3rd ed; John Wiley & Sons: 1980.

(13) Ikeda, T. Photomodulation of Liquid Crystal Orientations for Photonic Applications. *J. Mater. Chem.* **2003,** *13* (9), 2037-2057.

Chapter 5

Summary and Conclusion

In this thesis, the mechanism how mesoscopic aspects, i.e., structures and stiffness of inner networks and interaction and dynamics of components, contribute to mechanical properties was investigated on P-SiP/LC composite gels in order to accelerate the development of advanced functional materials. Using the revealed mechanism, the control of the mechanical properties of the composite gels and their application to the functional materials were attempted.

In chapter 2, temperature dependences of physical properties of the composite gels were examined. The composite gels exhibited the two gel states with different elastic modulus besides a sol (S) state depending on temperature. One is the hard gel (G_H) state and the other is the soft gel (G_S) one. The transition temperature of the G_H–G_S agreed with the glass transition temperature of the polymer components in the composite gels. Therefore, it was concluded that the G_H–G_S transition originates from the change of the stiffness of the inner networks by the glass transition of the grafted polymer of P-SiPs that constructs the percolation networks in the composite gels. The G_S–S transition was driven by the structural changes of the inner networks. The destruction of the network structure coincided with the solubilization of the grafted polymer into LC matrices. In addition, the effects of the concentration of P-SiP and the molecular weight of the grafted polymer on the viscoelasticity of the composites were also described in this chapter.

In chapter 3, the photoresponsivity of P-SiP/azo-doped LC composite gels and its origin were studied. The G_H–G_S and G_S–S transition temperatures were lowered under the irradiation of the UV light. The reductions of the viscoelastic transition temperatures were derived from the improvement of the miscibility between the grafted polymers and azo-doped LC matrix by the UV-light irradiation. Furthermore, from the analyses of the phase behavior of the polymer/azo-doped LC system, it was revealed that the improvement of the miscibility was caused by the change of the interaction between the solvent molecules by the photoisomerization of the azo additive. Using the reduction of the G_H–G_S transition temperature, the isothermal change of the elastic moduli of the composite was achieved by the changes of the stiffness of the inner networks upon

the photoinduced G_H–G_S transition. It was also found that the composite gels employing the nematic LCs with the higher $T_{N–I}$ exhibited the higher viscoelastic transition temperatures. Consequently, the elastic modulus of the P-SiP/azo-doped LC composites could be controlled in the wide elastic modulus range from below10^2 Pa to over 10^5 Pa using the change of the structures and stiffness of the inner networks by the thermal or photochemical manners (Figure 5-1).

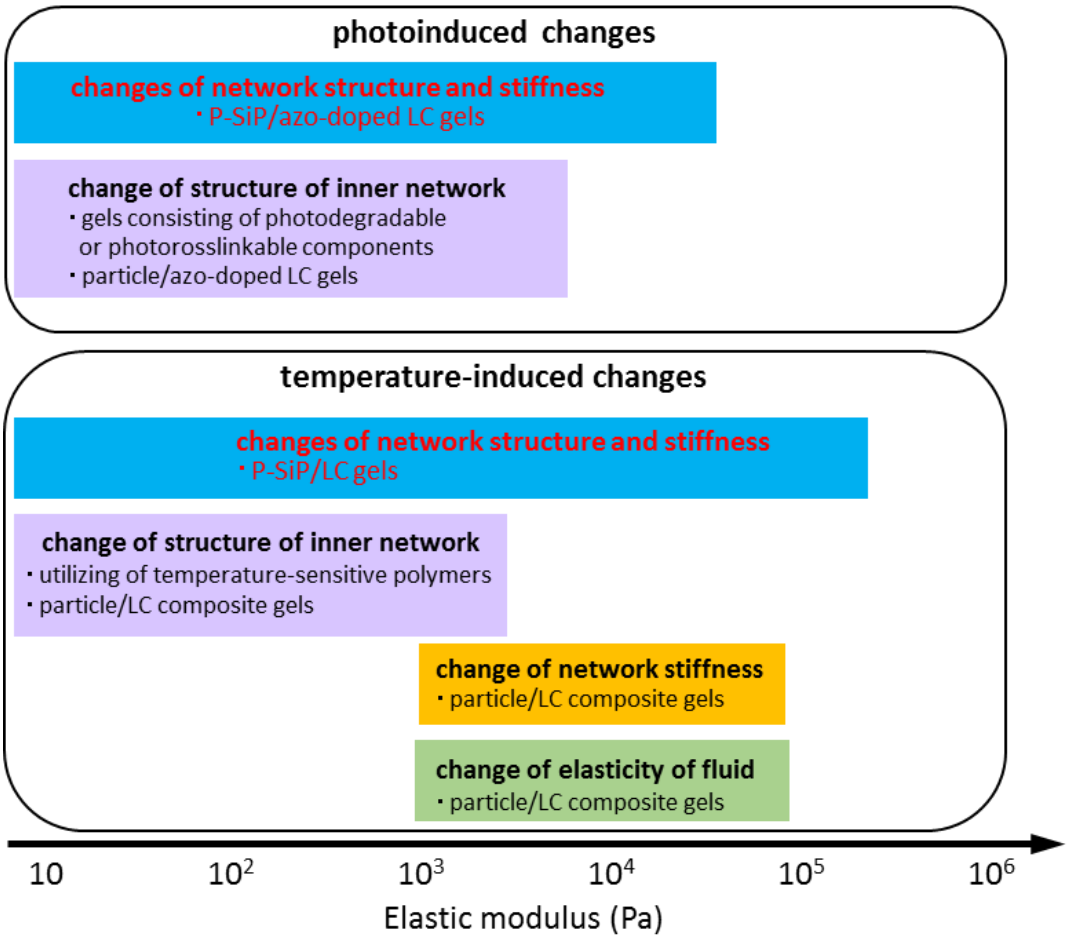

Figure 5-1. Control of elasticity in the wide elastic modulus range achieved in this study.

The control of the mechanical properties of the P-SiP/LC composite gels was able to confer the additional abilities to the functional materials. In chapter 2, it was found that the P-SiP/LC composite gels would be applicable to the self-supporting photonic materials. In the G_H state with the high elastic modulus regardless of the phase structure of the LC matrix, the photoswitching of

the transparency of the film prepared from the P-SiP/azo-doped LC composites was successfully achieved with keeping its self-supporting property. The good adjustability of the viscoelastic properties described in chapters 2 and 3 will make possible to develop cell culture media for tissue engineering, in which the sophisticated tuning of gel properties is required.

In chapter 4, the self-healing abilities of the composite gels were investigated on the basis of the precise control of the viscoelastic property. The good elasticity of the grafted polymer chains plasticized by LC enabled the composite gels to repair surface dents spontaneously. The photoinduced gel–sol transition was also achieved in the composite gel by the reduction of the G_S–S transition temperature upon the UV-light irradiation. Surface cracks were repaired by the photoinduced gel-sol transition in the damaged area. Consequently, the P-SiP/azo-doped LC composite gel exhibited dual self-healing abilities comprising of the spontaneous repairing of a surface dent and the light-assisted repairing of a surface crack.

In this study, the control of the elastic modulus of gels was achieved by the changes of both the structures and stiffness of the networks inside the gels. This control method can be universally applied to other numerous gel materials. Moreover, it was found that the photoinduced changes of the interaction between solvent molecules depending on the molecular shapes of the photoresponsive additive caused the macroscopic changes of materials properties. This mechanism has not been identified and will be utilized to develop new photofunctional materials. Furthermore, the role for the mechanical property was clarified of the mesoscopic structures inside the composites and the dynamics of the components to tune the mechanical property of the P-SiP/LC composites precisely. The elucidation of the correlation between the macroscopic properties and mesoscopic aspects is the common subject in soft matter science. Therefore, this study would contribute to the progress of the research and development of other soft matter.

List of Publications

Publications described in this thesis

(1) Kawata, Y.; Yamamoto, T.; Kihara, H.; Ohno, K. Dual Self-Healing Abilities of Composite Gels Consisting of Polymer-Brush-Afforded Particles and an Azobenzene-Doped Liquid Crystal. *ACS Appl. Mater. Interfaces* **2015**, *7*, 4185-4191.

(2) Kawata, Y.; Yamamoto, T.; Kihara, H.; Yamamura, Y.; Saito, K.; Ohno, K. Three Gel States of Colloidal Composites Consisting of Polymer-Brush-Afforded Silica Particles and a Nematic Liquid Crystal with Distinct Viscoelastic and Optical Properties. *ACS Appl. Mater. Interfaces* **2016**, *8*, 29649-29657.

(3) Kawata, Y.; Yamamoto, T.; Kihara, H.; Saito, K.; Ohno, K. Control of Elastic Moduli with Phototuning of Network Stiffness in Physical Gels Composed of Polymer-Brush-Afforded Silica Particles and Azobenzene-Doped Liquid Crystal. in preparation.

Other publications not described in this thesis

Original papers

(1) Kimura, Y.*; Sato, T. Remarkable Expansion of the Poly(acrylic acid) Chain by Acid-Base Complexation with Low Molecular Weight Amines. *Polymer Journal* **2006**, *38*, 190–196.

* maiden name

(2) Yamamoto, T.; Kawata, Y.; Yoshida, M. Contrasting roles of layered structures in the molecular assembly of liquid crystal matrices on the viscoelastic properties of microparticle/liquid crystal composite gels leading to rigidification and destabilization. *J. Colloid Interf. Sci.* **2013**, *397*, 131-136.

(3) Yamamoto, T.; Kawata, Y.; Kihara, H.; Yoshida, M. Helical-structure-induced softening of particle/liquid-crystal composite gels. *Trans. MRS- J* **2015**, *40*, 335–338.

Review Articles

(1) 光修復性塗料への応用を目指した液晶性光応答ゲルの開発
山本貴広，川田友紀，吉田勝

塗装工学, **2014**, 49, 34.

(2) 液晶の機能を利用した自己修復材料の開発　凹みと破断、２種の損傷修復を実現
川田友紀，山本貴広，木原秀元

コンバ―テック, **2015**, 12, 74-77.

(3) 凹みと破断を修復することが可能な新規自己修復材料の開発
山本貴広，川田友紀，木原秀元

プラスチックスエージ, **2016**, *62*, 86-90.

Acknowledgement

First of all, I would like to express my deep gratitude to Professor Kazuya Saito of the University of Tsukuba for his granting me an opportunity to study in his laboratory, constant guidance throughout the duration of this work. I received generous support as regards the thermal analyses and submission of papers from Associated Professor Yasuhisa Yamamura of the University of Tsukuba. I am deeply grateful to Professor Tetsuo Arai, Professor Hiroki Oshio, and Professor Tatsuya Nabeshima of the University of Tsukuba and Professor Kazuyuki Hiraoka of the Tokyo Polytechnic University for giving insightful comments and suggestions.

I have greatly benefited from Associated Professor Kohji Ohno. He kindly supplied me the series of polymer-brush-afforded silica particles and gives me insightful suggestions. I would like to express my deep gratitude here.

I would like to express the deepest appreciation to Dr. Takahiro Yamamoto of the National Institute of Advanced Industrial Science and Technology (AIST) for his generous supporting. He has given me constant guidance, warm encouragement, and wonderful research environment for 5 years. I feel grateful to members in Smart Materials Group of AIST. I received hearty encouragement from them. I would like to offer my special thanks Dr. Hiroyuki Minamikawa of AIST for his support to the X-ray diffraction experiments.

Needless to say, I am deeply grateful to my family. Without their support and encouragement, I could not enter the doctoral program and complete this thesis.